

TECHNISCHE UNIVERSITÄT MÜNCHEN

Institut für Klinische Neuroimmunologie,
Universitätsklinikum Großhadern,
Ludwig-Maximilians-Universität München

Abteilung für Neuroimmunologie,
Max Planck Institut für Neurobiologie
Martinsried bei München

**Sporadic Inclusion Body Myositis:
Inflammatory and Degenerative Disease Mechanisms**

Jana Ivanidze

Vollständiger Abdruck der von der Fakultät für Medizin der Technischen Universität München zur Erlangung des akademischen Grades eines

Doctor of Philosophy

genehmigten Dissertation.

Vorsitzender: Univ.-Prof. Dr. Juliane Winkelmann

Prüfer der Dissertation: 1. Priv.-Doz. Dr. Klaus Dornmair,
Ludwig-Maximilians-Universität München
2. Univ.-Prof. Dr. Thomas Misgeld

Die Dissertation wurde am 17.05.2011 bei der Technischen Universität München eingereicht und durch die Fakultät für Medizin am 24.05.2011 angenommen.

Dedicated to my grandmother, Regina Bat Hanna Yagnyatynska, Of Blessed Memory.

"Many daughters have attained valor, yet you have surpassed them all."

Acknowledgements.

Having completed this dissertation, I am greatly indebted to many brilliant people.

I would like to begin by thanking my supervisor, PD Dr. Klaus Dornmair, who gave me the opportunity to pursue an exciting and highly rewarding research topic, and has always been a source of moral and scientific support and guidance throughout the years. I further would like to thank my co-supervisor, Prof. Dr. Reinhard Hohlfeld, for having been a wonderful mentor from the start. Of course, I am grateful to Prof. Dr. Hartmut Wekerle for hosting me at this outstanding institute and allowing me to benefit tremendously from constant exchange with exceptional scientists in and beyond my field.

I am grateful to PD Dr. Reinhard Hoffmann, who has been tremendously supportive with the microarray analysis and far beyond, and who served as a member of my thesis committee. I would further like to thank Prof. Dr. Thomas Mísgeld and Prof. Dr. Juliane Winkelmann, who have readily agreed to serve as referees for this dissertation. I am most grateful to Dr. Katrin Offe and Prof. Dr. Arthur Konnerth from the TUM PhD Program "Medical Life Sciences and Technology", for providing me with the opportunity to pursue my PhD in such an inspiring scientific environment.

I would like to thank Dr. Andrew G. Engel, who has shaped the field of myositis research for the last three decades, for having provided his guidance and support, as well as valuable biopsy material.

I am grateful to the Gerhard C. Starck Foundation for financial and moral support throughout this PhD dissertation. In particular, I would like to thank Dr. Charlotte Knobloch, an inspiring mentor.

Mrs. Ingrid Eiglmeier and Mr. Joachim Malotka have tremendously contributed to the successful completion of this dissertation by being warm and wonderful colleagues who created an enjoyable working atmosphere every day.

It's a very fortunate situation when one's colleagues also happen to be one's friends. Big thanks to Latika, Judy, Kathrin, Katherina, Sarah, Birgit, Anna, Jessica, Joachim Z, Martina, Wakiro, and Reinhard. I really enjoyed working with you! I am especially indebted to Latika and Judy for three wonderful years of unparalleled friendship and support. Beyond the lab, special thanks goes out to Amin and Andrew for last-minute proofreading.

I am thankful to my mentors in Radiology, Prof. Dr. Maximilian Reiser, PD Dr. Birgit Ertl-Wagner, Dr. Pina Sanelli, and Dr. Robert Zimmerman, for their moral support.

I thank Prof. Dr. Harry K. MacWilliams for having been my source of inspiration since 1998.

Finally, no words can describe my gratitude to my wonderful mother, my grandmother "Z", my grandfather, my uncle, and my entire family in Munich, Israel and New York, as well as my dear friends in Munich and on all continents, who have always been there for me.

Table of content

	Page	
Table of Content	1	
Used abbreviations	9	
Chapter	Title	Page
1.	Introduction	13
1.1	The adaptive immune system	14
1.2	Inflammatory disease mechanisms	15
1.2.1	Antiviral and antibacterial immunity	15
1.2.2	Autoimmune disease mechanisms	18
1.3	The Inflammatory Myopathies	20
1.4	Sporadic Inclusion Body Myositis – clinical background and pathophysiological considerations	22
1.4.1	Sporadic Inclusion body myositis – Clinical background	22
1.4.2	sIBM Pathophysiology: Inflammatory mechanisms	25
1.4.3	sIBM Pathophysiology: Degenerative mechanisms, similarities to established degenerative diseases	26

Table of content

Chapter	Title	Page
2.	Aims of the study	29
3.	Materials and methods	31
3.1	Patients	31
3.2	Materials	33
3.2.1	Consumables	33
3.2.2	TaqMan quantitative PCR primers and probes	34
3.2.3	Buffers and solutions	36
3.2.4	Antibodies	37
3.2.5	Reaction kits and special reagent solutions	38
3.2.6	Cells and cell culture material	39
3.2.7	Instruments	40
3.3	Methods	41
3.3.1	Frozen tissue cryosectioning	41
3.3.2	Pre-treatment of glass slides for subsequent laser microdissection of single cells	41
3.3.3	Fluorescence labelling of antibodies	42
3.3.4	Basic principles of immunofluorescence imaging	42
3.3.5	Different immunofluorescence staining approaches	43

3.3.5.1	Anti-CD8-/ Anti-HLA-ABC- double immunofluorescence staining for immunofluorescent and confocal microscopy	43
3.3.5.2	Anti-CD8-/ Anti-HLA-ABC- double immunofluorescence staining for subsequent laser microdissection	44
3.3.5.3	Anti-CD8-/ Anti-IFNGR2 - double immunofluorescence staining for subsequent confocal microscopy	45
3.3.5.4	Anti-CD8-/ Anti-CIITA-/ DAPI- triple immunofluorescence staining for subsequent confocal microscopy	45
3.3.5.5	Anti-CD8-/ Anti-HLA-DR/DP/DQ- double immunofluorescence staining for immunofluorescent and confocal microscopy	46
3.3.5.6	Anti-CD8-/ Anti-CXCL9- double immunofluorescence staining for immunofluorescent microscopy	47
3.3.5.7	Anti-CD8-/ Anti-CXCR3- double immunofluorescence staining for immunofluorescent microscopy	48
3.3.5.8	Anti-RER1/ DAPI - double immunofluorescence staining for subsequent confocal microscopy	49
3.3.6	Image acquisition	50
3.3.6.1	Immunofluorescence imaging	50
3.3.6.2	Confocal imaging	51
3.3.7	Laser microdissection	51
3.3.8	RNA Isolation	52
3.3.8.1	RNA isolation from cryosectioned biopsy material	52
3.3.8.2	RNA isolation from laser microdissected cells	54

Table of content

3.3.9	RNA quality control using the Agilent Bioanalyzer	54
3.3.10	Linear transcriptome amplification	57
3.3.11	Microarray hybridization and analysis	59
3.3.12	cDNA synthesis from total RNA	61
3.3.13	TaqMan quantitative PCR	61
3.3.14	Statistical analysis of IFNGR2 distribution on myofibers in sIBM	64
3.3.15	Cell culture	64
4.	Results	65
4.1	Establishment of the methodology and experimental conditions	65
4.1.1	Detection of HLA-ABC and CD8 in sIBM biopsy cryosections	65
4.1.2	Laser microdissection	67
4.1.3	Preservation of RNA quality	68
4.1.4	Establishment and validation of the linear amplification method	69
4.2	CD8 ⁺ T cells focally attack HLA-ABC ⁺ myofibers in the axial as well as the longitudinal plane	71
4.2.1	Demonstration of focal inflammatory infiltrates in sIBM	71
4.2.2	CD8 ⁺ T cells follow a focal attack pattern in the longitudinal plane	72
4.3	Global transcriptome analysis in laser microdissected myofibers	74
4.3.1	Establishment of a classification system for the sampling attacked versus non-attacked myofibers	74

4.3.2	Global microarray analysis of aRNA from laser microdissected myofibers	76
4.4	Evaluation of transcripts involved in antigen presentation and IFN γ -induced signaling by means of TaqMan quantitative PCR	82
4.4.1	TaqMan quantitative PCR analysis confirms global HLA-I upregulation in sIBM myofibers	82
4.4.2	Differential regulation of IFN γ downstream effector transcripts	84
4.5	Confocal microscopy confirms differential IFNGR2 Expression in A _{IBM} versus N _{IBM} myofibers	86
4.6	Upregulation of IFN γ - and TNF α - inducible chemokines	94
4.7	Upregulation of class II HLA on the protein level	99
4.8	Upregulation of CIITA on the protein level	100
4.9	RER1 – a novel candidate biomarker in sIBM and other amyloid-associated diseases	102
4.9.1	Microarray results indicate highly significant regulation of RER1 across all samples	102
4.9.2	RER1 protein expression patterns in inflammatory and degenerative myopathies compared with non-diseased controls	104
4.9.3	Analysis of RER1 mRNA expression in inflammatory and degenerative muscle diseases compared to non-diseased controls	110
4.9.4	RER1 mRNA expression in laser microdissected myofibers versus muscle biopsy samples from patients with sIBM	111
4.9.5	Starvation of TE671 cells induces downregulation of RER1	113

5.	Discussion	115
5.1	sIBM pathophysiology – inflammatory aspects	116
5.1.1	Ubiquitous upregulation of HLA-class I	116
5.1.2	Upregulation of IFN γ receptor in CD8 ⁺ T cell-attacked myofibers	117
5.1.3	Upregulation of IFN γ -induced transcripts	119
5.1.4	Comparison with other microarray studies in human inflammatory myopathies and animal models	121
5.1.5	Inflammatory aspects of sIBM - conclusions and model	122
5.2	sIBM pathophysiology – degenerative aspects	123
5.2.1	Role of the amyloidogenic pathway in sIBM	123
5.2.2	RER1 – a novel potential early regulator of amyloid biosynthesis	123
5.2.3	Myofiber-specific RER1 downregulation demonstrated in laser microdissected sIBM myofibers	125
5.2.4	RER1 mRNA and protein downregulation in sIBM versus other inflammatory and degenerative myopathies	125
5.2.5	RER1 expression may predict the disease course in a patient with myositis	127
5.2.6	Possible regulatory mechanisms of RER1	127
5.2.7	RER1: Conclusions and possible clinical and pathophysiological implications	128
5.3	Inclusion body myositis – a paradigm for the interplay of immunological and degenerative disease mechanisms	128

6.	Summary	131
7.	References	133
8.	Curriculum vitae	147
9.	Published data from the manuscript	149

Used abbreviations

Used abbreviations

AD	Alzheimer's disease
AP	Alkaline phosphatase
APC	Antigen-presenting cell(s)
APH1	Anterior pharynx defective 1
Aqua dest.	Distilled water
aRNA	Amplified ribonucleic acid
BACE1	beta-site APP-cleaving enzyme 1 (β -secretase)
bp	Basepairs
CCL	Chemokine (C-C-motif) ligand
CCR	Chemokine (C-C-motif) receptor
CD	Cluster of differentiation
CNS	Central nervous system
COX	Cytochrome-oxidase
CTL	Cytotoxic T lymphocyte(s)
CXCL	Chemokine (C-X-C-motif) ligand
CXCR	Chemokine (C-X-C-motif) receptor
cDNA	complementary desoxy-ribonucleic acid
DM	Dermatomyositis
DMD	Duchenne muscular dystrophy

Used abbreviations

DNA	Desoxy-ribonucleic acid
EMG	Electromyography
FAM	6-Carboxyfluorescein
Fig	Figure
GAPDH	Glycerinaldehyde-3-dehydrogenase
GAS	Gamma-activated sequence
h	Hour(s)
HBSS	Hank's balanced salt solution
hIBM	Hereditary inclusion body myopathy
HLA	Human leukocyte antigen
HLA-I	HLA class I
HLA-II	HLA class II
IBM	Inclusion body myositis
IF	Immunofluorescence
IFN α	Interferon α
IFN β	Interferon β
IFN γ	Interferon γ
IFNAR	Interferon α receptor
IFNGR	Interferon γ receptor
Ig	Immunoglobulin
IHC	Immunohistochemistry

IP10	IFN γ -inducible protein 10 kDa
IVIg	Intravenous immunoglobulin
kDa	Kilodalton
LDA	Low Density Arrays (“TaqMan cards”)
LM	Laser microdissection
MFM	Myofibrillar myopathy
MGB	Minor groove binder
MHC	Major histocompatibility complex
MIG	Monokine induced by IFN γ
mRNA	messenger ribonucleic acid
NCT	Nicastrin
PBS	Phosphate buffered saline
PEN2	Presenilin enhancer 2
PM	Polymyositis
PPIA	Peptidyl prolyl isomerase A (cyclophilin)
PS1	Presenilin 1 (γ -secretase)
PSMB	Proteasome subunit β
qPCR	TaqMan quantitative polymerase chain reaction
RER1	Retention in endoplasmic reticulum 1 homolog (<i>Saccharomyces cerevisiae</i>)
rpm	Rounds per minute
RQ	Relative quantification

Used abbreviations

sIBM	Sporadic inclusion body myositis
STAT	Signal transducer and activator of transcription
TBS	Tris buffered saline
TCR	T cell receptor
TNF α	Tumor necrosis factor alpha
U	Unit(s)
UV	Ultra-violet light

1. Introduction

Sporadic inclusion body myositis (sIBM) is the paradigm of a myopathy with distinctive degenerative and inflammatory pathogenetic components (Dalakas, 2006b). There is no treatment (Griggs, 2006), and the cause is as yet unknown; both inflammatory and degenerative mechanisms are implicated in sIBM pathogenesis (Dalakas, 2010b).

With a prevalence of around 1 in 100.000, sIBM is the most common inflammatory myopathy in the adult population over the age of 50 years (Mastaglia, 2009). Clinically, sIBM is characterized by progressive weakness and atrophy of both proximal and distal muscle groups, leading to disability within 5 to 10 years after diagnosis (Needham and Mastaglia, 2007). Patients often present with falls, and experience progressive difficulty performing certain tasks, such as tying knots. Involvement of facial and nuchal muscles is common (Dalakas, 2006b).

Myofibers of healthy persons do not express HLA-I (McDouall et al., 1989). sIBM is characterized by a unique mechanism of inflammatory myofiber injury with myocytotoxic CD8⁺ T cells that focally surround and invade HLA-class I positive, non-necrotic myofibers ((Engel and Arahata, 1984) reviewed in (Dalakas, 2006b; Dalakas, 2010b)). Immunological synapses are formed between the attacking CD8⁺ T cells and the myofibers (Goebels et al., 1996). Certain myofibers are heavily attacked, whereas others remain spared by the myocytotoxic T cells (Engel and Arahata, 1984). This observation, while pertinent for the last three decades, has not been explained to this date.

The inflammatory mechanism of myofiber injury is crucial in sIBM pathophysiology, however, it is only one part of the story. In sIBM, but not in other inflammatory myopathies, myofibers harbor disease-specific amyloid deposits. The resulting similarity between IBM and Alzheimer's disease, as well as other neurodegenerative central nervous system (CNS) disorders, is intriguing, albeit barely understood (reviewed in (Askanas and Engel, 2008)).

1.1 The adaptive immune system

The human immune system consists of the innate and the adaptive immune system and protects the body against various pathogens including viruses, bacteria, fungi and parasites. The innate immune system represents a non-specific “first-line defense” and consists of the epithelial barriers, the complement system, as well as macrophages, monocytes, mast cells, granulocytes and natural killer (NK) cells. The adaptive immune system consists of a humoral and a cell-mediated component. The high diversity and specificity of the adaptive immune system, along with its high adaptability and its ability to differentiate between self and non-self, make it such a strong weapon in the battle against offending agents that have overcome the innate immune system. The humoral adaptive immune system is composed of B lymphocytes that produce specific antibodies targeting extracellular antigens. The antibodies enter the circulation system via the bone marrow and lymphatic tissues where they have been produced, and act at anatomically distant sites of infection. The cell-mediated adaptive immune system is composed of T lymphocytes and mainly targets intracellular antigens. The two major types of T lymphocytes are $CD4^+$ and $CD8^+$ T lymphocytes ($CD4^+$ and $CD8^+$ T cells), both types carrying T cell receptors (TCR) which specifically recognize antigens. Antigens are presented to T cells via human leukocyte antigen molecules (HLA). There are two major classes of HLA: HLA class I (HLA-I) and HLA class II (HLA-II). In a healthy human organism, the expression of HLA-II is restricted to “professional” antigen-presenting cells (APC) such as B-cells, macrophages, dendritic cells and tissue-specific APC, e.g. microglia cells in the brain. $CD4^+$ T cells have specific TCR that recognize antigen presented via HLA-II, regulating the activity of “professional” APC (Murphy et al., 2008a). HLA-I, on the other hand, are expressed on almost all nucleated cells, one prominent exception being healthy muscle cells (myofibers) (McDouall et al., 1989). $CD8^+$ T cells have specific TCR that recognize antigen presented via HLA-I. The $CD8^+$ T cell – somatic cell interaction is crucial in the defense against intracellular pathogens, and plays a major role in anti-cancer immunity and autoimmune diseases (see 1.2). This interaction has also been called the “cytotoxic immunological synapse” (**Figure 1.1**). There are two modes of $CD8^+$ T cell-mediated killing: Ca^{2+} -dependent killing by perforin and granzymes and Ca^{2+} -independent killing mediated by Fas ligand (FasL) binding to Fas (CD95) on target cells (Dustin and Long, 2010). Once a $CD8^+$ T cell recognizes a “foreign” or otherwise

immunogenic antigen it becomes activated, undergoes clonal expansion and is capable of killing its target cell (Murphy et al., 2008c).

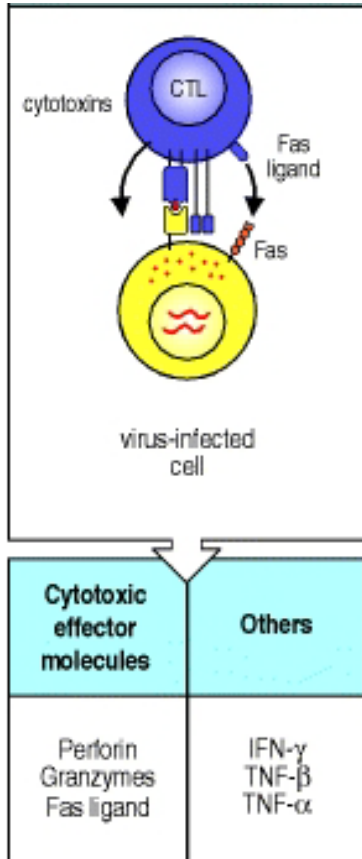


Figure 1.1: Upon recognition of pathogen-derived, HLA-class I bound, peptides, CD8⁺ T cells (CTL, in blue) release perforin and granzymes, initiating pores in the target cell (yellow) membrane and inducing apoptosis. Moreover, CD8⁺ T cells express Fas ligand (FasL). When FasL binds to Fas on a target cell it activates apoptosis in the Fas-bearing cell. Other important effector molecules expressed by CD8⁺ T cells include IFN γ and TNF α . (Murphy et al., 2008c).

1.2 Inflammatory disease mechanisms

1.2.1 Antiviral and antibacterial immunity

Viral and bacterial infections, as well as autoimmune reactions, tumor progression, and other pathogenic changes evoking an inflammatory response, prompt the host cells to produce a subset of proteins called interferons (IFN). IFN were first described in 1957 as signalling proteins capable of “interfering” with viral infections by blocking the spread of intracellular pathogens to non-infected cells (ISAACS and LINDENMANN, 1957). IFN are further divided into type I and

type II IFN. Type I IFN (mainly IFN α and IFN β) regulate early immune response to viral and bacterial infections, acting directly or indirectly on T and B lymphocytes, dendritic cells, macrophages, monocytes and granulocytes (Prchal et al., 2009). The induction of IFN α/β -associated gene expression occurs through IFN α/β -receptor-coupled Janus kinases (JAK). The main downstream regulator proteins in IFN α/β -signalling are members of the signal transducer and activator of transcription (STAT) family, in particular heterodimers of STAT1 and STAT2 (Decker et al., 2005).

Type II IFN (IFN γ) is produced later in the course of infection by activated T lymphocytes and NK cells, as well as B lymphocytes, dendritic cells, and macrophages (Schroder et al., 2004). IFN γ induces the expression of HLA-I and HLA-II expression in host cells, thus driving efficient antigen presentation in intracellular infections. The receptor for IFN γ consists of two distinct chains, IFNGR1 and IFNGR2 (Stark et al., 1998). It is of particular importance to note that upon binding of IFN γ , IFNGR1 rapidly translocates to the nucleus in a complex with IFN γ and STAT1, while IFNGR2 remains on the cell surface (Ahmed and Johnson, 2006; Larkin, III et al., 2000). JAK1 and JAK2 are subsequently activated and perpetuate the phosphorylation of STAT1 and formation of STAT1 homodimers (**Figure 1.2**) (Pestka, 1997; Young and Bream, 2007) which then induce the transcription of IFN γ -responsive genes. There is however also a role for STAT1-independent IFN γ signaling (Gough et al., 2008).

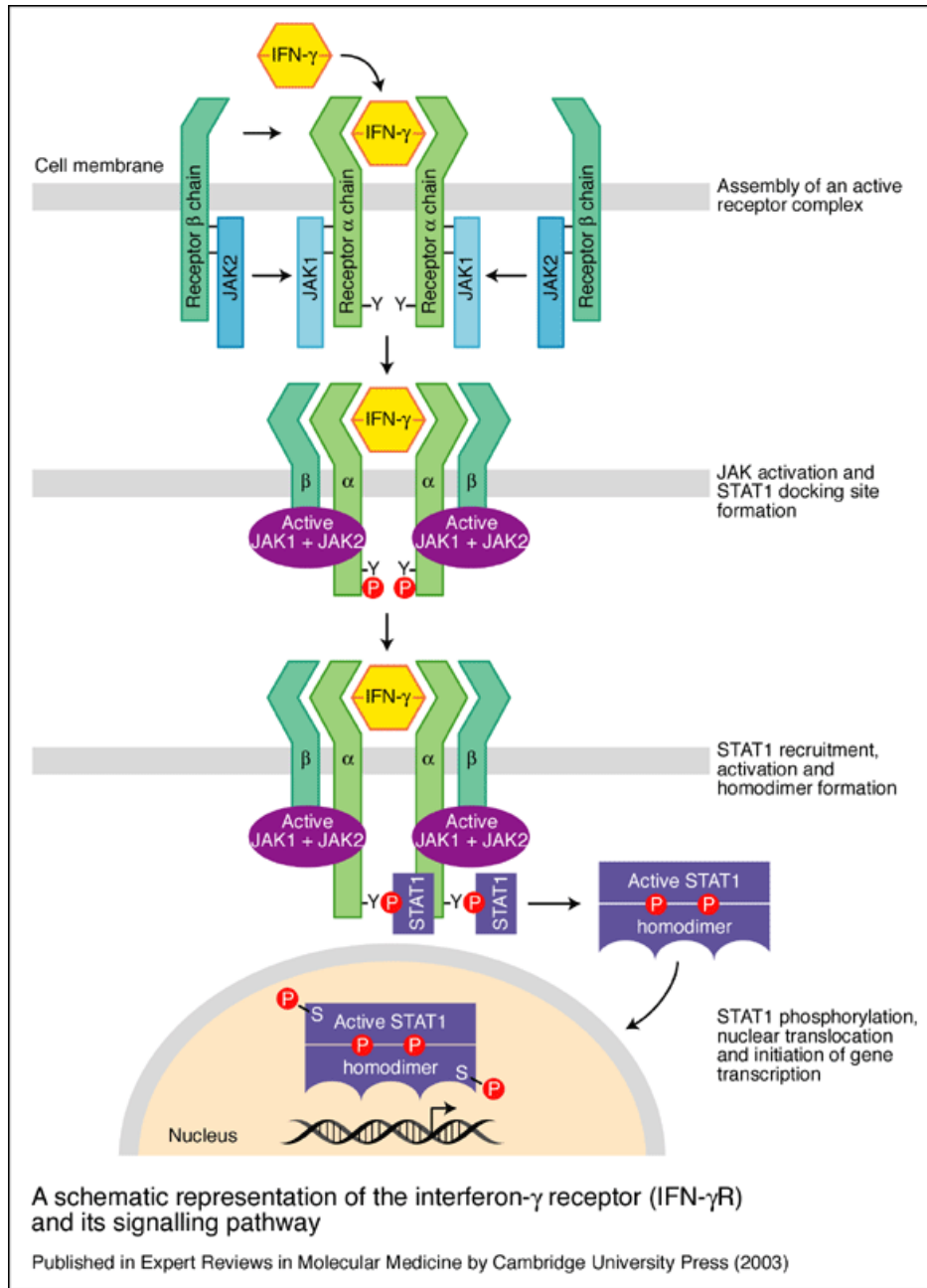


Figure 1.2: Signaling via the IFN γ receptor (IFNGR). The receptor for IFN- γ has two subunits: IFNGR1, the ligand-binding, constitutively expressed chain and IFNGR2, the signal-transducing, TNF α -inducible chain (also known as the β chain or accessory factor 1). Binding of IFN- γ leads to dimerization of two IFNGR1 chains, and association with two IFNGR2 chains. This in turn activates the Janus kinases JAK1 and JAK2 which phosphorylate a tyrosine residue on the intracellular domain of IFNGR1. This leads to the recruitment and phosphorylation of STAT1, which forms homodimers and translocates to the nucleus to activate a wide range of IFN- γ -responsive genes. After signalling, the ligand-binding chains are internalised and dissociate. The chains are then recycled to the cell surface. (from *Expert Reviews in Molecular Medicine* 2003, adapted from (Stark et al., 1998)).

Through binding to their respective GAS sequences, STAT1 directly activates many immune effector genes, including genes involved in antiviral response, microbicidal proteins, phagocytic receptors, chemokines, cytokines, and antigen-presenting molecules (Hu and Ivashkiv, 2009; Stark, 2007).

An important downstream effector of the IFN γ -induced JAK/STAT signalling cascade is the MHC Class II transactivator (CIITA). CIITA drives the expression of HLA-II and to a smaller extent HLA-I. HLA-I is present on most nucleated cells, with one of the few exceptions being skeletal muscle (McDouall et al., 1989). HLA-II expression is restricted to professional APC (van den Elsen et al., 2004). Overexpression of HLA-I in muscle cells has been demonstrated to induce myositis-like disease in mice, further supporting the pathophysiological role of HLA-I in the development of sIBM (Nagaraju et al., 2000; Li et al., 2009).

The immunoproteasome is an IFN γ -inducible multisubunit ATP-dependent protease which generates antigenic peptides optimized for antigen presentation via HLA-I in non-immune cells, and via HLA-II in professional APC (Coux et al., 1996). IFN γ is the major trigger for the expression of immunoproteasome components, thus directly activating antigen presentation (Kloetzel, 2001).

1.2.2 Autoimmune disease mechanisms

One of the most critical functions of the immune system is to distinguish between self and nonself. In order to do this, lymphocytes have three basic mechanisms: 1.) during their maturation, lymphocytes that react strongly with ubiquitous self antigens (autoantigens) are eliminated by induction of apoptosis, 2.) mature naïve lymphocytes are exposed to chronically high concentrations of self antigens, which induces tolerance, 3.) autoantigens are normally presented in the absence of co-stimulatory signals that are crucial for an effective immune response. However, these mechanisms are not perfect; self-reactive lymphocytes are always present in the immune repertoire, but are not often activated (Murphy et al., 2008b).

Just like immune responses to pathogens that are specifically triggered by antigens, autoimmune responses are elicited by autoantigens which give rise to autoreactive effector T cells and

autoreactive B cells producing autoantibodies. Autoimmunity usually arises spontaneously, i.e. the initial events triggering an autoimmune response are unknown. Whereas certain infectious agents expressing epitopes similar to autoantigens are implicated in certain autoimmune diseases, a preceding infection is not a general precondition for the induction of autoimmunity (Murphy et al., 2008b).

Autoimmune diseases are difficult to classify given how little is known about their pathogenesis. In some of the diseases, the exact antigen(s) are known, whereas in most autoimmune diseases the search for the autoantigen(s) is still ongoing. Clinically, autoimmune diseases are commonly differentiated into organ-specific diseases, where the autoimmune mechanisms are restricted to specific organs of the body, and systemic diseases affecting multiple organs. One of the most common examples of organ-specific autoimmune diseases is type I diabetes mellitus, where autoreactive T cells attack and destroy pancreatic islet β -cells, completely abolishing endogenous insulin production, resulting in rising blood glucose levels in affected individuals (Powers, 2008). An important example of a systemic autoimmune disease is Systemic lupus erythematoses (SLE). In SLE, both autoreactive antibodies and autoreactive T-cells target DNA and other nuclear components such as histones, resulting in damage to the skin, the kidneys, the vasculature, as well as the central nervous system (Powers, 2008).

Many autoimmune diseases seem not to be triggered by autoreactive immune response alone, in contrast, other mechanisms, such as degeneration, are present in the local milieu of ongoing attack. The interrelation between inflammatory and non-inflammatory mechanisms in

IFN play a complex role in autoimmune responses (Munz et al., 2009). IFN-induced autoimmunity is thought to stem from increased activation of dendritic cells, as well as increased production of antibodies (Jego et al., 2003; Rizza et al., 2010). An increased IFN signature, i.e. upregulation of IFN-inducible genes, is seen in various autoimmune diseases such as systemic lupus erythematoses (Bennett et al., 2003; Ronnblom and Alm, 2003) and dermatomyositis (Greenberg, 2010).

1.3 The inflammatory myopathies

The inflammatory myopathies inclusion body myositis (IBM), polymyositis (PM), and dermatomyositis (DM) are the most common cause of acquired muscle disease in adults. The estimated annual incidence equals 5 to 10 per million in adults and 1 to 5 per million in children. The estimated prevalence is 50 to 100 cases per million (Miller, 2005).

Features common to all inflammatory myopathies are inflammation of the endomysium, muscle fiber necrosis, elevation of serum muscle enzymes and progressive muscle weakness. However, each subset has unique clinical and pathophysiological features, and therapy and prognosis of the different inflammatory myopathies are fundamentally different (Dalakas, 2010a).

The most common inflammatory myopathy in older individuals is sporadic Inclusion body myositis (sIBM). The sporadic form of IBM is by far more common than the hereditary form (hIBM). sIBM is also the most common inflammatory myopathy in the adult population over the age of 50 years (Mastaglia, 2009). Clinically, sIBM is characterized by progressive weakness and atrophy of both proximal and distal muscle groups, leading to disability within 5 to 10 years after diagnosis (Needham and Mastaglia, 2007). If the clinical presentation gives rise to suspicion of sIBM, muscle biopsy is essential for a diagnosis. Other important diagnostic measures are electromyography (EMG) and serum muscle enzyme levels. The main characteristics of sIBM muscle biopsy are focal infiltrates mainly consisting of CD8⁺ T cells surrounding and invading myofibers, ubiquitous HLA-I upregulation on myofibers, and Congo red positive amyloid deposits and rimmed vacuoles within myofibers. The amyloid deposits are immunoreactive for a number of amyloid-associated proteins. There is currently no treatment available for sIBM (Mastaglia, 2009).

Dermatomyositis (DM) presents with a symmetrical, proximal muscle weakness of a variable degree, along with skin changes including a so-called heliotrope rash on the upper eyelids, face, knees, elbows, neck, anterior chest, back, and shoulders, along with a so-called Gottron's rash (scaly eruptions on the knuckles). A thorough workup for a possible underlying malignancy is mandatory given that 15% of DM patients develop cancer within three years of diagnosis. The pathophysiology is still not entirely understood, however, it is known that dermatomyositis is mainly driven by CD4⁺ T cells that activate B cells and plasmacytoid dendritic cells in the

perimysial and perivascular regions. There is moreover a strong activation of the complement cascade leading to the formation of the membranolytic attack complex leading to destruction of endomysial capillaries. Migration of B cells and CD4⁺ T cells to the endo- and perimysium follows a chemotactic gradient of type I interferon-inducible cytokines and chemokines. There is perifascicular atrophy with a strong upregulation of HLA-I, neural cell adhesion molecule (NCAM), and $\alpha\beta$ -crystallin (Dalakas, 2005).

Polymyositis (PM) clinically represents a diagnosis of exclusion: it is an acquired myopathy affecting proximal muscles in a symmetrical fashion and occurring subacutely in adults who do not have an accompanying rash, a positive family history, or previous exposure to myotoxic drugs. Muscle biopsy shows ubiquitous HLA-I upregulation, with clonally expanded cytotoxic CD8⁺ T cells focally attacking apparently healthy myofibers. The nature of the (auto-)antigens presented to CD8⁺ T cells via HLA-I-positive myofibers is unknown, as is the reason for the focal nature of the CD8⁺ T cell attacks.

The classification of the inflammatory myopathies was first established by Bohan and Peter in 1975. The Bohan and Peter criteria include 1.) subacute, symmetric proximal weakness; 2.) histological abnormalities (necrosis, regeneration, perifascicular atrophy, inflammatory exudates); 3.) elevated serum creatine kinase (CK) activity, 4.) pathological EMG; and 5.) typical skin abnormalities (for DM). Exclusion criteria are a slowly progressive course, a positive family history, and the concomitance of other neuromuscular disorders (Bohan and Peter, 1975a; Bohan and Peter, 1975b). According to the Bohan and Peter classification, a definitive diagnosis of PM can be made if criteria 1 through 4 are fulfilled. If skin abnormalities are present in addition to three of the other criteria, DM can be diagnosed. Thus, skin abnormalities are the only feature that differentiates PM from DM according to the Bohan and Peter classification (Bohan and Peter, 1975a; Bohan and Peter, 1975b).

Arahata and Engel showed in 1984 that there are important histologic differences between PM, and DM (Arahata and Engel, 1984). Dalakas then refined the diagnostic criteria, including histopathological differences between the three entities (Dalakas, 1991). Despite this refinement, several large studies have kept using the Bohan and Peter criteria in evaluating patients with inflammatory myopathies (IM) and have come to the conclusion that PM constitutes 30 to 60%

of the IM patient population (Hill et al., 2001; Love et al., 1991; Joffe et al., 1993). In a 2003 study that included 165 patients with IM it was shown that PM made up only 5% of the IM patient population (van der Meulen et al., 2003). Moreover, these nine patients with “definite PM” all exhibited a longer disease duration, presentation at older age, and less pronounced serum CK elevation, all features suggestive of sIBM. Out of these 9 patients with “definite PM”, five had no improvement or progression under high-dose steroid treatment, and exhibited rimmed vacuoles, a histopathological sign of sIBM, at re-biopsy one year after the initial diagnosis (van der Meulen et al., 2003). Other authors have shown that a large number of patients with therapy-resistant PM have retrospectively been diagnosed with sIBM (Amato et al., 1996; van der Meulen et al., 1998). Based on these findings, it has been widely debated whether PM can be considered an entity of its own (van der Meulen et al., 2003; Chahin and Engel, 2008).

As opposed to sIBM which is therapy-resistant, DM and PM tend to respond very well to corticosteroid treatment. Prednisone is usually the first-line drug, even though there are no controlled trials to support this choice of medication. A high dose is initially started, and then slowly reduced after three to four weeks until the lowest possible dose necessary for disease control is reached. Additionally, so-called “steroid-sparing” drugs are used, including azathioprine, mycophenolate mofetil, methotrexate and cyclosporine. In cases where steroid treatment fails to induce remission, or in cases of rapidly progressive disease, preference is given to intravenous immunoglobulin (IVIg) over the above mentioned steroid-sparing agents (Dalakas, 2011).

1.4 Sporadic Inclusion Body Myositis – clinical background and pathophysiological considerations

1.4.1 Sporadic Inclusion body myositis – Clinical background

The sporadic form of IBM is by far more common than the hereditary form. sIBM is also the most common inflammatory myopathy in the adult population over the age of 50 years. The prevalence is around 1 in 100.000, however, it varies based on observed population and HLA haplotype. Men are more frequently affected than women; and Caucasians are more commonly affected than other ethnic groups (Mastaglia, 2009).

Clinically, sIBM is characterized by progressive weakness and atrophy of both proximal and distal muscle groups and leading to disability within 5 to 10 years after diagnosis (Needham and Mastaglia, 2007). Involvement of quadriceps as well as deep finger flexors are important clinical clues (Sekul and Dalakas, 1993). Patients often present with falls owing to proximal muscle weakness; as well as difficulty performing certain tasks, such as tying knots, due to distal wrist and finger flexor weakness. There is frequent involvement of facial and nuchal muscles, and dysphagia is present in up to 60% of patients with sIBM. Most patients require an assistive device for walking within several years of onset (Dalakas, 2006b).

If the clinical presentation gives rise to suspicion of sIBM, muscle biopsy is essential for a diagnosis. Other important diagnostic measures are electromyography (EMG) showing increased spontaneous activity and serum creatine kinase levels which can be elevated up to ten-fold in the initial stage of the disease. Muscle biopsy shows signs of a chronic disease process with atrophic as well as hypertrophic myofibers, occasionally internalized nuclei and increased fibrous tissue. The main characteristics of sIBM muscle biopsy are focal infiltrates mainly consisting of CD8⁺ T cells surrounding and invading myofibers, ubiquitous HLA-I upregulation on myofibers, and congo-red positive amyloid deposits and rimmed vacuoles within myofibers. The amyloid deposits are immunoreactive for a number of amyloid-associated proteins. Further, there are tubulo-filamentous inclusions that can be visualized on electron microscopy, and signs of abnormal mitochondria such as cytochrome-oxidase (COX) negative fibers (**Figure 1.2**).

In summary, (sIBM) is thus the paradigm of a myopathy with distinct degenerative and inflammatory pathogenetic components. At present, it is unknown how exactly the two pathways interact, which of the two mechanisms is the mechanism primary injury, and which is secondary.

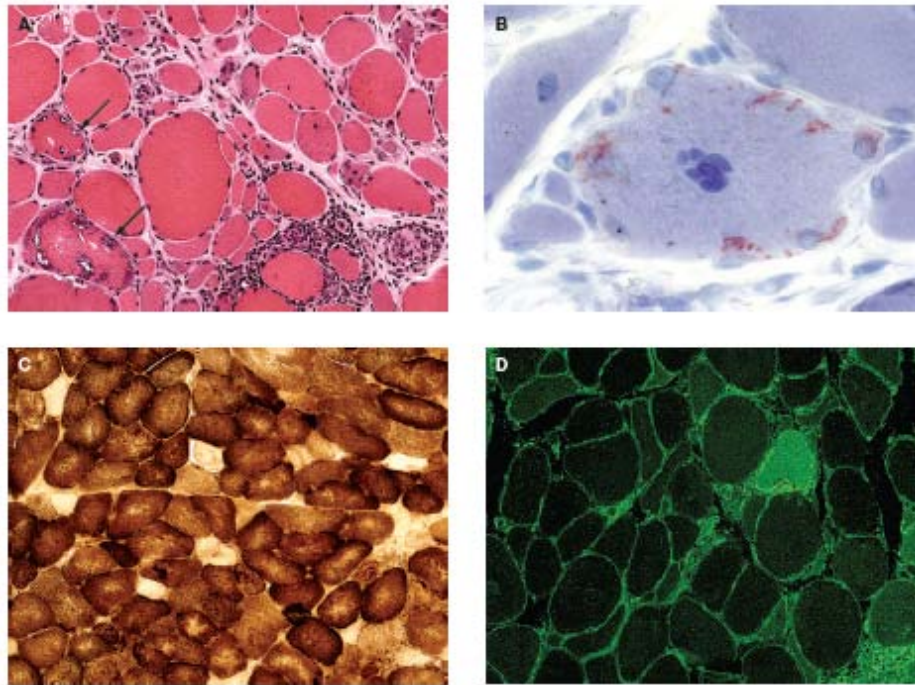


Figure 1.2: Histological features in muscle biopsies of patients with sIBM.

A. Endomysial inflammation with multifocal lymphocytic invasions of healthy appearing myofibers. Two myofibers contain vacuoles (arrows). **B.** Intracellular amyloid deposits, visualized here with crystal violet staining. **C.** COX-negative myofibers. **D.** Ubiquitous HLA-I upregulation.

Figure adapted from Dalakas, 2006.

Hereditary inclusion body myositis (hIBM) is a very rare disease which was first described in 1984 as being specific to a population of Iranian Jews; meanwhile, affected individuals have been characterized worldwide (Argov and Yarom, 1984; Sadeh et al., 1993; Nishino et al., 2002). Clinically, hIBM features progressive systemic muscle atrophy with sparing of the quadriceps. Histologically, small myofibers with rimmed vacuoles and tubulofilamentous inclusions are seen, however there is no evidence of inflammation. The most common mutations associated with hIBM are located in the ubiquitously expressed *GNE* gene which encodes glucosamine (UDP-N-acetyl)-2-epimerase/ N-acetylmannosamine kinase (GNE/ MNK), an enzyme catalyzing acetylneuraminic acid biosynthesis. No established treatment is currently available for hIBM (Huizing and Krasnewich, 2009).

1.4.2 sIBM Pathophysiology: Inflammatory mechanisms

A substantial body of evidence supports an autoinflammatory mechanism as the primary cause for sIBM.

There are studies reporting an association with certain HLA alleles and haplotypes including the so-called “autoimmune haplotype” (HLA-A*01, -B*0801, -DRB1*0301, -DQB1*0201, -DQA1*05), one of the strongest known HLA-disease associations that is also associated with a number of other autoimmune diseases and with increased production of inflammatory cytokines (Price et al., 1999). Other sIBM-associated HLA haplotypes include the 35.2 AH (HLA-B35, DR1) and the 52.1 AH (HLA-B*5201, DRB1*1502), whereas the HLA-DR4 and DR7 alleles may be protective (Mastaglia et al., 2009).

Further, sIBM bears resemblance to other autoimmune diseases in that association of sIBM within families is seen in members of the same generation (Sivakumar et al., 1997). An association of sIBM with other autoimmune diseases has been reported, including pernicious anemia, dermatitis herpetiformis and psoriasis; moreover, non-specific autoantibodies are present in the serum of patients with sIBM (Koffman et al., 1998; Badrising et al., 2004).

Further, an association with human immunodeficiency virus (HIV) and human T-lymphotropic virus (HTLV) infections has been reported, suggesting immune mechanisms to be of major relevance in sIBM pathophysiology (Dalakas, 2006b). Moreover, a strong upregulation of inflammatory cytokines, chemokines and their receptors in sIBM muscle tissue have been shown (Figarella-Branger et al., 2003; Raju et al., 2003).

The focal attack and invasion of non-necrotic myofibers by CD8⁺ T cells and macrophages represents an unparalleled mechanism of inflammatory myofiber injury ((Engel and Arahata, 1984) reviewed in (Dalakas, 2006b; Dalakas, 2010b)). Occasional autoantibodies found in sIBM are non-specific, and there is no role for autoantibody-mediated injury in sIBM; hence, no systemic or long-distance mechanisms of injury are present. By contrast, direct contact between cytotoxic CD8⁺ T cells and affected myofibers leads to local injury with the formation of specific “immunological synapses” with vectorial excretion of perforin towards the attacked myofibers (Goebels et al., 1996). The myofiber-specific cytotoxic T cells likely recognize – currently still unidentified – antigen(s) presented by HLA-class I (HLA-I) molecules on the myofiber

membrane (Dustin and Long, 2010). Accumulating evidence of oligoclonal restriction of the T cell receptor repertoire supports the hypothesis of an antigen-driven recruitment of the myocytotoxic T cells (Lindberg et al., 1994; Amemiya et al., 2000; Bender et al., 1998; Seitz et al., 2006; Hofbauer et al., 2003). Moreover, these clonal expansions were shown to persist over time in individual patients (Amemiya et al., 2000; Hofbauer et al., 2003; Dimitri et al., 2006). On the other hand, CD8⁺ T cells that are found in the perimysial space and are not attacking myofibers (so-called “bystander CD8⁺ T cells) are clonally diverse (Bender et al., 1998).

Myofibers of healthy subjects do not express HLA-I (McDouall et al., 1989). In sIBM, HLA-I is ubiquitously induced in all myofibers as shown in **Figure 2D** and previously demonstrated by other authors (Karpati et al., 1988; Bartoccioni et al., 1994; Jain et al., 2007; Emslie-Smith et al., 1989). On the other hand, CD8⁺ T cells attack and invade sIBM myofibers in a strictly focal pattern ((Arahata and Engel, 1984) reviewed in (Dalakas, 2007)). HLA-I expression is a necessary but not sufficient precondition for a myofiber to be attacked. Despite the high numbers of immune cells present in muscle biopsies of sIBM patients, immune mechanisms alone cannot provide sufficient explanation for the pathophysiological mechanisms leading to sIBM. This is supported by the fact that all immunosuppressive therapies have failed in sIBM patients (Griggs, 2006; Dalakas, 2010b). There seem to be additional factors rendering muscle fibers susceptible to inflammatory attack.

1.4.3 sIBM Pathophysiology: Degenerative mechanisms, similarities to established degenerative diseases

Because sIBM is notoriously refractive to immunosuppressive therapies (Griggs, 2006), it has been argued that sIBM may not represent a primary autoimmune myopathy but that the inflammatory changes may be secondary to as yet unknown viral or degenerative trigger(s) (Hilton-Jones et al., 2010). Indeed, sIBM does bear features characteristic of classic degenerative disorders of the CNS such as Alzheimer’s disease (AD) and Parkinson’s disease (PD) and has been repeatedly compared to these entities (Askanas and Engel, 2008).

One hallmark of sIBM suggesting a role for degenerative mechanisms are vacuolated myofibers (**Figure 1.2A**) (Dalakas, 2006a). Such vacuolated fibers have been observed in other myopathies

that are purely degenerative, such as hIBM, myofibrillar myopathy, X-linked Emery Dreifus muscular dystrophy, rigid-spine-syndrome, and post-Polio syndrome (Fidzianska et al., 2004; Semino-Mora and Dalakas, 1998; Selcen et al., 2004). Moreover, β -Amyloid and a number of related proteins including APP, phosphorylated tau, presenilin-1, apolipoprotein-E, α -tubulin, clusterin, α -synuclein, gelsolin, oxidative stress proteins, and proteasome components have been detected in sIBM biopsies, with expression levels comparable to myofibrillar myopathy (Fidzianska et al., 2004; Semino-Mora and Dalakas, 1998; Selcen et al., 2004; Ferrer et al., 2004; Ferrer et al., 2005).

Similarities between sIBM muscle and AD brain include the accumulation of AD-characteristic proteins, namely β -Amyloid (Askanas and Engel, 2008; Askanas and Engel, 1998). While some researchers have argued that the accumulation of β -Amyloid is the initiating event in sIBM pathophysiology (Askanas and Engel, 2007), others have demonstrated that certain chemokines, namely Interleukin-1 β , can induce intracellular β -Amyloid accumulation in cultured muscle cells, and have shown a colocalization of Interleukin-1 β and β -Amyloid in biopsies of sIBM patients (Schmidt et al., 2008), arguing that the inflammatory mechanisms are the primary event in sIBM.

Alzheimer's disease (AD) is a progressive, fatal degenerative disease of the aging brain, and the most common cause of dementia, as well as one of the leading causes of death in the elderly population of industrialized nations (Alzheimer's Association, 2010). AD is characterized by a loss of short-term memory and deterioration in behavior and higher cognitive function (Mattson, 2004). AD is clinically differentiated into early-onset (age of onset younger than 60-65 years) and late-onset (age of onset older than 60-65 years), the latter being the more common form. A definitive diagnosis is only possible through histopathological examination of post-mortem brain, and demonstration of the two histopathological hallmarks of AD, neuritic or senile plaques containing β -Amyloid and neurofibrillary tangles in the cortex and limbic system (LaFerla and Oddo, 2005; Gouras et al., 2005).

In the recent years, more and more evidence has accumulated that progressive deposition of β -

amyloid, derived from β -amyloid precursor protein (APP), plays a major role in AD pathophysiology (Selkoe, 1989; Sisodia and Price, 1995). One of the major enzymes responsible for the production of β -Amyloid is γ -Secretase (Wolfe and Guenette, 2007). γ -Secretase represents a complex machinery consisting of four subunits that have to be assembled within the endoplasmic reticulum (ER) and the cytoplasm before γ -Secretase can successfully cleave its substrates (Spasic and Annaert, 2008). AD research in the recent years has focused on the regulation and assembly of γ -Secretase, given its potential applicability as a drug target in future AD therapies (Woo et al., 2011).

Parkinson's disease (PD) is characterized by loss of dopaminergic neurons in the substantia nigra. On the molecular level, a hallmark of PD is the development of Lewy bodies, protein aggregates of filamentous material within degenerating neurons (Braak et al., 2003). The protein components of the Lewy bodies arise from proteins such as α -synuclein, parkin, and components of the ubiquitin-proteasome system (Fornai et al., 2003). The hypothesis that proteasome dysfunction and associated unfolded protein response play a pivotal role in PD pathogenesis provides an interesting link between PD and sIBM (Askanas and Engel, 2008)

Senile systemic amyloidosis is characterized by intracellular accumulation of amyloid, mainly consisting of transthyretin (prealbumin). The deposition of transthyretin can occur in a variety of tissues (the heart is a common manifestation). The similarities to other degenerative diseases discussed here lie in the toxic, self-perpetuated accumulation of amyloid components. There is emerging evidence that transthyretin and β -amyloid interact on a molecular level (Du and Murphy, 2010).

Myofibrillar myopathy (MFM) is a heterogeneous muscle disorder characterized by the accumulation of myofibrillar degradation products and a dysregulated ubiquitin-proteasome system. There is a wide variety of aberrantly expressed proteins in MFM, including desmin and α B-crystallin. Strikingly, proteins overexpressed in Alzheimer's disease such as β -amyloid and phosphorylated tau protein, are aberrantly expressed in MFM as well, suggesting a mutual pathogenetical component of the two conditions (Ferrer and Olive, 2008).

2. Aims of the study

The main aim of this work was to apply an unbiased global transcriptome analysis approach to shed light on the question why in sIBM certain myofibers are attacked by CD8⁺ T cells whereas other myofibers remain spared.

To analyze differential expression in attacked versus non-attacked myofibers, methods were established that allowed to perform specific immunofluorescence staining and laser microdissection of muscle tissue, as well as global qualitative and quantitative transcriptome analysis of laser microdissected cells. The unique properties and distinct morphology of myofibers were used to establish experimental conditions necessary for RNA isolation and analysis. Since RNA isolated from laser microdissected muscle cells was sparse, linear transcriptome amplification was required to yield sufficient material for further analysis.

The aim was then to apply these methods to identify subsets of transcripts which are differentially regulated in attacked versus non-attacked muscle fibers using an unbiased approach. The results were then validated with quantitative methods on the mRNA by quantitative PCR and on the protein level by immunohistochemistry.

sIBM is unique in that inflammatory and degenerative mechanisms are closely interrelated, in fact, it is still unknown which mechanism leads to the primary initiating event in sIBM pathophysiology. In the third part of this dissertation, the expression of a potential new molecular marker of amyloid biosynthesis was investigated in sIBM, other inflammatory myopathies, as well as degenerative muscle diseases.

3. Materials and methods

3.1 Patients

For establishment of experimental conditions as described in section 4.1, fresh frozen tonsillitis specimens were kindly provided by the department of general surgery, Munich University Hospital. The tissue was immediately frozen upon surgical extraction from patients with tonsillitis.

For the first two parts of this thesis, i.e. establishment of RNA-preserving experimental conditions for the analysis of laser microdissected cells (see section 4.1) and analysis of the IFN γ downstream signaling in sIBM (see section 4.2), muscle-biopsy specimens from five patients with sIBM (IBM1-5) and three healthy controls (C1-3) were used (**Table 3.1**). sIBM biopsy samples were kindly provided by Professor Dr. Andrew G. Engel of the Neuromuscular Laboratory, Mayo Clinic, Rochester, MN, USA. The study was approved by the local IRB (IRB # 1278-03). Patients' consent was acquired according to the Declaration of Helsinki (BMJ 1991; 302: 1194). None of the five sIBM patients had received prior immunomodulating therapy. The diagnosis of definitive sIBM was made by Dr. Engel according to published criteria, including visualization of congophilic deposits in Congo-red stained sections viewed under rhodamine optics. Three individuals who had clinically presented with non-specific myalgia, but whose serum creatine kinase values and diagnostic biopsy findings were normal served as controls (C1-3) and were kindly provided by Professor Dr. Hanns Lochmüller of the Institute of Human Genetics, Newcastle University, International Centre for Life, Newcastle upon Tyne, NE1 3BZ, United Kingdom. C-1 had a clinically silent leukocytosis with elevated C-reactive protein levels at the time of biopsy.

For the third part of this thesis, i.e. analysis of the expression of RER1 in sIBM and other myopathies, all muscle biopsy material was kindly provided by Dr. Andrew G. Engel, except for three healthy controls mentioned above which were provided by Dr. Hanns Lochmüller. All muscle blocks were stored at -80° C at all times. **Table 3.1** provides a summary of all patient and control samples.

Patient ID	Source	Diagnosis	Sub-project
10804 = C1	H.L.	Healthy control	4.2, 4.3
12701 = C2	H.L.	Healthy control	4.2, 4.3
19400 = C3	H.L.	Healthy control	4.2, 4.3
20059	A.G.E.	Healthy control	4.3
20239	A.G.E.	Healthy control	4.3
20350	A.G.E.	Healthy control	4.3
20387	A.G.E.	Healthy control	4.3
21545	A.G.E.	Healthy control	4.3
15701	A.G.E.	Polymyositis	4.3
16288	A.G.E.	Polymyositis	4.3
17936	A.G.E.	Polymyositis	4.3
16093	A.G.E.	Polymyositis	4.3
15876	A.G.E.	Polymyositis	4.3
18495	A.G.E.	Polymyositis	4.3
16825	A.G.E.	Polymyositis	4.3
17336	A.G.E.	Polymyositis/ Inclusion body myositis	4.3
16646	A.G.E.	Polymyositis/ Inclusion body myositis	4.3
18747	A.G.E.	Polymyositis/ Inclusion body myositis	4.3
19116 =	A.G.E.	Inclusion body myositis	4.2, 4.3
18592 =	A.G.E.	Inclusion body myositis	4.2, 4.3
19142 =	A.G.E.	Inclusion body myositis	4.2, 4.3
14715 =	A.G.E.	Inclusion body myositis	4.2, 4.3
13515 =	A.G.E.	Inclusion body myositis	4.2, 4.3
27453	A.G.E.	Inclusion body myositis	4.3
27525	A.G.E.	Inclusion body myositis	4.3
27464	A.G.E.	Inclusion body myositis	4.3
27433	A.G.E.	Inclusion body myositis	4.3
15551	A.G.E.	Inclusion body myositis	4.3
20424	A.G.E.	Dermatomyositis	4.3
20589	A.G.E.	Dermatomyositis	4.3
20647	A.G.E.	Dermatomyositis	4.3
21708	A.G.E.	Myofibrillar myopathy	4.3
23697	A.G.E.	Myofibrillar myopathy	4.3
22874	A.G.E.	Myofibrillar myopathy	4.3
22208	A.G.E.	Duchenne muscular dystrophy	4.3
20542	A.G.E.	Duchenne muscular dystrophy	4.3

Table 3.1: Patient and control muscle biopsy samples used for this PhD thesis. For each patient, the respective patient ID is listed along with the source (Andrew G. Engel or Hanns Lochmüller), diagnosis, and respective result section in this PhD thesis.

Table 3.2 provides an overview over the number of patients and disease groups included in the RER1 expression analysis project.

Disease	Patient ID	Disease	Patient ID
Healthy controls	10804	IBM	19116
	12701		18592
	19400		19142
	20059		14715
	20239		13515
	20350		27453
	20387		27525
	21545		27464
PM	15701		15551
	16093		DM
	15876	20589	
	16288	24716	
	17936	MFM	23697
	18495		22874
PM/ IBM	17336	DMD	22208
	16646		20542
	18747		

Table 3.2: Patients and healthy controls included in the RER1 expression study. RER1 protein expression was analysed via confocal microscopy and blinded scoring in 8 healthy controls, 6 patients with polymyositis (PM), 9 patients with inclusion body myositis (IBM), 3 patients with 4 patients with dermatomyositis (DM), 2 patients with myofibrillar myopathy (MFM), and 2 patients with Duchenne muscular dystrophy (DMD).

3.2 Materials

3.2.1 Consumables

Consumable materials such as pipette tips, reaction tubes, and centrifuge tubes were purchased from Biozym (Hess, Oldendorf, Germany), Eppendorf (Hamburg, Germany) and Becton

Dickinson. If required, specially made sterile pipette tips and reaction tubes made from polypropylene (Biozym, Germany) were used in order to minimize adsorption of nucleic acids and proteins to the wall of the reaction tube.

3.2.2 TaqMan quantitative PCR primers and probes

Table 3.3 provides an overview of the primers and probes used for TaqMan qPCR.

Gene	TaqMan qPCR Primers/Probes
HLA-A	Forward: 5'-CTGAGATGGGAGCTGTCTTC -3'
	Reverse: 5'-CTATCTGAGCTCTTCCTCCT-3'
	Probe: 5'-FAM-GTAAAGTGTGAGACAGCTGCCTTG-TAMRA-3'
HLA-B	Forward: 5'-CTGAGATGGGAGCCGTCTT-3'
	Reverse: 5'-CTCCTTTTCCACCTGAACTC -3'
	Probe: 5'-FAM-GAGCTTGAAAAGCCTGAGAGAGC-TAMRA-3'
HLA-C	Forward: 5'-GAGCTGGGAGCCATCTTCC-3'
	Reverse: 5'-CTGTTGCTGCACGCAGCCT-3'
	Probe: 5'-FAM-CCATCATGGGCATCGTTGCTGG-TAMRA-3'
HLA-E	Forward: 5'-GTCACCCTGAGATGGAAGC-3'
	Reverse: 5'-CTTGGATCTGTGGTCTCTGG-3'
	Probe: 5'-FAM-CCATCGTGGGCATCATTGCTGG-TAMRA-3'
HLA-F	Forward: 5'-CCTCAAAGGCACACGTTG-3'
	Reverse: 5'-GATAGAAACAGAGGGAGCTAC-3'
	Probe: 5'-FAM-CAAGACACACGTGACCCACCAC-TAMRA-3'

Table 3.3: TaqMan quantitative PCR primers and probes (continued on next two pages). Forward and reverse primers, and FAM/TAMRA-labeled probes are listed. All primer-/probesets where the sequence is provided were designed by the author, with the exceptions of ¹IFNGR1 (Wang et al., 2008) and ²CIITA (Buttice et al., 2006). The primer-/probesets for CCL5, STAT3, CXCL9, CXCL10 and RER1 were ordered ready-to-use from Applied Biosystems, in which case the Assay ID is provided (the recommended primer-/probeset was ordered in each case, as indicated by the ending “_m1*”). The internal controls PPIA and GAPDH were ordered ready-to-use from Applied Biosystems as well.

HLA-G	Forward: 5'-CCACAGATACCTGGAGAACG-3'
	Reverse: 5'-GATCATACTGACCTGGCAGC-3'
	Probe: 5'-FAM-CAAGACACACGTGACCCACCAC-TAMRA -3'
IFNGR1 ¹	Forward: 5'-CATCACGTCATACCAGCCATTT -3'
	Reverse: 5'-CTGGATTGTCTTCGGTATGCAT-3'
	Probe: 5'-FAM-GGTCTGTGAAGAGCCGTTGTCTC-TAMRA-3'
IFNGR2	Forward: 5'-CCACCAAGCATCCCATTACA -3'
	Reverse: 5'-CCTTGGACAAGGACAGCTC-3'
	Probe: 5'-GACCCAACTCAGCCCATCTTAGA-3'
STAT1	Forward: 5'-GAGCAGGTTCCACCAGCTTTATG -3'
	Reverse: 5'-GAAAACGGATGGTGGCAAATG-3'
	Probe: 5'-FAM-CAAGACTGGGAGCACGCTGCCAA-TAMRA
CIITA ²	Forward: 5'-ACGCCCTGCTGGGTCC
	Reverse: 5'-AACTCCATGGTGGCACACTG
	Probe: 5'-FAM-ACCTGTGACAGCCCCAAGGCAGC-TAMRA-3'
PSMB8	Forward: 5'-GTCCTACATTAGTGCCTTACG -3'
	Reverse: 5'-GATAGTACAGCCTGCATTCC-3'
	Probe: 5'-FAM-GCTGTGCAGACTGTCAGTAC-TAMRA-3'
HLA-DRA	Forward: 5'-GGCTTGGATGAGCCTCTTC-3'
	Reverse: 5'-GGACCATCTTCATCATCAAGG-3'
	Probe: 5'-FAM-CAAGCACTGGGAGTTTGATGCTC-TAMRA-3'
HLA-DRB	Forward: 5'-GGAGAGGTTTACACCTGCC-3'
	Reverse: 5'-GCAAGATGCTGAGTGGAGTC-3'
	Probe: 5'-FAM-GAATGGAGAGCACGGTCTGAATC-TAMRA-3'
HLA-DPA	Forward: 5'-CACAAGTTCCATTACCTGACC-3'
	Reverse: 5'-GAGCAAGAAAGTTCAACGAGG-3'
	Probe: 5'-CTTCTATGACTGCAGGGTGGAGC-3'

Table 3.3: TaqMan quantitative PCR primers and probes (*continued*).

HLA-DPB	Forward: 5'-GGAGTGGGAAGGCACAGTCT-3'
	Reverse: 5'-GAGCAAGAAAGTTCAACGAGG-3'
	Probe: 5'-CGGAGTAAGACATTGACGGGAGC-3'
HLA-DQA	Forward: 5'-CACCAAGGGCCATTGTGAAT-3'
	Reverse: 5'-CCAGAGAATAGTGCTAGGTC-3'
	Probe: 5'-FAM-CCATCTACAGGAGCAGAAGAATGG-TAMRA-3'
HLA-DQB	Forward: 5'-CCAGAGCAAGATGCTGAGTG-3'
	Reverse: 5'-GTGCAGAAGCCCTTTCTGAC-3'
	Probe: 5'-FAM-GGCTGGGCCTTATCATCCGTCAA-TAMRA-3'
CCL5	Applied Biosystems Assay ID Hs00174575_m1*
STAT3	Applied Biosystems Assay ID Hs01047580_m1*
CXCL9	Applied Biosystems Assay ID Hs00171065_m1*
CXCL10	Applied Biosystems Assay ID Hs00171042_m1*
RER1	Applied Biosystems Assay ID Hs00199824_m1*
PPIA	Applied Biosystems #4333763
GAPDH	Applied Biosystems #4333764

Table 3.3: TaqMan quantitative PCR primers and probes (*continued*).

3.2.3 Buffers and solutions

Name	Reagents		Manufacturer
6x DNA-Buffer:	50 %	Glycerin	Merck (Darmstadt, GER)
	0,02 %	Bromphenole blue	Sigma-Aldrich (Steinheim, GER)
		Xylencyanole FF	Bio-Rad
	0,02 %	Tris	Sigma-Aldrich
	10 mM	H ₂ O	
10x PBS:	1,5 M	NaCl	Merck
	84 mM	Na ₂ HPO ₄	Merck
	19 mM	NaH ₂ PO ₄ H ₂ O	Merck
DEPC-H₂O:	0,1 % DEPC (Sigma-Aldrich) dissolved in H ₂ O overnight, and autoclaved.		

Table 3.4: Buffers and solutions.

3.2.4 Antibodies

Mouse-anti-human CD8 α antibody clone LT8 (Serotec, Oxford, United Kingdom), which had previously been labeled with the Cy3-mAb Labeling Kit (GE/Amersham, Freiburg, Germany) was used at 2 μ g/ml. Mouse-anti-human HLA-ABC antibody clone W6/32 (directly labeled with Alexa-488 by the manufacturer, AbD Serotec, Düsseldorf, Germany) was used at 0.5 μ g/ml. Rabbit-anti-human IFNGR2 antibody, polyclonal (Sigma, Deisenhofen, Germany), was used at 1.6 μ g/ml with a goat-anti-rabbit Alexa-594-labeled secondary antibody (Invitrogen) at 4 μ g/ml. Unlabeled mouse-anti-human CD8 α antibody clone LT8 (Serotec, dilution 10 μ g/ml) was used in conjunction with a secondary goat-anti-mouse Alexa488-labeled antibody (Invitrogen, dilution 2 μ g/ml). To assess RER1 expression, Rabbit-anti-human RER1 antibody, polyclonal (Sigma) was used at 1.6 μ g/ml with a goat-anti-rabbit Alexa-594-labeled secondary antibody (Invitrogen, order no. A-11037) at 4 μ g/ml. For negative controls, isotype-matched IgGs (mouse-IgG1, BD Pharmingen; mouse IgG2a, AbD Serotec) were used for monoclonal antibodies, and purified rabbit IgG (IgG from rabbit serum, Sigma) were used for polyclonal antibodies.

3.2.5 Reaction kits and special reagent solutions

Product name	Manufacturer	Used for
10x PCR buffer	Roche (Mannheim, GER)	PCR
Cy3 TM mAb Labelling Kit	Amersham (Freiburg, GER)	Cy3 TM -Labelling of antibodies
dNTP-Mix (10 mM)	Qiagen	PCR
Easy Pure [®] DNA-Purification Kit	Biozym	DNA isolation from agarose gel
EB-buffer	Qiagen	DNA experiments
Fluorescent Mounting Medium	Dako	Immunohistochemistry
Protector RNase Inhibitor	Roche	Laser microdissection
TRIzol LS reagent	Invitrogen	RNA analysis Laser microdissection
Glycogen	Sigma Aldrich	RNA analysis
Trichlormethan	Merck	RNA analysis
QIAquick PCR-Purification Kit	Qiagen	Purification of PCR products
RNA 6000 Pico Assay Reagent Kit	Agilent	RNA Quality control
Taq-DNA-Polymerase (5 U/ μ L)	Roche	PCR
ExpressArt kit (<i>pico</i> Version)	AmpTec GmbH, Hamburg, GER	Linear transcriptome amplification

Table 3.5: Reaction kits.

3.2.6 Cells and cell culture material

Cell line	Cell type	Supplier
Jurkat	Human lymphoma	ATCC
TE671	Human rhabdomyosarcoma	ATCC

Table 3.6: Human cell lines.

Reagent	Supplier
RPMI1640	Invitrogen
L-Glutamin	Invitrogen
Fetal calf serum	PAA Laboratories GmbH
Penicillin/Streptomycin	Invitrogen
MEM Non-essential aminoacids	Invitrogen
MEM Sodium pyruvate 100mM	Invitrogen
1x PBS (CaCl ₂ , MgCl ₂)	Invitrogen
Trypsin/ EDTA	Invitrogen
Propidium iodide	Sigma Aldrich
Trypane blue solution	Sigma Aldrich

Table 3.7: Cell culture reagents.

3.2.7 Instruments

Bioanalyzer	Agilent Bioanalyzer	Agilent, Palo Alto, CA, USA
Cryostat:	LEICA CM 3050	Leica Microsystems (Wetzlar, GER)
Agarose gel electrophoresis:	LKB ECPS 3000/150	Pharmacia Biotech (Munich, GER)
	Gel camera Universal Hood	Bio-Rad (Hercules, USA)
	UV-Transilluminator	Bachofer (Reutlingen, GER)
Thermomixer:	Thermomixer Comfort	Eppendorf (Hamburg, GER)
Magnetic stirrer:	Ikamag RCT	IKA® (Staufen, GER)
Microscopes:	Mikroskop Axioplan 2	Zeiss (Jena, GER)
	Mikroskop Axiovert 200M	Zeiss
	Robo-Mover	Microlaser Technologies (Munich)
	SP2 UV Confocal microscope	Leica
PCR machines:	GeneAmp PCR System 9600	Perkin Elmer (Wellesley, USA)
	T3 Thermocycler	Biometra (Göttingen, GER)
	T personal Thermocycler	Biometra
	Mastercycler 5333	Eppendorf
	TaqMan 5700	Applied Biosystems
	TaqMan 7900	Applied Biosystems
pH-Meter:	pH 521	Bruno Kummer (Freiburg, GER)
Photometer:	Nanodrop ND-1000	Thermo Fisher Scientific (MA, USA)
RNA Quality control:	2100 Bioanalyzer	Agilent (Santa Clara, USA)
Water purification:	Milli Q Biocel	Millipore (Champigneulles, FR)
Mixer:	Vortex Genie 2	Scientific Industries (NY, USA)
Centrifuges:	Centrifuge 5417 R	Eppendorf
	Megafuge 1.0 R	Heraeus

3.3 Methods

3.3.1 Frozen tissue cryosectioning

After thorough cleaning of the cryostat with 80% Ethanol and “RNase ZAP” to ensure RNase-free conditions, the biopsy blocks were embedded in “Tissue-Tek” medium (Sakura Finetek Europe B.V.) and the position of the biopsy block was adjusted according to the cutting conditions. Thereafter, 10 µm thick sections were cut, transferred to “superfrost plus” glass slides (VWR GmbH) and immediately stored on dry ice. After completion of the cryosectioning, all newly cut sections were stored at -80°C. For later laser microdissection, a special type of membrane-covered glass slides was used (Membrane Slide 1.0 PET P.A.L.M. Microlaser Technologies GmbH). All tissue was stored at -80°C before and after cryosectioning.

3.3.2 Pre-treatment of glass slides for subsequent laser microdissection of single cells

For isolation of single cells from muscle biopsies of sIBM patients and non-diseased controls, 10 µm thick cryosections were prepared as described in 3.3.5. The membrane-covered slides had to be pre-treated in order to ensure a better adhesion of the tissue to the slide.

The slides were thus baked at 180°C for 4 h 30 min. After cooling to room temperature, the slides were irradiated with ultraviolet (UV) light in an RNase-free hood for 30 min. Thereafter, 100 µl of “Poly-L-Lysine Hydrobromide” (Sigma) were dispersed across each membrane-covered glass slide. The slides were then incubated for 1 h in a wet chamber. Lastly, the slides were rinsed with DEPC-H₂O and air-dried. Afterwards, the slides were UV-irradiated once more under an RNase-free hood as described above. After the described pre-treatment, slides could be stored for several weeks until used.

3.3.3 Fluorescence labelling of antibodies

Since the mouse-anti-human CD8 antibody (clone LT8) was not available with an applicable fluorescent labelling, the “Cy3 mAb Labelling Kit“ was used to manually conjugate the antibody with the fluorescent dye Cy3TM prior to staining. An isotype control (mouse monoclonal IgG1) of the same concentration was Cy3TM-conjugated in a parallel setup.

The antibody was diluted to a concentration of 1mg/ml in PBS. 5µl of coupling buffer were added per 100µl of antibody solution and mixed thoroughly by vortexing for about 30s. Next, the entire antibody-coupling buffer-mix was transferred to the vial containing the reactive dye and gently mixed by pipetting up and down, taking care to avoid foaming. The solution was then incubated for 30min at RT, with additional mixing every ten minutes.

The gel filtration column was equilibrated with 3 ml fresh elution buffer for 30 min. Thereafter, the antibody-coupling buffer-dye mixture was added to the gel filtration column with two times 1.1 ml elution buffer. The labeled antibody (visualized as a pink band descending the column) was collected into a fresh collection tube.

3.3.4 Basic principles of immunofluorescence imaging

Immunofluorescence imaging is a central method for this work and shall be discussed in more detail here. Immunofluorescence microscopy enables researchers to specifically visualize macromolecules present within cultured cells or, as in this case, tissue sections. Compared to immunohistochemistry, immunofluorescence results in a much lower background, i.e. much less non-specific staining.

Indirect immunofluorescence microscopy uses a primary antibody which is unlabelled. Thereafter, a secondary antibody is used, which is covalently conjugated with a fluorescent dye (e.g. fluoresceine-isothiocyanate (FITC), or Cy3TM, or Alexa488). This fluorescent dye is later detected through excitation of the tissue at a specific excitation wavelength, and detection of a specific emission wavelength. The advantage of indirect immunofluorescence lies in the potentiation of the fluorescence intensity, which stems from several secondary antibodies binding to one primary antibody. A disadvantage is that the protocol requires more washing and

incubation steps, and thus is of longer duration compared to direct immunofluorescence microscopy, which can become a problem if RNA preservation is an issue. One more disadvantage is that more chemicals are required, thus further increasing the risk of contamination.

Direct immunofluorescence technique employs primary antibodies which are covalently conjugated with an immunofluorescent dye (e.g. Cy3TM). This technique does not require a secondary antibody and allows for significantly shorter protocol time, which in conjunction with the smaller number of chemicals required results in a lower contamination risk.

3.3.5 Different immunofluorescence staining approaches

Different immunofluorescence approaches were established in the course of this work, depending on whether RNA preservation or maximum visualization for subsequent imaging was the primary goal. For each antibody used in this dissertation, the ideal staining conditions had to be established on test tissue. For all described immunofluorescent and confocal microscopy applications, cryosections of 10 µm thickness were prepared as described in section 3.3.1 and stored at -80°C until use.

3.3.5.1 Anti-CD8-/ Anti-HLA-ABC- double immunofluorescence staining for immunofluorescent and confocal microscopy

Cryosections were air-dried at room temperature for 10 minutes, then immediately immersed in ice-cold acetone for 5 minutes. Thereafter, 100µl PBS was pipetted onto each slide to ensure re-hydration of the tissue. Immediately thereafter, the PBS was removed and replaced with 100µl “blocking solution”, consisting of 2% purified bovine serum albumin (BSA) (B4287, Sigma, Deisenhofen, Germany) BSA in PBS. The tissue was then left to incubate in the blocking solution for 30 minutes. The blocking solution was removed and replaced with the “antibody solution” consisting of 0,5 µg/ml mouse-anti-human HLA-ABC-Alexa488 and 4 µg/ml mouse-anti-human-CD8-Cy3 in 2% BSA in PBS, and the sections were incubated with the antibody solution for another 30 minutes. The sections were then rinsed with PBS by immersion in PBS for 5 minutes three times. Thereafter, the tissue was embedded in Fluorescence mounting

medium (Dako), and covered with a glass cover slip. Imaging was performed on the same day. Biological negative controls were performed in parallel to each experiment using muscle tissue from nondiseased controls. Technical negative controls were performed in parallel to each experiment by using mouse-IgG1-Cy3 as an isotype control for mouse-anti-human-CD8-Cy3 at the same concentration, and mouse-IgG2a-Alexa 488 as an isotype control for mouse-anti-human-HLA-ABC-Alexa 488 at the same concentration, respectively.

3.3.5.2 Anti-CD8-/ Anti-HLA-ABC- double immunofluorescence staining for subsequent laser microdissection

Membrane-covered slides suitable for laser microdissection were used for the experiments described in this section. All experiments were carried out in a specifically designated room which was decontaminated by daily UV light irradiation and cleaning with RNase ZAP and 80% Ethanol before and after each experiment. Protective sterile clothing (gloves, surgical headcovers, surgical masks, labcoats, shoecovers) was worn at all times when working with RNA. Sections were mounted on PET-films (P.A.L.M. Microlaser, Bernried, Germany) that had been previously been baked at 180°C for 4h, UV-irradiated and coated with poly-L-lysine, as described in section 3.3.2. Upon taking the sections out of -80°C, sections were immediately dried in a desiccator for two minutes, then immersed in ice-cold acetone for one minute. After rehydration in phosphate-buffered saline (PBS) for 10 s the tissue was left to incubate in 100 µl “blocking solution”, consisting of 2% BSA and 3 U/ µl Protector RNase inhibitor in PBS-DEPC for three minutes. The blocking solution was removed and replaced with the “antibody solution” consisting of 0,5 µg/ml mouse-anti-human HLA-ABC-Alexa488 and 4 µg/ml mouse-anti-human-CD8-Cy3 and 2% BSA and 3 U/ µl Protector RNase inhibitor in PBS-DEPC, and the sections were incubated with the antibody solution for another 5 minutes. The sections were then rinsed by pipetting 3 ml of PBS-DEPC onto the tissue. Afterwards, 1 ml of 100% Ethanol was pipetted onto each specimen and the slides were dried in a desiccator for two minutes. Laser microdissection was performed immediately thereafter in the same room.

3.3.5.3 Anti-CD8-/ Anti-IFNGR2 - double immunofluorescence staining for subsequent confocal microscopy

After drying at room temperature for 10 minutes, cryosections immediately immersed in ice-cold 4% paraformaldehyde (PFA) for 5 minutes. Thereafter, slides were immersed in PBS three times for 5 minutes to remove PFA from the tissue. 100µl “blocking solution”, consisting of 2% BSA in PBS, were then applied to each sample and the tissue was then left to incubate in the blocking solution for 30 minutes. The blocking solution was removed and replaced with the “primary antibody solution” consisting of 10 µg/ml mouse-anti-human-CD8 and 1.6 µg/ml rabbit-anti-human-IFNGR2 in 2% BSA in PBS, and the sections were incubated with the primary antibody solution for another 30 minutes. The primary antibody solution was removed and replaced with the “secondary antibody solution” consisting of 2 µg/ml goat-anti-mouse-IgG-Alexa488 and 4 µg/ml goat-anti-rabbit-IgG-Alexa594 in 2% BSA in PBS, and the sections were incubated with the secondary antibody solution for another 20 minutes. The sections were then rinsed with PBS by immersion in PBS for 5 minutes three times. Thereafter, the tissue was embedded in Fluorescence mounting medium (Dako), and covered with a glass cover slip. Imaging was performed on the same day. Biological negative controls were performed in parallel to each experiment using muscle tissue from nondiseased controls. Technical negative controls were performed in parallel to each experiment by using mouse-IgG1 as an isotype control for mouse-anti-human-CD8 at the same concentration, and rabbit IgG as an isotype control for rabbit-anti-human-IFNGR2 at the same concentration, respectively.

3.3.5.4 Anti-CD8-/ Anti-CIITA-/ DAPI- triple immunofluorescence staining for subsequent confocal microscopy

Sections were air-dried at room temperature for 10 minutes and immersed in ice-cold 4% paraformaldehyde (PFA) for 5 minutes. Thereafter, slides were immersed in PBS three times for 5 minutes to remove PFA from the tissue. Following PFA fixation, slides were incubated in 0,01% Triton X permeabilization solution in PBS for 20 minutes to facilitate intracellular and intranuclear staining. 100µl “blocking solution”, consisting of 2% BSA in PBS, were then applied to each sample and the tissue was then left to incubate in the blocking solution for 30 minutes. The blocking solution was removed and replaced with the “primary antibody solution”

consisting of 2 µg/ml rabbit-anti-human-CIITA in 2% BSA in PBS, and 4 µg/ml mouse-anti-human-CD8-Cy3 and the sections were incubated with the primary antibody solution for another 30 minutes. The primary antibody solution was removed and sections were then rinsed with PBS by immersion in PBS for 5 minutes three times. Sections were then incubated with the “secondary antibody solution” consisting of 2 µg/ml goat-anti-rabbit-IgG-Alexa488 in 2% BSA in PBS for another 20 minutes. To visualize myofiber nuclei, DAPI (4',6-diamidino-2-phenylindole) diluted 1-1000 in PBS containing 2% BSA was added after the secondary antibody incubation time had elapsed, and the sections were incubated for another five minutes. The sections were then rinsed with PBS by immersion in PBS for 5 minutes three times. Thereafter, the tissue was embedded in Fluorescence mounting medium (Dako), and covered with a glass cover slip. Imaging was performed on the same day. Biological negative controls were performed in parallel to each experiment using muscle tissue from nondiseased controls. Technical negative controls were performed in parallel to each experiment by using mouse-IgG1-Cy3 as an isotype control for mouse-anti-human-CD8-Cy3 at the same concentration, and mouse-IgG2a as an isotype control for mouse-anti-human-CIITA at the same concentration, respectively.

3.3.5.5 Anti-CD8-/ Anti-HLA-DR/DP/DQ- double immunofluorescence staining for immunofluorescent and confocal microscopy

Cryosections were fixed in ice-cold acetone for 5 minutes after air-drying for 10 minutes. Thereafter, 100µl PBS was pipetted onto each slide to ensure re-hydration of the tissue. Immediately thereafter, the PBS was removed and replaced with 100µl “blocking solution”, consisting of 2% purified bovine serum albumin (BSA) (B4287, Sigma, Deisenhofen, Germany) BSA in PBS. The tissue was then incubated in the blocking solution for 30 minutes. The blocking solution was removed and replaced with the “antibody solution” consisting of 0,5 µg/ml mouse-anti-human HLA-DR/DP/DQ-Alexa488 and 4 µg/ml mouse-anti-human-CD8-Cy3 in 2% BSA in PBS, and the sections were incubated with the antibody solution for another 30 minutes. The sections were then rinsed with PBS by immersion in PBS for 5 minutes three times. Thereafter, the tissue was embedded in Fluorescence mounting medium (Dako), and covered with a glass cover slip. Imaging was performed on the same day. Biological negative controls were performed in parallel to each experiment using muscle tissue from nondiseased controls.

Technical negative controls were performed in parallel to each experiment by using mouse-IgG1-Cy3 as an isotype control for mouse-anti-human-CD8-Cy3 at the same concentration, and mouse-IgG2a as an isotype control for mouse-anti-human-HLA-DR/DP/DQ at the same concentration, respectively.

3.3.5.6 Anti-CD8-/ Anti-CXCL9- double immunofluorescence staining for immunofluorescent microscopy

Sections were subjected to 10 minutes acetone fixation at -20°C after air-drying at room temperature for 10 minutes. This was followed by an additional fixation step of 10 minutes in 4% PFA. Thereafter, sections were placed on top of a glass beaker containing 4% citrate buffer heated to 60°C, thus exposing the tissue to the evaporating citrate buffer. Citrate buffer exposure (“steaming”) times of 5, 10, 15, 20, 30 and 60 minutes were tried, ultimately standardizing all experiments to 20 minutes of steaming. The sections were then rinsed with PBS by immersion in PBS for 5 minutes three times. Immediately thereafter, the PBS was removed and replaced with 100 µl “blocking solution”, consisting of 2% BSA in PBS. The tissue was then left to incubate in the blocking solution for 30 minutes. The blocking solution was removed and replaced with the “primary antibody solution” consisting of 2 µg/ml mouse-anti-human CXCL9-FITC (R&D Systems, MN, USA) and 4 µg/ml mouse-anti-human-CD8-Cy3 in 2 % BSA in PBS, and the sections were incubated with the primary antibody solution for another 30 minutes. The sections were then rinsed with PBS by immersion in PBS for 5 minutes three times. Sections were then incubated with the “secondary antibody solution” consisting of 2 µg/ml goat-anti-FITC-Alexa488 in 2% BSA in PBS for another 20 minutes to enhance CXCL9 staining. The sections were then rinsed with PBS by immersion in PBS for 5 minutes three times. Thereafter, the tissue was embedded in Fluorescence mounting medium (Dako), and covered with a glass cover slip. Imaging was performed on the same day. Biological negative controls were performed in parallel to each experiment using muscle tissue from nondiseased controls. Technical negative controls were performed in parallel to each experiment by using mouse-IgG1-Cy3 as an isotype control for mouse-anti-human-CD8-Cy3 at the same concentration, and mouse-IgG1-FITC as an isotype control for mouse-anti-human-CXCL9-FITC at the same concentration, respectively. **Table 3.8** summarizes the protocol.

Protocol step	Time
Thawing of tissue cryosections at room temperature	10 min
Acetone fixation at -20°C	10 min
Additional fixation in 4% Paraformaldehyde at 4° C	10 min
<i>Steaming in citrate buffer at 95° C</i>	<i>Up to 60 min</i>
Three times washing in PBS (5 minutes each time)	15 min
Blocking of non-specific binding sites with 2% BSA in PBS	15 min
Incubation with primary antibody	40 min
Three times washing in PBS (5 minutes each time)	15 min
Incubation with secondary antibody	15 min
Three times washing in PBS (5 minutes each time)	15 min

Table 3.8: Immunofluorescence staining protocol for the detection of chemokines in muscle biopsy cryosections. including steaming in citrate buffer, intended for the detection of small, soluble proteins (e.g. chemokines) in cryosectioned tissue. (Bradl M and Lassmann H, personal communication).

3.3.5.7 Anti-CD8-/ Anti-CXCR3- double immunofluorescence staining for immunofluorescent microscopy

Upon removal from -80°C, sections were air-dried at room temperature for 10 minutes, then immediately immersed in ice-cold acetone for 5 minutes. Thereafter, 100µl PBS was pipetted onto each slide to ensure re-hydration of the tissue. Immediately thereafter, the PBS was removed and replaced with 100µl “blocking solution”, consisting of 2% purified bovine serum albumin (BSA) (B4287, Sigma, Deisenhofen, Germany) BSA in PBS. The tissue was then left to incubate in the blocking solution for 30 minutes. The blocking solution was removed and replaced with the “antibody solution” consisting of 1 µg/ml mouse-anti-human CXCR3-Alexa488 and 4 µg/ml mouse-anti-human-CD8-Cy3 in 2% BSA in PBS, and the sections were incubated with the antibody solution for another 30 minutes. The sections were then rinsed with PBS by immersion in PBS for 5 minutes three times. Thereafter, the tissue was embedded in Fluorescence mounting medium (Dako), and covered with a glass cover slip. Imaging was

performed on the same day. Biological negative controls were performed in parallel to each experiment using muscle tissue from nondiseased controls. Technical negative controls were performed in parallel to each experiment by using mouse-IgG1-Cy3 as an isotype control for mouse-anti-human-CD8-Cy3 at the same concentration, and mouse-IgG2a-Alexa 488 as an isotype control for mouse-anti-human-CXCR3-Alexa 488 at the same concentration, respectively.

3.3.5.8 Anti-RER1/ DAPI - double immunofluorescence staining for subsequent confocal microscopy

After 10 min of air-drying at room temperature, sections were immersed in 100% methanol for 10 minutes at -20°C. Thereafter, a post-fixation step followed, incubating the slides in a 1:1 methanol-acetone solution at -20°C for 10 minutes. Slides were then immersed in PBS three times for 5 minutes to remove the methanol/acetone from the tissue. 100µl “blocking solution”, consisting of 2% BSA in PBS, were then applied to each sample and the tissue was then left to incubate in the blocking solution for 30 minutes. The blocking solution was removed and replaced with the “primary antibody solution” consisting of 1.6 µg/ml rabbit-anti-human-RER1 antibody in 2% BSA in PBS, and the sections were incubated for another 25 minutes. The primary antibody solution was removed and the sections were then rinsed with PBS by immersion in PBS for 5 minutes three times. Sections were then incubated with the “secondary antibody solution” consisting of 4 µg/ml goat-anti-rabbit-IgG-Alexa594 in 2% BSA in PBS, and the sections were incubated with the secondary antibody solution for another 20 minutes. To visualize myofiber nuclei, DAPI (4',6-diamidino-2-phenylindole) diluted 1-1000 in PBS containing 2% BSA was added after the secondary antibody incubation time had elapsed, and the sections were incubated for another five minutes. The sections were then rinsed with PBS by immersion in PBS for 5 minutes three times. Thereafter, the tissue was embedded in Fluorescence mounting medium (Dako), and covered with a glass cover slip. Imaging was performed on the same day. Biological negative controls were performed in parallel to each experiment using muscle tissue from nondiseased controls. Technical negative controls were performed in parallel to each experiment by rabbit IgG as an isotype control for rabbit-anti-human-RER1 at the same concentration, respectively. The protocol is summarized in **Table 3.9**.

Protocol step	Time
Thawing of tissue cryosections at room temperature	10 min
Methanol fixation at -20°C	10 min
Post-Fixation in a 1:1 Methanol-Acetone solution at -20°C	10 min
Washing with PBS (three times 5 min)	15 min
Blocking of non-specific binding sites with 2% BSA in PBS	30 min
Incubation with anti-RER1 antibody	25 min
Washing with PBS (three times 5 min)	15 min
Incubation with goat-anti-rabbit-Alexa594 antibody	20 min
Incubation with DAPI	1 min
Washing with PBS (three times 5 min)	15 min
TOTAL STAINING TIME	~ 2.5 hours

Table 3.9 RER1 staining protocol. Since this protocol was primarily intended for RER1 visualization using confocal microscopy, and no RNA preservation was required, there was no need to employ minimal incubation times, or the other measures described in section 4.1. DAPI was included in the protocol to visualize nuclear staining. The fixation had to be carried out in methanol, including a post-fixation in a 1:1 methanol:acetone mixture. The slides were embedded in mounting medium immediately upon completion of the last washing step, and confocal microscopy was performed on the same day.

3.3.6 Image acquisition

3.3.6.1 Immunofluorescence imaging

For immunofluorescence imaging, a Zeiss Axiovert 200 M inverted microscope with fluorescence / phase or DIC (Nomarski) imaging was used. The filter sets used in this dissertation were Dapi, GFP, Texas Red and bright field. The microscope contained 10X, 20X, 40X and 63X high chromatic correction objectives.

Filter characteristics were as follows:

DAPI: Chroma set 31000V2, Excitation 325-375 nm, Emission 435-485 nm (bandpass filter).

GFP: Chroma set 41001, Excitation 460-500 nm, Emission 510-560 nm (bandpass filter).

Texas Red: Chroma set 41004, Excitation 530-580 nm, Emission 610-680 nm (bandpass filter).

Zeiss AxioVision LE software was used to analyze and overlay the images.

3.3.6.2 Confocal imaging

For confocal laser microscopy, a Leica TCS SP2 UV system was used. Excitation laser wavelengths used were 488 nm (Argon-Krypton laser) and 594 nm (Helium Neon laser), depending on the staining. For the detection of DAPI, a diode laser with an excitation wavelength of 405nm was used. Accompanying software used was the LCS Lite confocal software from Leica. Stacked series of confocal single z-planes were taken with a step size of 1µm to cover the full thickness of the tissue section. Sections were imaged with a pinhole of 1.0 Airy units, 512 x 512 pixel image format and four frame averages. Simultaneous image acquisition of samples stained with multiple dyes can result in crosstalk since all dyes will be excited at the same time. To avoid cross-talk of the various fluorochromes, the width of the detection channels and filter settings were carefully controlled, and images for Alexa Fluor 488, Alexa Fluor 594 and DAPI were acquired using sequential image recording. Hardware and software settings were assigned to each subproject and used continuously without further modifications.

3.3.7 Laser microdissection

A laser microdissection protocol similar to a previously published method (Junker et al., 2007) was used. 10 µm cryostat sections were prepared as described in sections 3.3.1 and 3.3.2 from muscle biopsy specimens of patients IBM-1 to IBM-5 and healthy controls C-1, C-2 and C-3. The sections were double-stained for CD8α and HLA-ABC as described in section 3.3.5. The tissue was then rinsed with PBS and immediately imaged at a P.A.L.M Microbeam-Z

microscope. A myofiber was defined as being attacked when at least three CD8⁺ T cells were clearly adhering to the myofiber, or at least one CD8⁺ T cell was invading the fiber. Fibers that were surrounded and superficially invaded by inflammatory cells were preferentially sampled. Fibers that were deeply invaded were avoided in order to minimize contamination of the myofiber transcriptome. A non-attacked myofiber was defined as such if no CD8⁺ T-cells could be seen in the proximity (**Figure 4.7 A, B**). “Intermediate” myofibers not corresponding to either category were not sampled. The fibers were dissected from transversally cut biopsy sections. When dissecting the myofiber content, a “safety margin” was left, avoiding contamination with surrounding and superficially invading immune cells (**Figure 4.7 C, D**). The specimens were evaluated within 10 min after staining for attacked and non-attacked myofibers. Qualifying myofibers were then marked electronically and subsequently microdissected and laser pressure catapulted into respective reaction tubes (either attacked or non-attacked) containing 20 µl Trizol. The reaction tubes were then immediately stored on dry ice. Because of a strong variability in myofiber diameter typically seen in sIBM, equal areas rather than equal numbers of myofibers were sampled. The area of each collected myofiber (automatically calculated by the P.A.L.M. software) was recorded, and a total of 100.000 µm² myofiber area was collected from each sIBM patient (attacked and non-attacked, respectively) and each control subject. The dried sections were assessed for artifacts by comparison with embedded tissue stained under the same conditions (embedded with Fluorescent Mounting Medium (Dako, DK-2600 Glostrup, Denmark)) to minimize contamination of the microdissected myofiber samples with T cells and macrophages. Potential contamination risk was further minimized by analyzing the microarray datasets for the expression of lymphocyte-, monocyte- and macrophage-specific transcripts (**Table 4.4**).

3.3.8 RNA Isolation

3.3.8.1 RNA isolation from cryosectioned biopsy material

Prior to enrolling a patient or control biopsy sample in a project (section 4.2, section 4.3), the baseline RNA quality was assessed in order to exclude potential samples which had suffered from RNA degradation (e.g. resulting from improper storage).

Tissue cryosections were prepared as described in section 3.3.1, however, instead of being spread out on glass slides, around 20 sections of 10 μm thickness, respectively, were collected in a 2 ml reaction tube. TRIzol LS reagent was immediately added to the freshly sectioned tissue, and the samples were stored at -80°C until further use if RNA isolation did not occur immediately thereafter.

RNA isolation was performed under a sterile workbench. All experiments were carried out in a specifically designated room which was decontaminated by daily UV light irradiation and cleaning all surfaces and instruments with RNase ZAP and 80% Ethanol before and after each experiment. Protective sterile clothing (gloves, surgical headcovers, surgical masks, labcoats, shoecovers) was worn at all times when working with RNA. The samples were equilibrated to room temperature, and resuspended in the TRIzol LS reagent until completely dissolved to ensure lysis of the tissue components. After adding 200 μl Trichlormethane the samples were shaken by hand for 15 s, then incubated at room temperature for 5 min. After centrifugation using the centrifuge 5417 R at 4°C and 14.000 rpm (20.800 g) for 15 min, phase separation occurred, with RNA being in the upper, transparent phase, and DNA being in the lower, pink phase. The upper phase was collected and transferred into fresh tubes. 10 μl Glycogen were immediately added and RNA was precipitated by adding 700 μl 70% Isopropanole, incubation for 20 min, and subsequent centrifugation for 20 min at 4°C and 14.000 rpm. After washing of the RNA-pellet with 1 ml 80% Ethanol, and centrifugation for 5 min at 4°C and 14.000 rpm, the pellet was air-dried. Lastly, RNA was dissolved in 22 μl DEPC- H_2O (Invitrogen) and stored at -20°C until use.

3.3.8.2 RNA isolation from laser microdissected cells

Upon collecting 100,000 μm^2 of each subgroup of myofibers, the samples were pooled according to their classification (see section 4.2). RNA was then isolated using the Trizol method (section 3.3.8.1), with the following modifications as recommended by the linear amplification protocol: 1 μl of N-carrier was added to each Trizol sample, and 1 μl of P-carrier was added to each isopropanol precipitation reaction to improve RNA yield. 0.1 volume units of 3 M sodium acetate and 1 μl of P-carrier were added to each aqueous RNA solution before ethanol precipitation, and the solution was incubated on ice for 10min before RNA recovery. After centrifugation and air-drying as described in section 3.3.8.1, the RNA pellet was dissolved in 6 μl DEPC- H_2O .

3.3.9 RNA quality control using the Agilent Bioanalyzer

The 2100 Bioanalyzer from Agilent Biotechnologies was used along with the “RNA 6000 Pico Assay” Kit to determine RNA quality in muscle biopsy samples. RNA was isolated as described in section 3.3.8.1. RNA samples were diluted 1:10 in DEPC- H_2O (Invitrogen) and denatured for 2 min at 70°C, then immediately stored on ice. The “RNA Ladder” a molecular mass standard provided by Agilent Biotechnologies, was heat denatured and aliquotted prior to use in the same fashion as the samples. Electrodes were cleaned according to the manufacturer’s recommendations before and after each electrophoresis run. The electrode cleaner chip was filled with 350 μl RNase-free water and placed in the Agilent 2100 bioanalyzer. The electrodes were incubated in the RNase-free water for 5 minutes, then air-dried by leaving the lid open for 30 seconds. To prepare the gel, all kit components were equilibrated to room temperature for 30 minutes. Thereafter, 550 μl RNA 6000 Pico gel matrix were pipetted into a spin filter and centrifuged at 4000 rpm for 10 minutes. The filtered gel was subsequently aliquotted in samples of 65 μl . The aliquots were immediately used or stored at 4°C for up to one month. To prepare the gel-dye mix, the vial containing the RNA 6000 Pico dye concentrate was vortexed for several seconds, following quick centrifugation to spin down the dye. 1 μl of dye was then added to 65 μl of filtered gel. The gel-dye mixture was then vortexed for several seconds and subsequently centrifuged at room temperature and 14000 rpm for 10 minutes. The gel-dye mix was then loaded into the wells designated “G” on the RNA 6000 Pico Chip. The chip was then placed inside the chip priming station and the plunger was pushed from 1 ml until held by the clip. After

30 seconds, the clip was released. RNA 6000 Conditioning solution and RNA 6000 Pico Marker were then added to the respective, appropriately marked wells. 1 μ l of the denatured RNA sample (or RNA Ladder, respectively) was then loaded into the designated wells. After loading of all wells was finished, the chip was placed into the vortex mixer and vortexed at 2000 rpm for 2 minutes. Immediately thereafter, the chip was placed into the bioanalyzer device and the run was started. Data analysis was performed using the software “Agilent Technologies 2100 Bioanalyzer 2100 Expert, VB.02.06.SI418” from Agilent Biotechnologies.

Using the Bioanalyzer, RNA can be separated according to molecular mass (comparable to a traditional agarose gel electrophoresis for DNA). In the case of the Bioanalyzer, the Gel is located inside a 4x4cm chip (**Figure 3.1**).

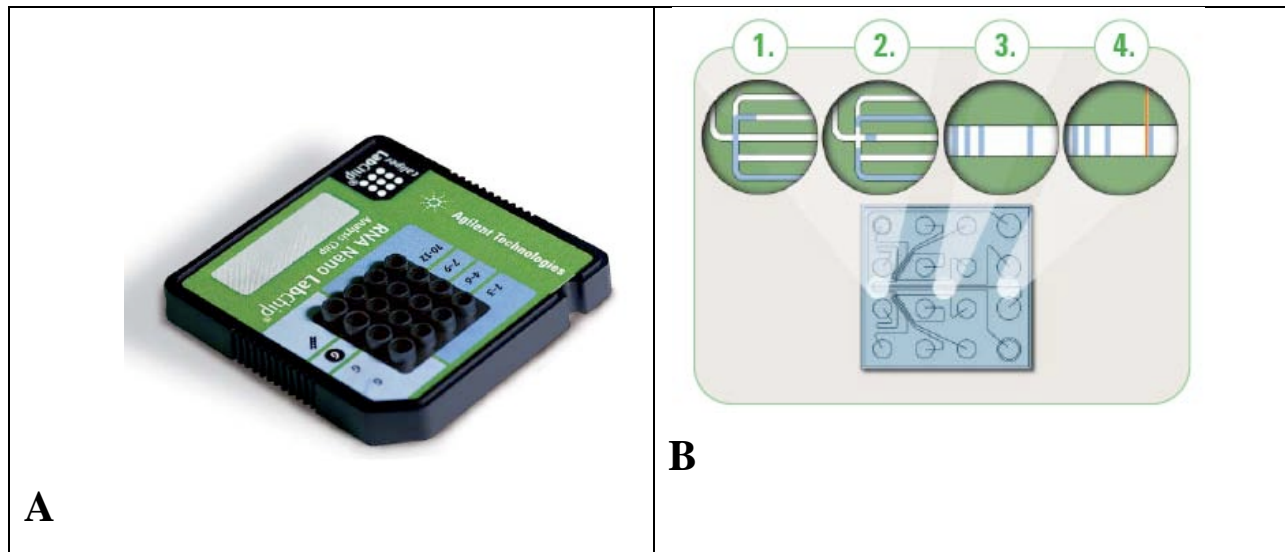


Figure 3.1: Agilent Bioanalyzer RNA-Chip. The chip contains 12 wells, suitable for 11 samples and a “ladder” (molecular mass standard) (A). The analysis is performed in four steps (B): 1. The sample moves from the well through the microchannels; 2. The sample is transferred into the separation channel; 3. Electrophoretic separation of the RNA sample components; 4. Detection of the sample components using a fluorescent dye, generation of gel-like images (bands) and electropherograms (peaks). Source: Agilent Technologies.

Figure 3.2 shows an exemplified analysis of total RNA from tissue (source: Agilent Technologies).

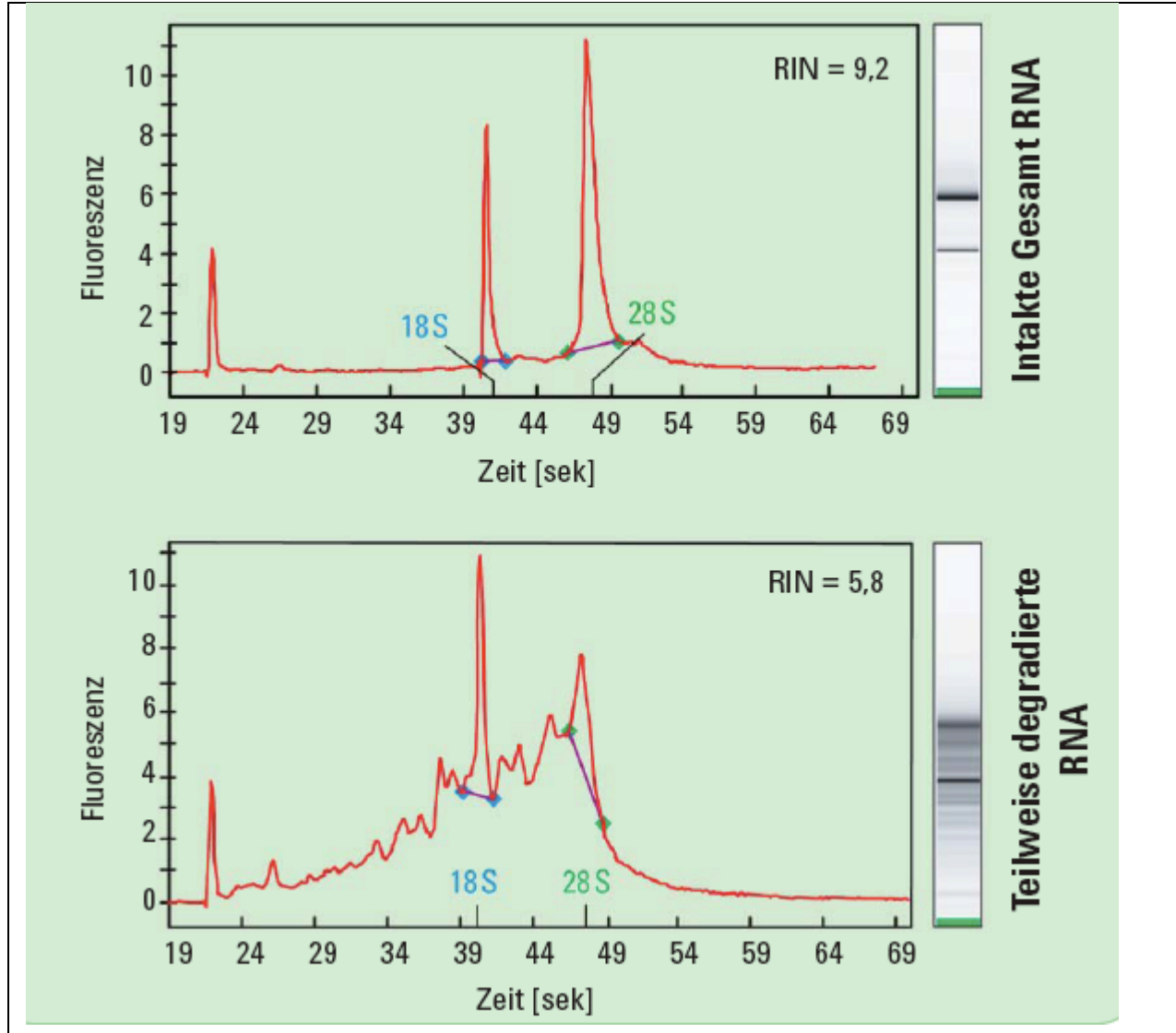


Figure 3.2: Analysis of total RNA using the 2100 Bioanalyzer (source: Agilent Technologies). The electrophoretic separation described in Figure 3.3 B results in electrophoretically separated bands (right) and electropherogram peaks (left). If RNA is preserved (upper panel), two bands can be sharply delineated in the gel-like image: the 18S- and the 28S-RNA, presenting as two distinct peaks in the electropherogram. If RNA is partially degraded (lower panel), the two bands will still be distinguishable, however, additional bands of various sizes will be present in the background (lower panel, right). This enables a quick visual estimation of the RNA quality of a biopsy sample.

3.3.10 Linear transcriptome amplification

Linear mRNA amplification was used to overcome the low starting amounts of RNA. A linear, T7-based in vitro transcription (IVT) method was established by Eberwine and van Gelder in 1990 (Van Gelder et al., 1990). In this approach, RNA templates are primed with an oligo(dT) primer that has been 5' modified to contain a promoter for the T7 RNA polymerase and are subsequently reverse transcribed into first-strand cDNA. The RNA-cDNA hybrid is then treated with *E. coli* RNase H, and priming for second-strand cDNA synthesis occurs by RNA nicking. Second-strand cDNA synthesis is then carried out with *E. coli* DNA polymerase and *E. coli* DNA ligase followed by blunt-ending with T4 DNA polymerase. The T7 RNA polymerase, which binds to the T7 promoter introduced during first-strand cDNA synthesis, is then used to accomplish transcription and amplification, producing amplified antisense RNA.

Three rounds of linear T7-based transcriptome amplification (**Figure 3.3**) were carried out using the ExpressArt-mRNA Amplification Kit, Pico Version (AmpTec, Hamburg, Germany) (Baugh et al., 2001). The method was established and tested according to the instructions of the supplier. Laser microdissected myofibers were stored in Trizol reagent at -80°C. Once a sufficient amount of myofibers had been collected from each subset, the samples were pooled accordingly. RNA was isolated as described in section 3.3.8.2. For the first amplification round, an oligo-(d)-T primer without promoter sequence was used. For dsDNA synthesis, a special “*TRiNucleotide*” primer was employed that preferentially binds near the 3' end and contains a special 5'-terminal “*Box*” sequence. Templates then were created using a T7-containing primer. The resulting, near-full-length, double stranded cDNA thus contained a T7 promoter. In vitro transcription then was performed using a T7 RNA polymerase, resulting in amplified RNA (aRNA) which contained the “*Box*” sequence at the 3' end. The second amplification round was then carried out using a primer which recognizes the “*Box*” sequence for cDNA synthesis, and T7-based in vitro transcription. The third amplification round mirrored the second round. After establishing the method according to the instructions of the supplier, the following modifications were included: for synthesis of the first cDNA strand, the master mix was pre-warmed at 45°C; and 1 µl of RNase R was added to each reaction for the RNA removal step. The resulting yields of aRNA were between 30-40 µg, derived from < 10 ng of input total RNA.

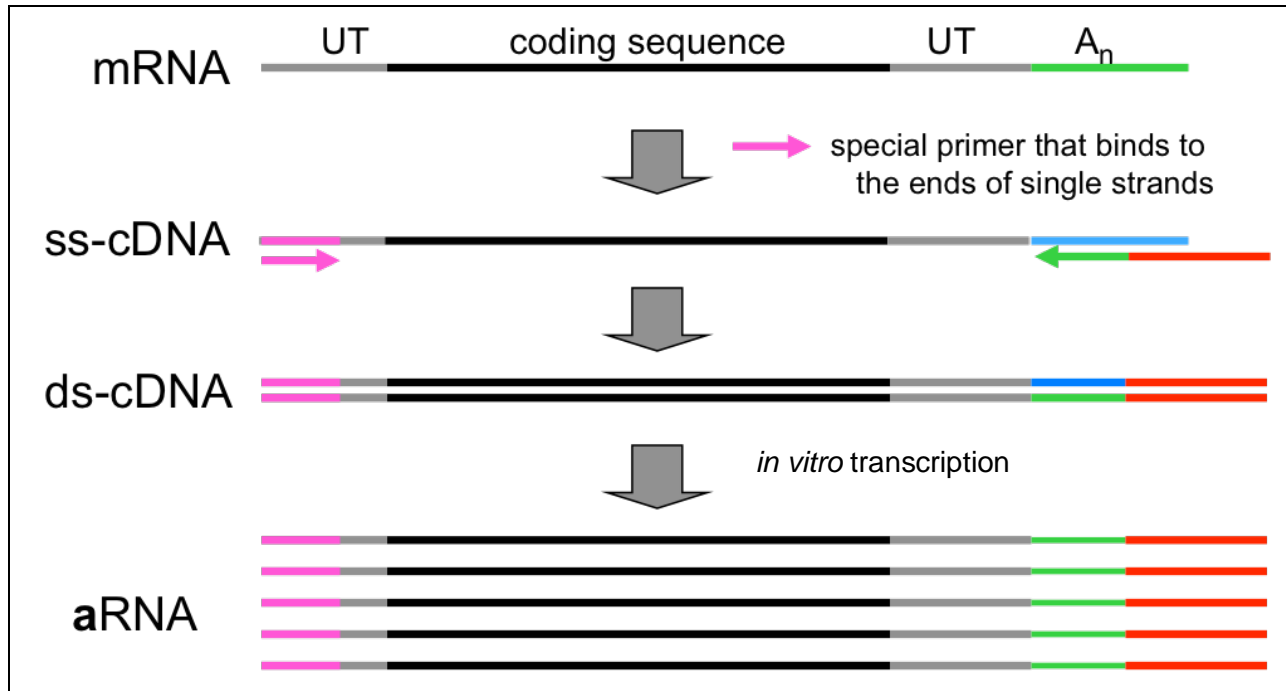


Figure 3.3: AmpTec-based linear amplification method. The three steps of linear mRNA amplification are shown from top to bottom. In the first step, a primer which can bind free 3' ends are used to reverse transcribe mRNA into single stranded (ss)-cDNA. Next, a primer that contains the sequence of a T7-promoter is used to synthesize the complementary cDNA strand, resulting in double stranded (ds)-cDNA. The “amplification round” is concluded by *in vitro* transcription of the ds-cDNA into amplified RNA (aRNA). At this stage, the linear amplification can be potentiated by adding one or two more amplification rounds.

Microarray probesets are usually located near the poly-(A)-tail, whereas TaqMan qPCR primer/probe-pairs can be located anywhere in the transcript. This may in fact be a reason for differences in microarray and TaqMan qPCR results. TaqMan quantitative PCR (section 3.3.13) was used to check for linearity of the amplification (results described in section 4.1.4).

3.3.11 Microarray hybridization and analysis

15 µg of amplified cDNA were biotinylated and transcribed into aRNA using the BioArray High Yield RNA labeling kit (Enzo Life Sciences, Plymouth Meeting, PA, USA). Biotinylated aRNA was hybridized to HU133 GeneChip arrays from Affymetrix in collaboration with PD Dr. Reinhard Hoffmann, Institute of Microbiology, Munich University of Technology. This type of array tests for over 48000 probesets on one chip. All chips were normalized using the robust multiarray average (RMA) (Irizarry et al., 2003) or the GC-RMA (Wu and Irizarry, 2004) procedure in R packages from Bioconductor (www.bioconductor.org). The q values were calculated for each probeset. The q value reflects the "False Discovery Rate" and thus the degree of heterogeneity (variability of expression levels) between different samples (Storey and Tibshirani, 2003), i.e. here between samples from different patients within each group ("attacked myofibers" (A_{IBM}) versus "non-attacked myofibers" (N_{IBM}) versus "controls" (H_{CTRL}), **Figure 3.4**). A low q value thus mirrors a high significance of a particular expression alteration across all samples. To achieve a high concordance across all patients, only transcripts with a q-value of 20% or less were considered.

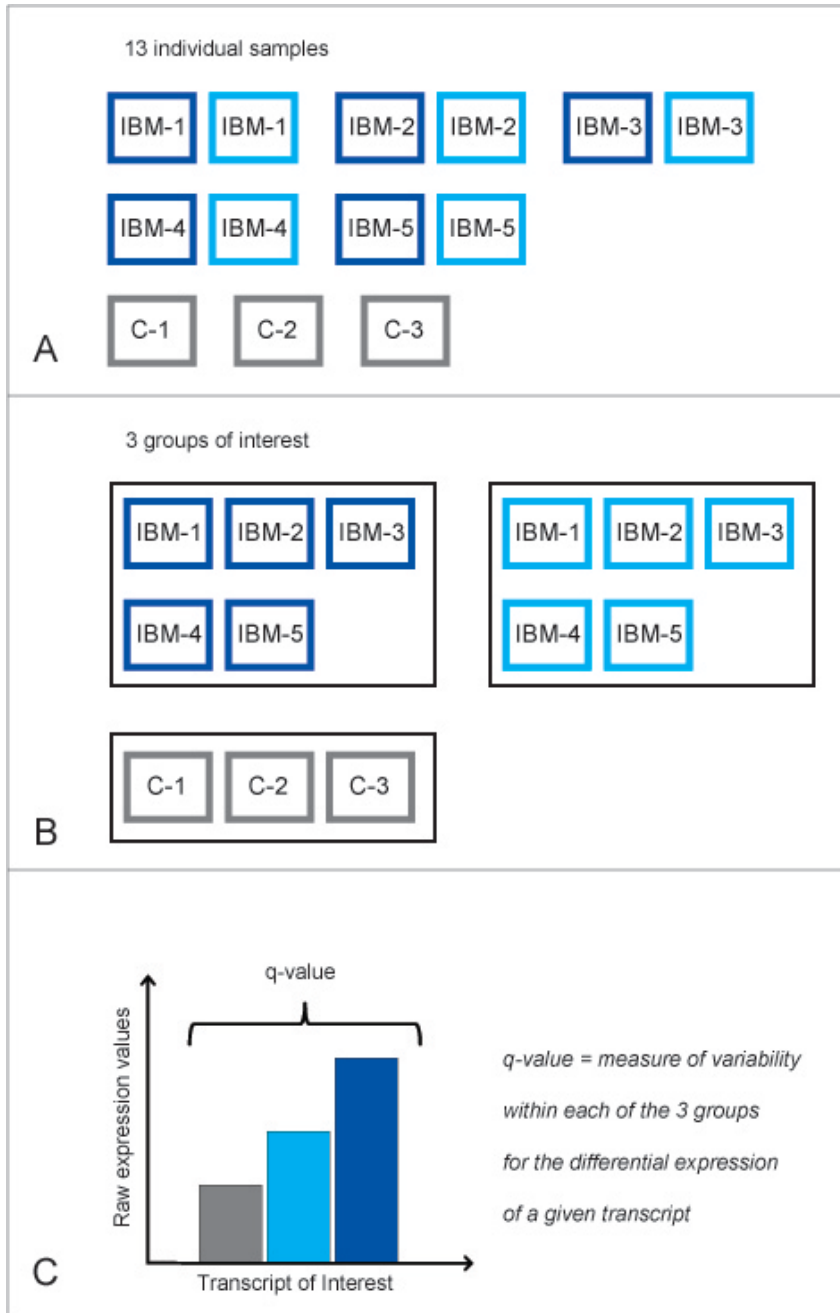


Figure 3.4: The q-value as a measure of significance of expression changes. RNA from laser microdissected myofibers from 13 individuals was isolated and subjected to linear amplification and biotinylation for subsequent Affymetrix microarray hybridization (A). The 13 samples were grouped into 3 groups (B): A_{IBM} (attacked myofibers from patients IBM-1 to IBM-5, dark blue), N_{IBM} (non-attacked myofibers from patients IBM-1 to IBM-5, light blue) and H_{CTRL} (myofibers from non-diseased controls C-1 to C-5). For each probeset, the q values were calculated as described (C) (Storey and Tibshirani, 2003). The q-value illustrates the degree of heterogeneity between samples from different patients within each group (A_{IBM} versus N_{IBM} versus H_{CTRL}), thus reflecting significance of a particular expression change across all samples.

3.3.12 cDNA synthesis from total RNA

For quantitative PCR experiments from muscle biopsy samples, RNA was isolated as described in section 3.3.8.1 and cDNA synthesis was performed using the SuperScript III First-Strand Synthesis System for RT-PCR (Invitrogen Life Technologies) according to the manufacturer's instructions, with modified incubation temperatures as follows. An oligo-(dT) primer was used for first strand synthesis. 3 µg of RNA were mixed with dNTPs and water and incubated for 10 minutes at 65°C. Subsequently, the oligo-(dT) primer was added with the first strand buffer and 0.1 M DTT as supplied by the manufacturer. The mixture was incubated for 1 minute at 45°C, before adding the SuperScript III RT enzyme and further incubation for 60 minutes at 45°C. The reaction was terminated by incubation of the sample at 75 °C for 15 minutes. Samples were then immediately placed on ice and stored at – 20 °C until further use.

3.3.13 TaqMan quantitative PCR

To establish quantitative gene expression analysis from laser microdissected tissue and amplified RNA (section 4.1), expression levels of the housekeeping genes cyclophilin (PPIA) and glyceraldehyde-3-dehydrogenase (GAPDH) were assessed. RNA from tonsillitis specimens was used that was either 1.) subjected to different experimental conditions to assess the extent of RNA degradation or 2.) subjected to a different number of rounds of linear amplification.

Quantitative PCR (qPCR) is based on the principle that a fluorescence signal is increasing with every amplification cycle. This normalized reporter signal (R_n) is measured by normalization versus the background fluorescence (a passive fluorescent dye contained in each reaction). The baseline of the qPCR reaction is defined as the initial reaction phase where reporter fluorescence is not yet observed, since reporter fluorescence does not yet exceed the signal from the passive fluorescent dye. Thus, baseline determines the background fluorescence. ΔR_n is obtained by subtracting the baseline value from R_n . Plotting ΔR_n versus the number of cycles results in a logarithmic curve with an initially exponential slope, then a linear slope, and finally saturation. The cycle threshold (CT) value is automatically determined by the TaqMan SDS software and corresponds to the PCR cycle in which the slope of the amplification curve is linear. Thus, the

lower the CT value, the earlier the linear phase of the amplification has been reached, and the higher the absolute copy number of the target gene in the analyzed sample. For the analysis of relative gene expression, CT values of a target gene and a housekeeping gene in a given RNA sample are mathematically correlated (Applied Biosystems, 2011).

Each primer-probe-set, regardless whether it had been designed by the author or purchased from Applied Biosystems, was tested in a dilution series of Tonsilla cDNA prior to the actual experiments. In such a dilution series, the difference between the CT value of a given cDNA concentration and a 10-fold dilution should be around 3 CT values. **Figure 3.5** shows examples of standard dilution series performed for primer-probe-sets to establish the qPCR conditions using test cDNA (cDNA prepared from total RNA of tonsillitis specimens).

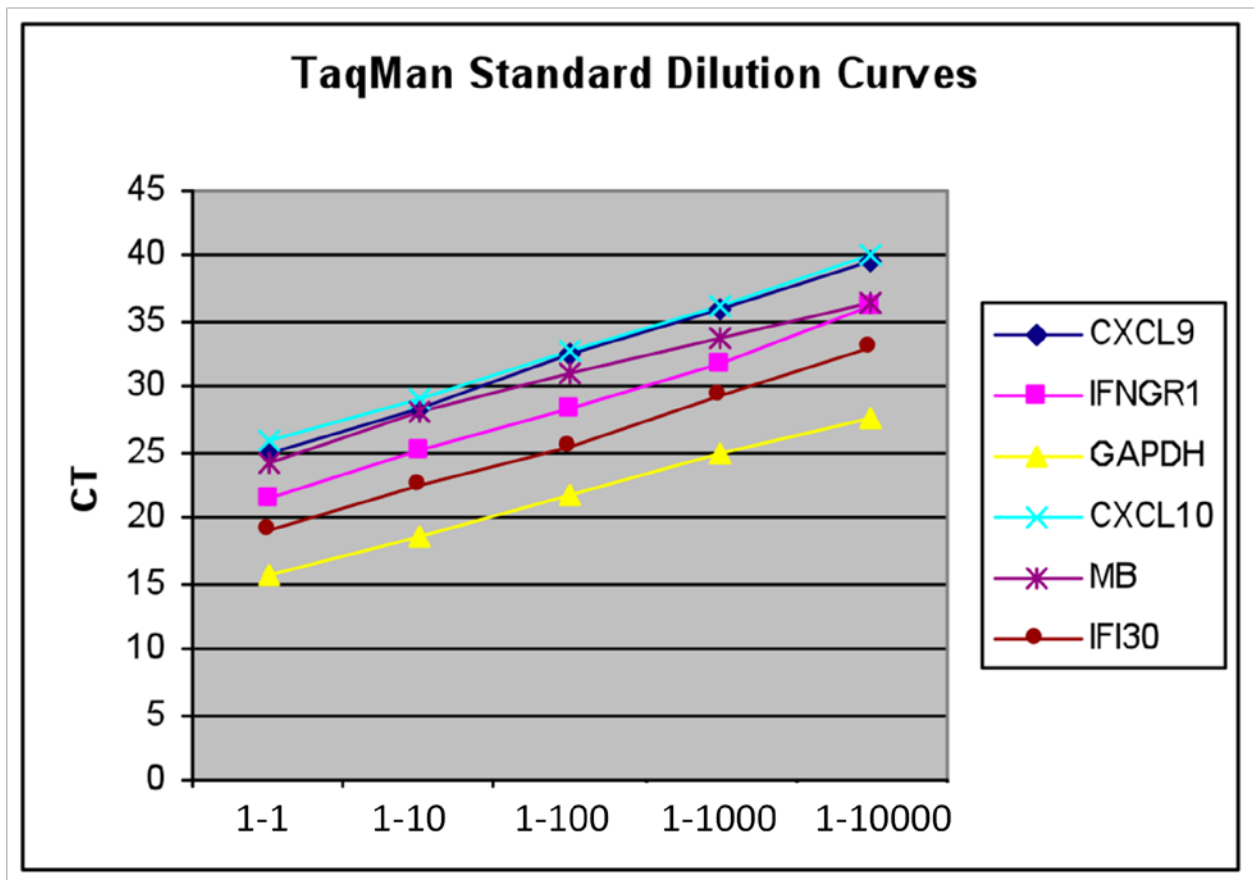


Figure 3.5: TaqMan quantitative PCR - standard dilution series exemplified on several primer-probe-sets used in this dissertation. The x-Axis shows serial 10-fold dilutions of tonsillitis cDNA, while raw CT values are depicted on the y-Axis. Each primer-probe-set was tested in such a dilution experiment prior to its use. The difference between two adjacent dilutions should be 3 CT values, which is the case for all tested primer-probesets.

TaqMan PCR was further used to check for linearity of the AmpTec amplification method (section 3.3.10). Untransfected *Jurkat* cells were sorted to aliquots of 100 cells and RNA was isolated from each aliquot as described above. Linear amplification was performed as described, and quantitative TaqMan PCR of three commonly occurring transcripts (Glyceraldehyde 3-phosphate dehydrogenase (GAPDH), Beta-2-Microglobulin (B2M), and Cyclophilin (PPIA)) was performed on the aRNA from the second and third amplification rounds, respectively. Ratios were calculated to demonstrate linearity of gene expression (results shown in **Table 4.3**).

For the evaluation of quantitative gene expression levels of genes involved in antigen processing and presentation, and IFN- γ receptor associated genes (section 4.2), expression levels of the following transcripts were analyzed in all 13 samples (attacked and non-attacked myofibers from each of the five patients, and C1-3) by real-time quantitative PCR using the 5700 Real-Time PCR System (Applied Biosystems, Foster City, CA): HLA-A, HLA-B, HLA-C, HLA-E, HLA-F, HLA-G, Interferon- γ Receptor- α -chain (IFNGR1) and - β -chain (IFNGR2), Signal transducer and activator of transcription 1 (STAT1), Class II transactivator (CIITA), Proteasome subunit β -type 8 (PSMB8), HLA-DRA, HLA-DRB, HLA-DPA, HLA-DPB, HLA-DQA, HLA-DQB, CCL5, STAT3. Amplified RNA was reverse transcribed into cDNA using primer D from the AmpTec ExpressArt-mRNA Amplification Kit. For each transcript, three replicates per sample were assayed for in a 96-well format plate. Cyclophilin (PPIA) was used as housekeeping gene for data normalization across samples. Normalization of CT values of each gene and calculation of fold changes in gene expression was performed according to the relative quantification (RQ) method, also known as the $2^{-\Delta CT}$ method (Schmittgen and Livak, 2008; Livak and Schmittgen, 2001a).

The $2^{-\Delta CT}$ method is preferred for presentation of qPCR data if individual data points from gene expression studies are to be compared, since it allows normalization of the data to an internal control (Livak and Schmittgen, 2001b). For certain genes, TaqMan[®] Gene expression Assays (Applied Biosystems) were used, and custom-made primers and probes (Metabion, Martinsried, Germany) were used to measure the expression levels of others (see section 3.2.2).

For the analysis of RER1 expression in inflammatory and degenerative muscle diseases versus nondiseased controls, expression levels of RER1 were measured in triplicate in the patients and healthy controls as described in section 4.4.3. Cyclophilin (PPIA) was used as housekeeping gene, and CT values were normalized across samples to determine gene expression fold changes according to the $2^{-\Delta CT}$ method as described above. **Table 3.2** (section 3.2.2) lists the primers and probes.

3.3.14 Statistical analysis of IFNGR2 distribution on myofibers in sIBM

Cryosections were stained for IFNGR2 and CD8 and imaging was performed as described in section 3.3.5.3. Myofibers were classified into four groups according to their extent of membrane circumference positivity for IFNGR2 and photographically documented: Group 1, > 80%; Group 2, 50-80%; Group 3, 20-50%, and Group 4, < 20%. For each myofiber, the number of adjacent CD8⁺ T cells was noted, and the median was calculated for each group. Two investigators (J.I. and Mrs. Ingrid Eiglmeier) independently performed this analysis for each patient. A Mann-Whitney U-Test was performed to determine whether the medians of adjacent CD8⁺ T cells of group 1 (>80% IFNGR2 positivity) and group 4 (<20% IFNGR2 positivity) differed significantly. The two-tailed p-value was calculated, as well as the Mann-Whitney U. This analysis was performed for four out of five sIBM patients due to lack of biopsy material from Patient 4.

3.3.15 Cell culture

For the experiments described in section 4.4.5, TE671 cells were thawed and cultivated in Roswell Park Memorial Institute (RPMI)-1640 cell culture medium supplemented with 10% fetal calf serum (FCS), 2mM glutamin, penicillin and streptomycin at 37°C and 5% CO₂. The RPMI-1640 medium was exchanged once every 24h. For cell transfer, medium was removed, adherent cells were washed and trypsinized with PBS containing 0.5 mg/ ml trypsin and 0.22 mg/ ml EDTA. The detached cells were transferred into a collection tube and centrifuged at 1200 rpm for six minutes at 4°C. Cells were then plated at a density of 100.000 / ml in a T75 flask.

To induce starvation of TE671 cells, cultured cells were transferred into Hering's buffered salt solution (HBSS) at a density of 100.000 /ml and cultured in HBSS (starved) for 2h and 24h, respectively.

4. Results

4.1 Establishment of the methodology and experimental conditions

4.1.1 Detection of HLA-ABC and CD8 in sIBM biopsy cryosections

Since the initial approach, i.e. global transcriptome analysis, was non-hypothesis-driven, the whole transcriptome – rather than any specific gene – had to be detected with the best possible quality. Thus, a staining and laser microdissection protocol had to be established that is specific enough to detect CD8⁺ T cells and HLA-I⁺ myofibers in the biopsy, yet rapid enough to prevent RNA degradation.

The starting point to establish the double immunofluorescence for CD8 and HLA-I was a previously described immunohistochemistry protocol (Seitz et al., 2006). In that protocol, the total time from defrosting the slides to cell isolation is at least 3h. To obtain RNA quality suitable for global, unbiased transcriptome analysis, the protocol had to be completely modified.

The approach to design a new protocol was guided by three major experimental improvements: 1.) exchanging immunohistochemistry for immunofluorescence for better visualization, less background, and ability to detect multiple antigens at once; 2.) shortening the incubation and washing time to a minimum; and 3.) supplementation of RNase-inhibiting reagents to the incubation solutions to further minimize RNA degradation. To address the first point, HLA-I staining was established with the W6/32 monoclonal mouse-anti-human antibody which was directly labeled with the immunofluorescent dye Alexa-488. Moreover, CD8 staining was established with a monoclonal mouse-anti-human CD8 antibody that had to be directly labeled with the immunofluorescent dye Cy3. The protocol then had to be optimized for simultaneous application of the two antibodies, bearing in mind that conditions required for laser microdissection (no coverslip) will invariably lead to reduced image quality. Thus, higher antibody concentrations had to be applied in the new protocol. The immunofluorescence staining protocol was dramatically shortened to a total time of 10 min.

Figure 4.1 demonstrates the finalized results on a representative image from sIBM patient 19142 (IBM-3). The finalized staining protocol, including the addition of RNase inhibitor to all blocking and antibody suspensions (see following sections), is outlined in **Table 4.1**.

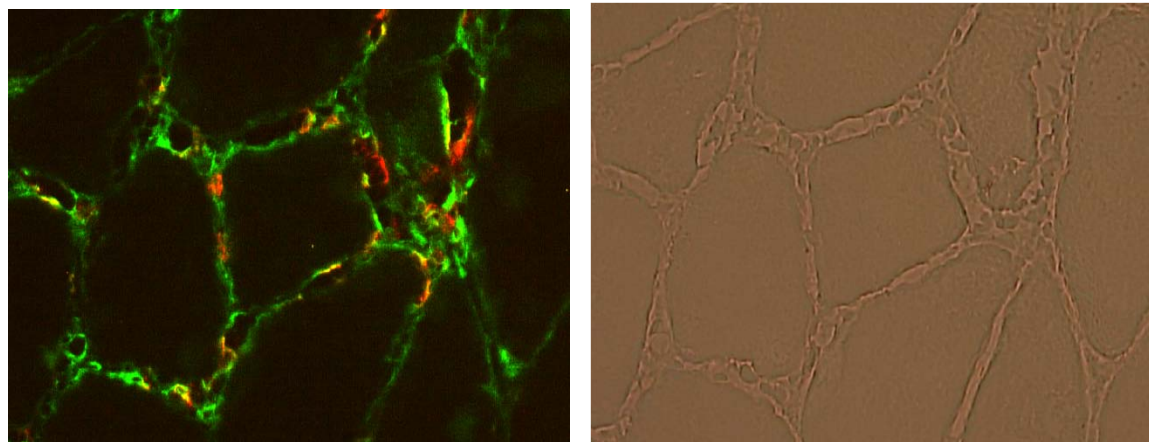


Figure 4.1: Double immunofluorescence staining for HLA-I (visualized in green with Alexa488) and CD8 (visualized in red with Cy3) of sIBM patient 19142 (IBM-3). Axially cut, HLA-I positive myofibers can be seen, as they are being attacked by CD8⁺ T cells (A). A corresponding transmission image is provided for correlation (B). Magnification: 400x.

Protocol step	Time
Thawing of tissue cryosections in desiccator	3 min
Acetone fixation at -20°C	1 min
Rinse tissue with PBS	5 s
Blocking of non-specific binding sites with 1% BSA in PBS + 3 U/ml Protector RNase inhibitor (Roche)	3 min
Incubation with both directly labeled antibodies	5 min
Rinse tissue with PBS (pour three times 1 ml onto slide)	10 s
Rinse tissue with 1ml of 100% Ethanol	5 s
Dry tissue in desiccator	2 min
TOTAL TIME FROM THAWING TO CELL ISOLATION (EXCLUDING DESICCATOR TIME)	~ 10 min

Table 4.1: Newly established double immunofluorescent staining protocol suitable for subsequent laser microdissection and transcriptome analysis. Desiccator times are not included in the total protocol time of 10 min, since RNase is inactive in completely dry tissue (as under vacuum conditions inside the desiccator).

4.1.2 Laser microdissection

Muscle tissue from patients with sIBM and healthy control individuals was stained as described in 4.1.1. The experimental conditions for laser microdissection had to be established. Thus, focus and energy of the laser beam had to be adjusted according to the specifics of muscle tissue (**Figure 4.2**).

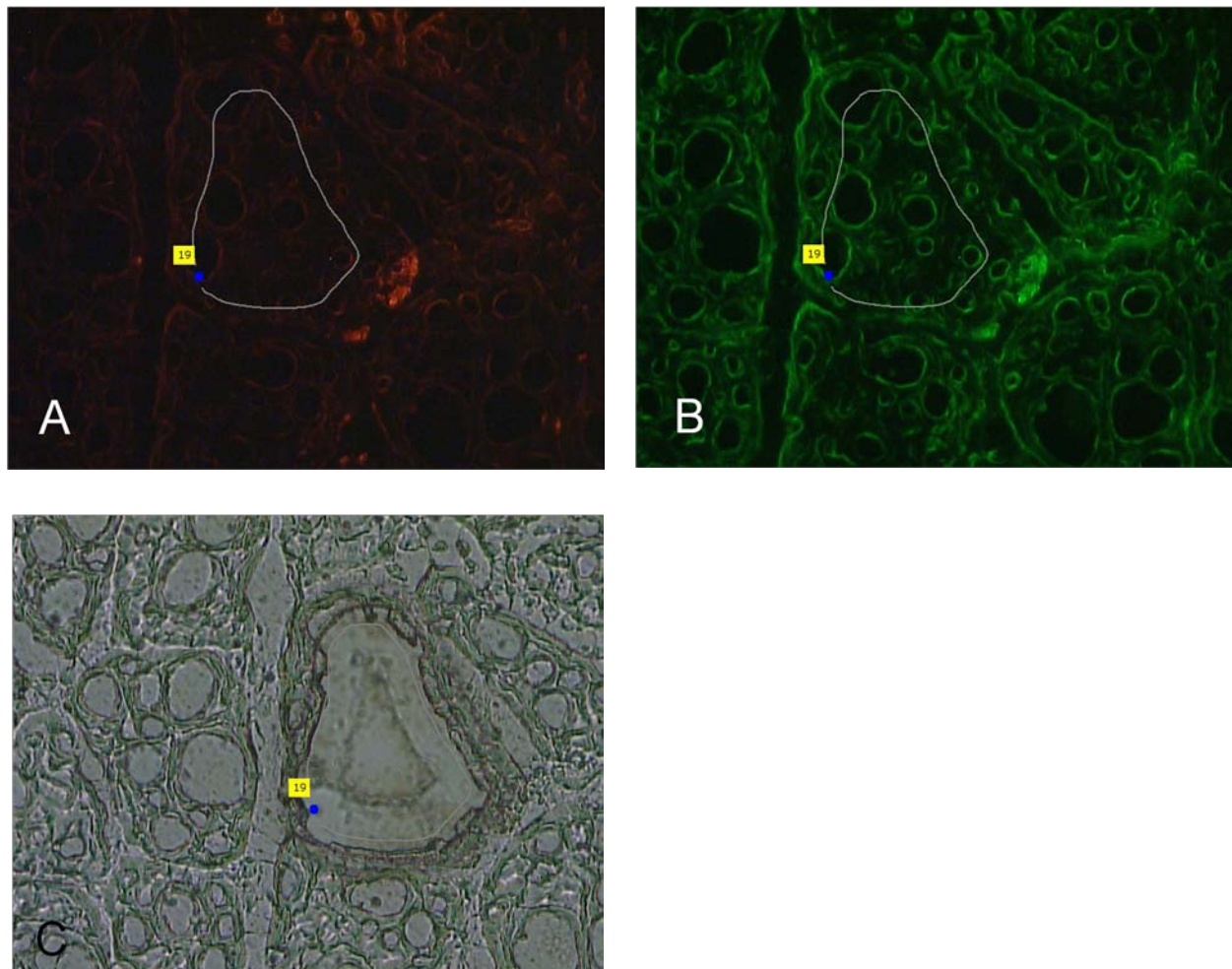


Figure 4.2 Laser microdissection of myofibers from patients with sIBM. Stained cryosections from sIBM patient 13515 (IBM-5) are shown before (A, B) and after (C) laser microdissection. Myofibers fulfilling the criteria (attacked or non-attacked) were identified via immunofluorescence staining as described. Figure A shows CD8 staining, with three CD8⁺ T cells attacking a myofiber, thus rendering it eligible for isolation. Figure B shows the same field of view highlighting HLA-ABC staining. Care was taken to avoid disrupting the myofiber membrane, thus minimizing contamination with surrounding lymphocytes (Figure C).

4.1.3 Preservation of RNA quality

In addition to dramatically shortening the incubation times and increasing antibody concentrations, further measures had to be taken to preserve RNA quality. The tissue was dried in a desiccator before and after the staining procedure to minimize endogenous RNase activity. Frozen tonsilla tissue was then used to test and compare outcomes of different protocol conditions, and the quality of RNA isolated from each tissue sample was assessed using the Agilent Bioanalyzer (Agilent Technologies). Different commercially available RNase inhibitors were tested, and Protector RNase inhibitor from Roche yielded the best results. **Figure 4.3** illustrates the influence of varying protocol conditions on RNA quality.

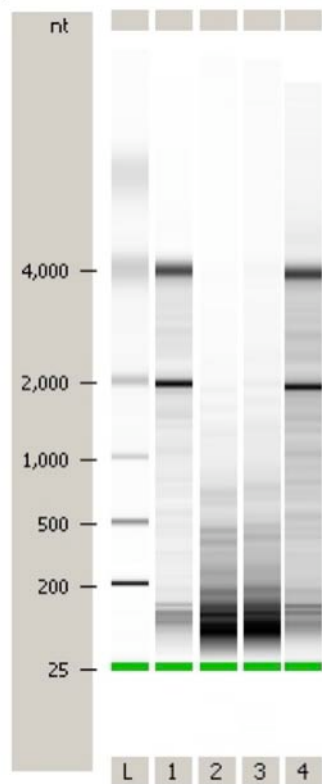


Figure 4.3: RNA degradation depends on protocol conditions.

Lane "L" represents the "ladder" or reference standard used to compare molecular mass sizes.

Lane 1 shows fresh, unstained tissue that was directly immersed in Trizol reagent once taken out of -80°C (positive control for RNA preservation).

Fresh frozen tonsilla tissue was stained with two fluorescent antibodies for 10 min. If no RNase inhibitor was included in the protocol, RNA degradation occurred invariably (*lanes 2 and 3*).

If fresh frozen tissue was treated in the same way as in lanes 1 and 2, however Protector RNase inhibitor (Roche) was included in the protocol, RNA remained very well preserved (*lane 4*).

All relevant protocol modifications resulting in the new, RNA-preserving immunofluorescent staining protocol are summarized in **Table 4.1**.

4.1.4 Establishment and validation of the linear amplification method

One of the challenges of the laser microdissection technique is the low amounts of RNA in the starting material (around 15 pg total RNA, thus around 0.5 pg mRNA) in comparison to the relatively large RNA amounts required for gene expression analysis, especially for high resolution microarray technology (about 10µg).

A recently established linear amplification technology called “ExpressArt” from the company AmpTec GmbH (Hamburg, Germany) derives from the method by Van Gelder and Eberwine described in the section 3.3.10. The advantage of the AmpTec linear amplification method (**Figure 3.6**) lie in the decreased shortening of fragments compared to random priming as it occurs with the method developed by Eberwine et al. RNA amplification starting from few picograms of total RNA was performed using the ExpressArt kit.

To assess output aRNA quality, Agilent Bioanalyzer analysis was performed on defined numbers of *Jurkat* cells and an RNA control sample (corresponding to RNA from around 3000 cells) provided in the AmpTec linear amplification kit. The results are depicted in **Figure 4.4**.

A number of modifications to the manufacturer’s protocol were introduced to the original protocol as described in section 3.3.10.

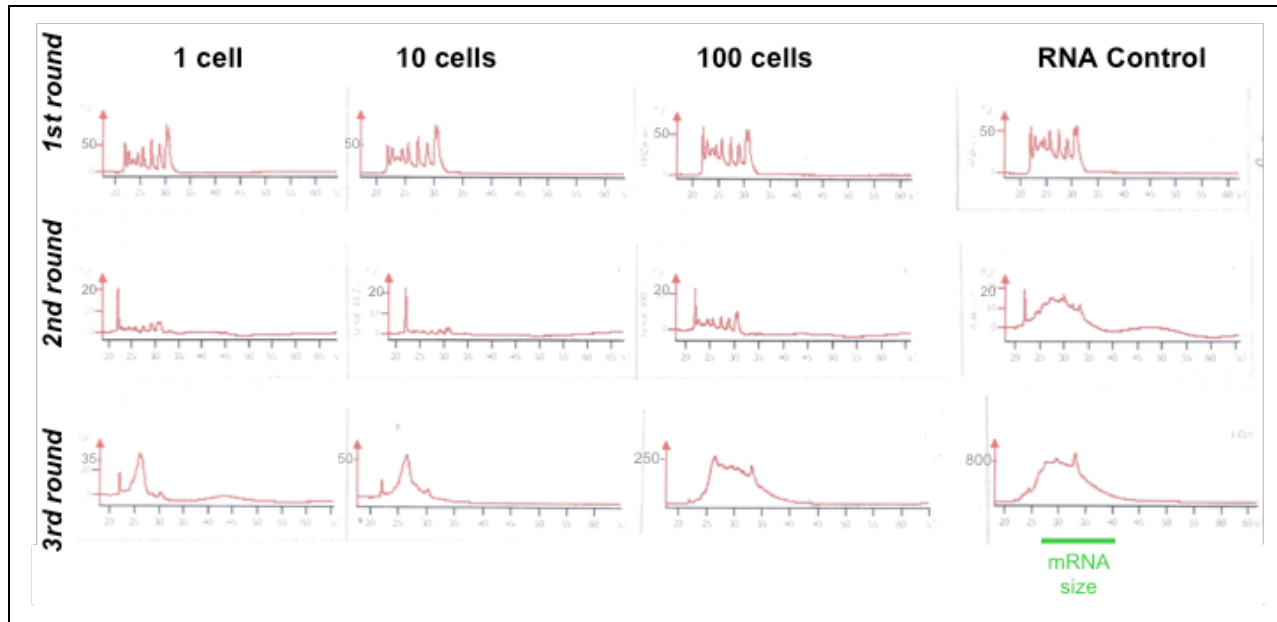


Figure 4.4: RNA Quality assessed after 1, 2, and 3 amplification rounds of defined numbers of cells. Defined numbers of untransfected Jurkat cells were FACSsorted into individual columns and RNA isolation was performed. The total RNA was then subjected to linear transcriptome amplification. Agilent Bioanalyzer analysis was run after each amplification round. The rounds are organized in rows, and the numbers of cells are organized in columns. As a control (RNA Control), control RNA from the AmpTec linear amplification kit was used. The green scale bar refers to the approximate mRNA size of the respective sample.

To check for linearity of the AmpTec amplification method, quantitative TaqMan PCR of three commonly occurring transcripts (Glyceraldehyde 3-phosphate dehydrogenase (GAPDH), Beta-2-Microglobulin (B2M), and Cyclophilin (PPIA)) was performed on RNA isolated from 100 *Jurkat* cells (**Table 4.2**) from the second and third amplification rounds, respectively. This experiment showed that the ratio between two given transcripts remained constant throughout amplification rounds, and that the linear amplification method was indeed reliable.

C_T Ratio – 100 cells	2nd round	3rd round
GAPDH/ PPIA	1.58	1.55
GAPDH/ B2M	1.28	1.31
B2M/ PPIA	1.24	1.20

Table 4.2: Demonstration of the linearity of RNA amplification from 100 cells. *Jurkat* cells were grown under standard conditions and sorted into individual tubes to obtain 100 cells per sample. RNA was isolated and subjected to three rounds of AmpTec linear amplification following the manufacturer’s recommendations. TaqMan quantitative PCR for the following transcripts was performed on such amplified RNA from the 2nd and 3rd amplification rounds, respectively: Glyceraldehyde 3-phosphate dehydrogenase (GAPDH), Beta-2-Microglobulin (B2M), and Cyclophilin (peptidyl prolyl isomerase A or PPIA). Ratios of the respective C_T values were then calculated. Linearity of amplification can be assumed if the ratio of two given transcripts remains constant between the 2nd and 3rd amplification round.

4.2 CD8⁺ T cells focally attack HLA-ABC⁺ myofibers in the axial as well as the longitudinal plane

4.2.1 Demonstration of focal inflammatory infiltrates in sIBM

This work aimed to compare expression patterns of myofibers attacked and non-attacked by CD8⁺ T cells. Axially cut myofibers were examined after immunofluorescent visualization of HLA-ABC and CD8 as described, and a clearly focal pattern of CD8⁺ T cell attack was observed (example illustrated in **Figure 4.5**). While individual myofibers were attacked heavily by CD8⁺ T cells (A_{IBM} in Figure 4.5), as well as other cells which were HLA-ABC-positive but CD8-negative (likely macrophages), other myofibers remained unattacked (N_{IBM} in Figure 4.5).

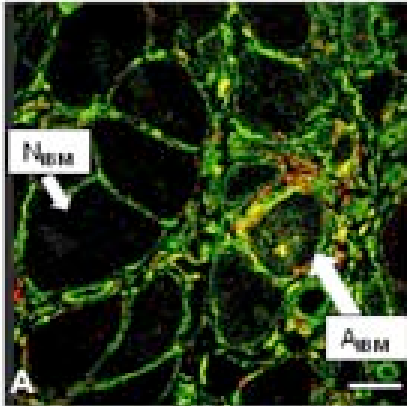


Figure 4.5: Overview of an axially sectioned biopsy sample from sIBM patient 19116. Cryosections were prepared as described in the methods section. Cryosections were stained for HLA-ABC (visualized with Alexa-488 in green) and CD8 (visualized with Cy3 in red) as described. In this example, confocal microscopy was performed as described in the methods section. In sIBM, some myofibers are heavily attacked (A_{IBM}) by numerous CD8⁺ T cells (“A_{IBM}”) while other myofibers remain spared (“N_{IBM}”).

4.2.2 CD8⁺ T cells follow a focal attack pattern in the longitudinal plane

Since myofibers are the longest cells in the human body, a scenario could be imaginable where a myofiber would appear as non-attacked in a given section, however in reality would have been attacked several sections below or above the visualized plane. It was thus important to check whether the focal nature of CD8⁺ T cell attack followed the same pattern in the longitudinal plane. Serial sections would have been the “gold standard” for checking continuity across multiple axial planes. However, serial sections require large amounts of material which was not available for the purposes of this dissertation. Thus, cryosections were prepared such that as many myofibers as possible were oriented longitudinally rather than axially, and subsequently double immunofluorescent staining was performed as described (**Figure 4.6**). The oblique orientation of myofibers resulted in examples such as Figure 4.6 A and B, with coexistence of axial and longitudinal sections.

As shown in **Figure 4.6**, even if A_{IBM} myofibers are heavily attacked in the proximity, N_{IBM} myofibers remain spared in the longitudinal plane.

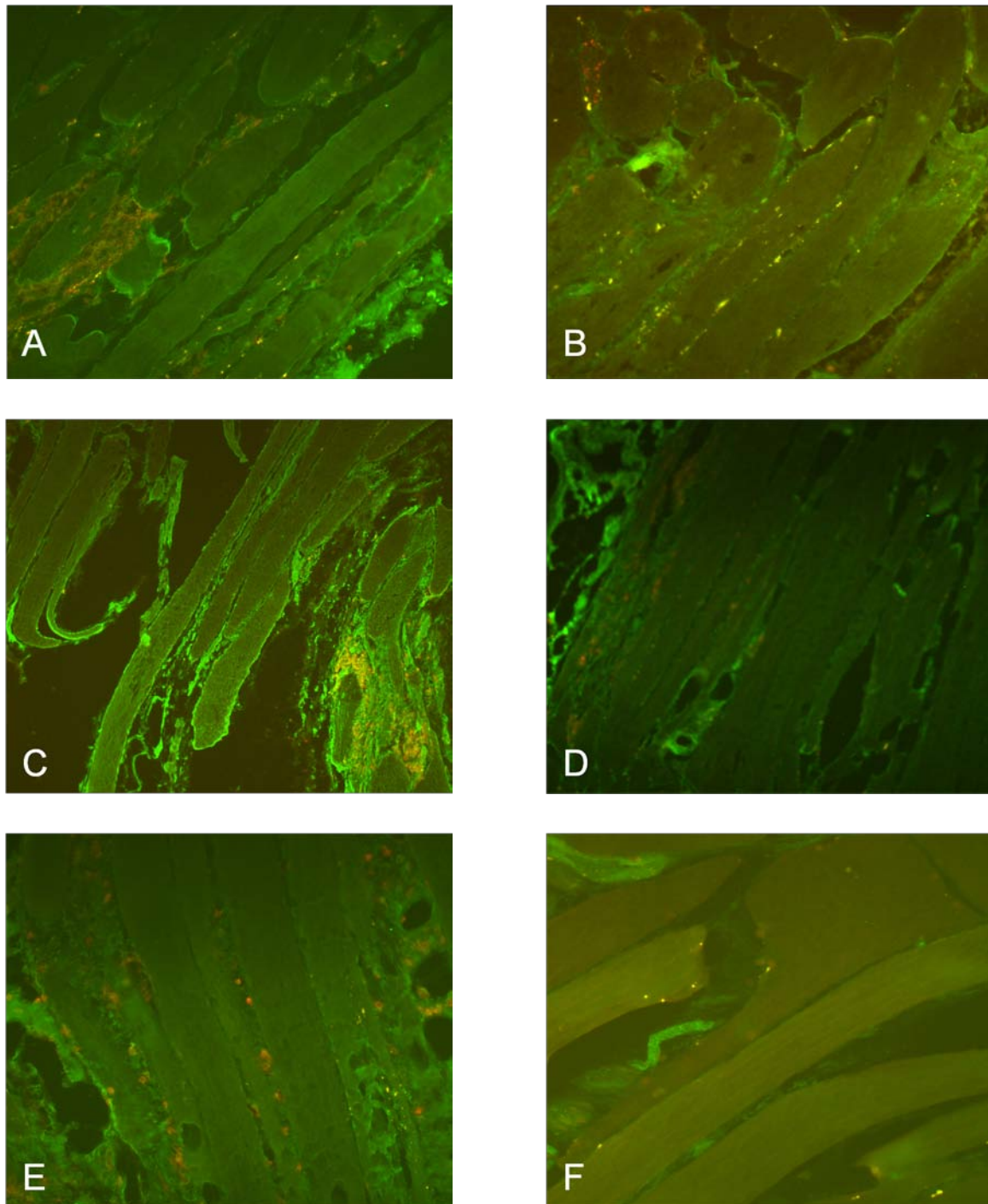


Figure 4.6: Overview of longitudinally, or partially longitudinally sectioned biopsy samples from sIBM patients 18592 (A), 19142 (B), 14715 (C), 18653 (D), 15551 (E) and healthy control 19400 (F). Cryosections were prepared as described in the methods section, however, longitudinal orientation of myofibers was checked for by immediately inspecting the sections under a transmission light microscope and re-orienting the biopsy blocks in the cryostat as necessary. Staining for HLA-ABC (visualized with Alexa-488 in green) and CD8 (visualized with Cy3 in red) was performed as described.

4.3 Global transcriptome analysis in laser microdissected myofibers

4.3.1 Establishment of a classification system for the sampling attacked versus non-attacked myofibers

IBM muscle sections were stained for CD8 and HLA-ABC using the protocol established in section 4.1.1 to distinguish attacked and non-attacked myofibers. IBM myofibers were defined as “attacked” or “A_{IBM}” if at least three CD8⁺ T cells could be identified in direct contact, or if a CD8⁺ T cell superficially invaded the myofiber. IBM myofibers were classified as “non-attacked” or “N_{IBM}” if no CD8⁺ T cell could be detected in their proximity (**Figure 4.7 A, B.**).

Laser microdissection was then used to isolate A_{IBM} and N_{IBM} myofibers (**Figure 4.7 C, D**). As controls, myofibers from control muscle specimens or “H_{CTRL}” were laser-microdissected. In all cases the inner core of the fibers was dissected, taking care to avoid any surrounding or invading inflammatory cells. The microdissected samples were pooled according to the myofiber subset, resulting in at least 100,000 μm^2 of total myofiber area from each myofiber subset of each patient, and from each control.

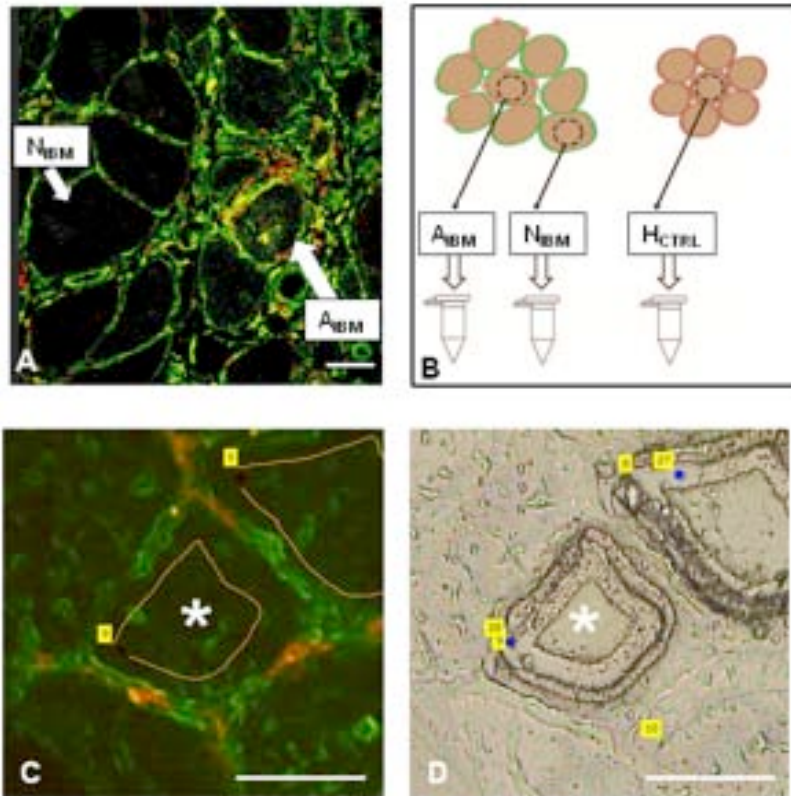


Figure 4.7 Experimental approach for separate analysis of attacked and non-attacked myofiber subsets in sIBM. (A) demonstrates the focal nature of inflammatory infiltrates in IBM. Muscle tissue was stained with anti-CD8 (red) and anti-HLA-ABC (green) antibodies as described in the text. (A) shows a confocal image, and (C) shows unembedded, dry tissue. All myofibers are HLA-ABC positive, but only some are attacked by CD8⁺ T cells (“A_{IBM}”), while others are spared (“N_{IBM}”). (B) myofibers in direct contact with at least three CD8⁺ T cells or invaded by at least one CD8⁺ T cell were defined as “A_{IBM}“. Myofibers not in contact with any CD8⁺ T cells were defined as “N_{IBM}“. Ambiguous myofibers were not sampled. Laser-capture microdissection was used to pressure-catapult the different types of myofibers into collecting tubes. In total, 100,000 μm² of A_{IBM} and N_{IBM} myofibers were sampled from each sIBM patient, and the same amount of H_{CTRL} myofibers from each control subject. (C), Double immunostaining for HLA-ABC (green) and CD8 (red) according to the protocol described in the text. Only myofiber tissue (marked by an asterisk), was isolated, avoiding surrounding lymphocytes (shown in red). (D) shows the corresponding bright-light image after the myofiber was dissected and catapulted out of the tissue. White scale bars represent 50μm.

4.3.2 Global microarray analysis of aRNA from laser microdissected myofibers

RNA from myofibers isolated as described in section 4.3.1 was then amplified according to the method established in section 4.1.2 and subsequently hybridized to Affymetrix microarrays. The microarray hybridization and analysis was performed in the laboratory of PD Dr. Reinhard Hoffmann, Institute for Microbiology, University of Technology, Munich. Microarray results were checked for inflammatory cell specific transcripts, and as demonstrated in **Table 4.3**, T-cell, macrophage and B-cell-related transcripts were essentially undetectable in the laser-microdissected samples.

Unintended sampling of lymphocytes and macrophages surrounding the myofibers was carefully avoided by only dissecting the inner core of each myofiber (**Figure 4.7 C, D**).

To minimize inter-patient variation, only transcripts that were regulated with q-values of 20% or lower were included in the subsequent data analysis (**Table 4.4**). The significance of q-values is explained in detail in methods section 3.3.11. A low q value thus mirrors a high significance of the differential expression across all samples. Out of the 34 transcripts with a q value of 20% or lower, 19 transcripts represented HLA-I, HLA-II, or inflammatory signaling genes (highlighted in yellow in **Table 4.4**).

The results for these genes involved in antigen processing and presentation are illustrated in **Figures 4.8, 4.9 and 4.10**. Given the high frequency of these genes among the significantly regulated transcripts, their expression was further evaluated using quantitative PCR and immunohistochemistry as described in the following sections.

Probe.Set.ID	Gene.Symbol	Healthy	Non-attacked	Attacked	q-value(%)
201743_at	CD14	5.14	22.04	11.61	94.60
219669_at	CD177	5.31	4.85	4.81	94.60
206398_s_at	CD19	5.51	5.46	5.40	94.60
213539_at	CD3D	9.27	13.62	37.27	94.60
205456_at	CD3E	4.39	4.34	4.41	94.60
205264_at	CD3EAP	26.48	18.23	19.98	94.60
206804_at	CD3G	5.00	5.07	4.95	94.60
203547_at	CD4	5.92	5.80	6.29	94.60
216424_at	CD4	5.46	5.96	5.37	94.60
203507_at	CD68	13.75	15.34	15.13	94.60
205758_at	CD8A	4.69	4.73	4.68	94.60
207979_s_at	CD8B	6.50	7.01	7.81	94.60
215332_s_at	CD8B	9.68	10.76	8.30	94.60
1553562_at	CD8B	6.91	7.02	6.10	80.48
205488_at	Granzyme A	8.30	8.40	14.65	80.48
210164_at	Granzyme B	7.22	6.05	31.20	94.60
210321_at	Granzyme H	5.02	6.59	7.43	94.60
206666_at	Granzyme K	5.38	25.62	6.50	94.60
207460_at	Granzyme M	4.90	4.89	4.89	97.17
211639_x_at	Immunoglobulin heavy (IGH) locus	5.89	5.63	5.55	94.60
211637_x_at	IGH locus	5.80	5.74	5.67	94.60
211638_at	IGH locus	4.86	4.86	4.80	94.60
211835_at	IGH locus	5.29	4.96	4.91	94.60
217217_at	IGH locus	5.24	5.62	5.16	94.60
217236_x_at	IGH locus	4.96	5.35	4.89	94.60
217281_x_at	IGH locus	7.02	7.13	6.98	97.17
211635_x_at	IGH locus	4.23	4.17	4.11	94.60
211636_at	IGH locus	8.04	7.80	7.51	94.60
211649_x_at	IGH locus	5.49	5.28	5.22	80.48
211646_at	IGH locus	7.53	7.53	7.16	94.60
217169_at	IGH constant A1	12.28	10.84	9.27	94.60
234477_at	IGH constant A1	6.55	6.59	6.41	94.60
216558_x_at	IGH constant A1	12.27	14.22	13.27	97.17
211650_x_at	IGH constant A1	6.27	7.11	7.72	94.60
211868_x_at	IGH constant A1	6.96	6.91	6.18	94.60
216557_x_at	IGH constant A1	5.28	6.09	5.34	94.60
217360_x_at	IGH constant A1	7.11	6.66	6.70	94.60
212827_at	IGH constant mu (IGHM)	11.93	11.42	11.99	94.60
211634_x_at	IGHM	4.54	4.53	4.49	94.60
215949_x_at	IGHM	52.78	36.06	30.76	94.60
211655_at	IG Lambda joining	5.52	5.69	5.68	97.17
215214_at	IG Lambda joining	12.55	12.37	12.30	94.60
216412_x_at	IG Lambda locus	7.26	6.77	6.79	94.60
210356_x_at	MS4A1 (CD20)	4.03	4.00	3.98	94.60
217418_x_at	MS4A1 (CD20)	3.71	3.71	3.69	94.60
1553681_a_at	Perforin 1	6.76	6.62	6.90	94.60
214617_at	Perforin 1	8.00	7.70	7.60	94.60

Table 4.3: Leukocyte markers in myofiber microarray data. Possible contamination was checked for by examining the obtained myofiber microarray data for the expression of B-cell-, T-cell- and macrophage-specific transcripts. Raw microarray expression values are shown. As demonstrated by the low expression values, T-cell, macrophage-, B-cell- and Neutrophil-related transcripts are essentially absent from the laser microdissected myofiber samples. The significance of q-values is explained in detail in section 3.3.11.

Results

Probe Set ID	Gene Title	Raw Expression Values				Fold Change		
		A _{IBM}	N _{IBM}	H _{CTRL}	q-value (%)	A _{IBM} /H _{CTRL}	A _{IBM} /N _{IBM}	N _{IBM} /H _{CTRL}
205132_at	actin, alpha, cardiac muscle 1	9926.55	5275.13	338.44	0.00	29.33	1.88	15.59
201891_s_at	beta-2-microglobulin	12436.09	11093.17	1570.33	0.00	7.92	1.12	7.06
216526_x_at	major histocompatibility complex, class I, B /// major histocompatibility complex, class I, C /// MHC class I polypeptide-related sequence A /// MHC class I polypeptide-related sequence B	8959.71	7976.71	705.27	0.00	12.70	1.12	11.31
209140_x_at	major histocompatibility complex, class I, B /// major histocompatibility complex, class I, C /// MHC class I polypeptide-related sequence A /// MHC class I polypeptide-related sequence B	9521.62	7469.66	297.92	0.00	31.96	1.27	25.07
200905_x_at	major histocompatibility complex, class I, E	3383.98	1638.89	57.90	0.00	58.44	2.06	28.30
217456_x_at	major histocompatibility complex, class I, E	1503.90	827.43	75.69	0.00	19.87	1.82	10.93
221875_x_at	major histocompatibility complex, class I, F	1959.54	1293.23	101.36	0.00	19.33	1.52	12.76
211529_x_at	major histocompatibility complex, class I, G	250.88	163.19	12.87	0.00	19.49	1.54	12.68
209040_s_at	proteasome (prosome, macropain) subunit, beta type, 8 (large multifunctional peptidase 7)	1751.19	613.20	4.05	0.00	432.37	2.86	151.40
202296_s_at	RER1 retention in endoplasmic reticulum 1 homolog (<i>S. cerevisiae</i>)	16.24	23.27	706.64	0.00	0.02	0.70	0.03
200887_s_at	signal transducer and activator of transcription 1, 91kDa	7963.49	6296.56	94.89	0.00	83.92	1.26	66.35
AFFX- HUMISGF3A/M97935_3_at	signal transducer and activator of transcription 1, 91kDa	1928.89	1828.85	34.57	0.00	55.80	1.05	52.91
221087_s_at	apolipoprotein L, 3	605.96	373.82	25.70	5.12	23.58	1.62	14.55
208812_x_at	major histocompatibility complex, class I, C	9337.37	6540.77	430.46	5.12	21.69	1.43	15.19
214459_x_at	major histocompatibility complex, class I, C	6556.01	4679.25	371.30	5.12	17.66	1.40	12.60
204806_x_at	major histocompatibility complex, class I, F	753.67	512.69	59.87	5.12	12.59	1.47	8.56
211071_s_at	myeloid/lymphoid or mixed-lineage leukemia (trithorax homolog, <i>Drosophila</i>); translocated to, 11	4511.40	2944.13	205.20	5.12	21.99	1.53	14.35
202237_at	nicotinamide N-methyltransferase	1944.88	1365.55	21.27	5.12	91.44	1.42	64.20
212845_at	sterile alpha motif domain containing 4A	22.95	44.53	554.77	5.12	0.04	0.52	0.08
215076_s_at	collagen, type III, alpha 1 (Ehlers-Danlos syndrome type IV, autosomal dominant)	6542.53	3846.48	12.69	8.84	515.45	1.70	303.05
213932_x_at	major histocompatibility complex, class I, A	9857.13	7352.34	2127.78	8.84	4.63	1.34	3.46
201137_s_at	major histocompatibility complex, class II, DP beta 1	1817.92	684.36	37.08	8.84	49.02	2.66	18.46
225061_at	DnaJ (Hsp40) homolog, subfamily A, member 4	1906.51	1525.02	29.68	11.67	64.24	1.25	51.39
211528_x_at	major histocompatibility complex, class I, G	195.97	149.47	16.23	11.67	12.08	1.31	9.21
200814_at	proteasome (prosome, macropain) activator subunit 1 (PA28 alpha)	4007.01	3496.38	405.11	11.67	9.89	1.15	8.63
232500_at	chromosome 20 open reading frame 74	1047.84	210.09	12.61	14.41	83.07	4.99	16.66
217436_x_at	major histocompatibility complex, class I, J (pseudogene)	141.93	114.16	19.59	14.41	7.24	1.24	5.83
226470_at	gamma-glutamyltransferase 7	51.17	51.41	1893.54	16.21	0.03	1.00	0.03
228098_s_at	myosin regulatory light chain interacting protein	794.08	85.92	27.30	16.21	29.09	9.24	3.15
200743_s_at	tripeptidyl peptidase I	1741.52	1749.31	337.65	16.21	5.16	1.00	5.18
238431_at	Transcribed locus	1251.44	347.59	22.14	20.02	56.52	3.60	15.70
215313_x_at	major histocompatibility complex, class I, A	11623.07	9764.78	968.10	20.02	12.01	1.19	10.09
204070_at	retinoic acid receptor responder (tazarotene induced) 3	3065.52	1516.95	88.87	20.02	34.49	2.02	17.07
209118_s_at	tubulin, alpha 1a	1608.79	1037.65	48.98	20.02	32.85	1.55	21.19

Table 4.4: Transcripts most significantly regulated across all patients and controls (legend continued on next page). Raw expression values are shown along with fold expression changes depicting regulation of transcripts in A_{IBM} versus H_{CTRL}, A_{IBM} versus N_{IBM} and N_{IBM} versus H_{CTRL}. Here, transcripts that were expressed with a q-value of 20 % or less (section 3.3.11) are shown. Among these 34 transcripts, 19 can be attributed to components of antigen processing and presentation (highlighted in yellow). Figures 4.7-4.9 demonstrate a graphical depiction of these results grouped in subsets.

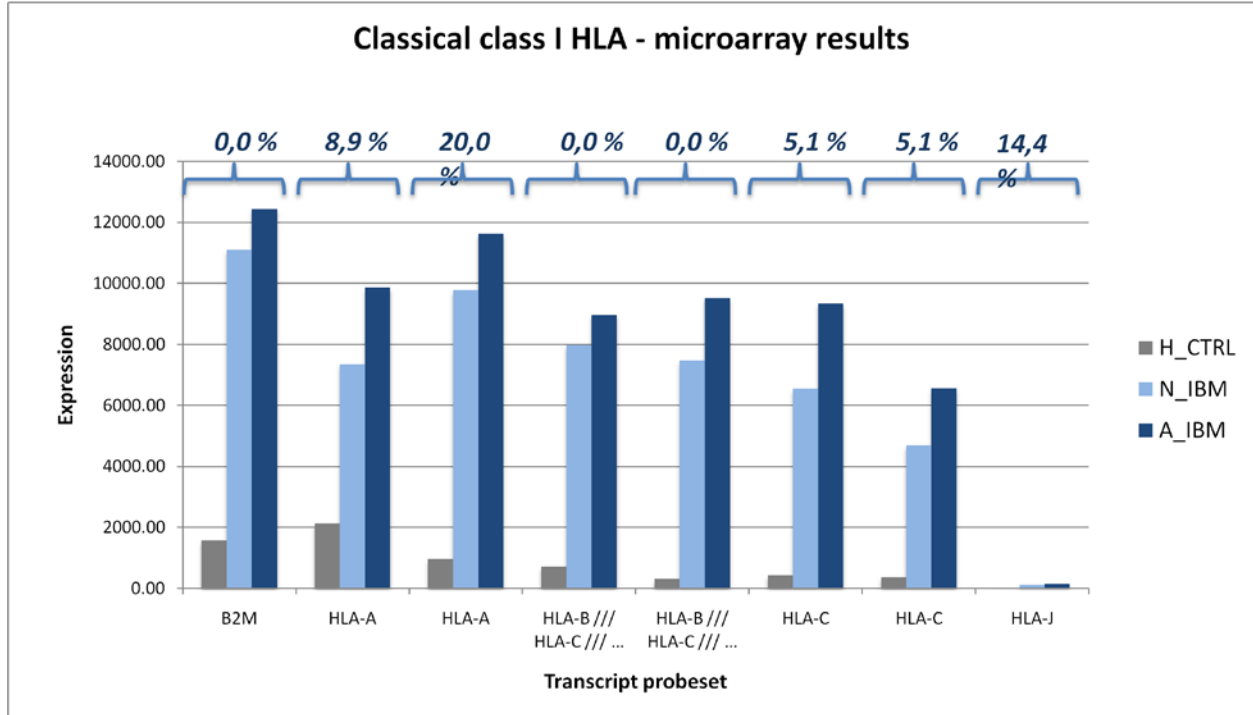


Figure 4.8: Graphical depiction of microarray expression values of significantly regulated probesets – Classical class I HLA transcripts (data from table 4.5). Presented here is same dataset as in Table 4.5. Expression values indicate a very strong expression of classical class I HLA in A_{IBM} and N_{IBM} myofibers. The expression in H_{CTRL} myofibers is considerably lower. The q-values are all 20% or less (as indicated by the numbers above the brackets), indicating a high significance of the differential expression across all samples.

Among the 34 transcripts regulated with a q-value of 20% or lower, there were seven transcripts from the polymorphic HLA-I molecules (HLA-A, HLA-B, HLA-C, **Figure 4.8**). Both A_{IBM} and N_{IBM} showed a strong upregulation of HLA-ABC expression compared to H_{CTRL} (average fold change A_{IBM}/H_{CTRL} = 16.78, N_{IBM}/H_{CTRL} = 12.95 and A_{IBM}/N_{IBM} = 1.29). Moreover, seven non-polymorphic HLA class I transcripts (HLA-E, HLA-F, HLA-G, **Figure 4.9**) were upregulated with low q values (average fold change A_{IBM}/H_{CTRL} = 23.63, N_{IBM}/H_{CTRL} = 13.74 and A_{IBM}/N_{IBM} = 1.62). HLA-DPB1 was the only HLA-II transcript found to have a q value of lower than 20% (**Figure 4.9**). In contrast to HLA-I, HLA-DPB1 was upregulated 2.66-fold in A_{IBM} versus N_{IBM} myofibers.

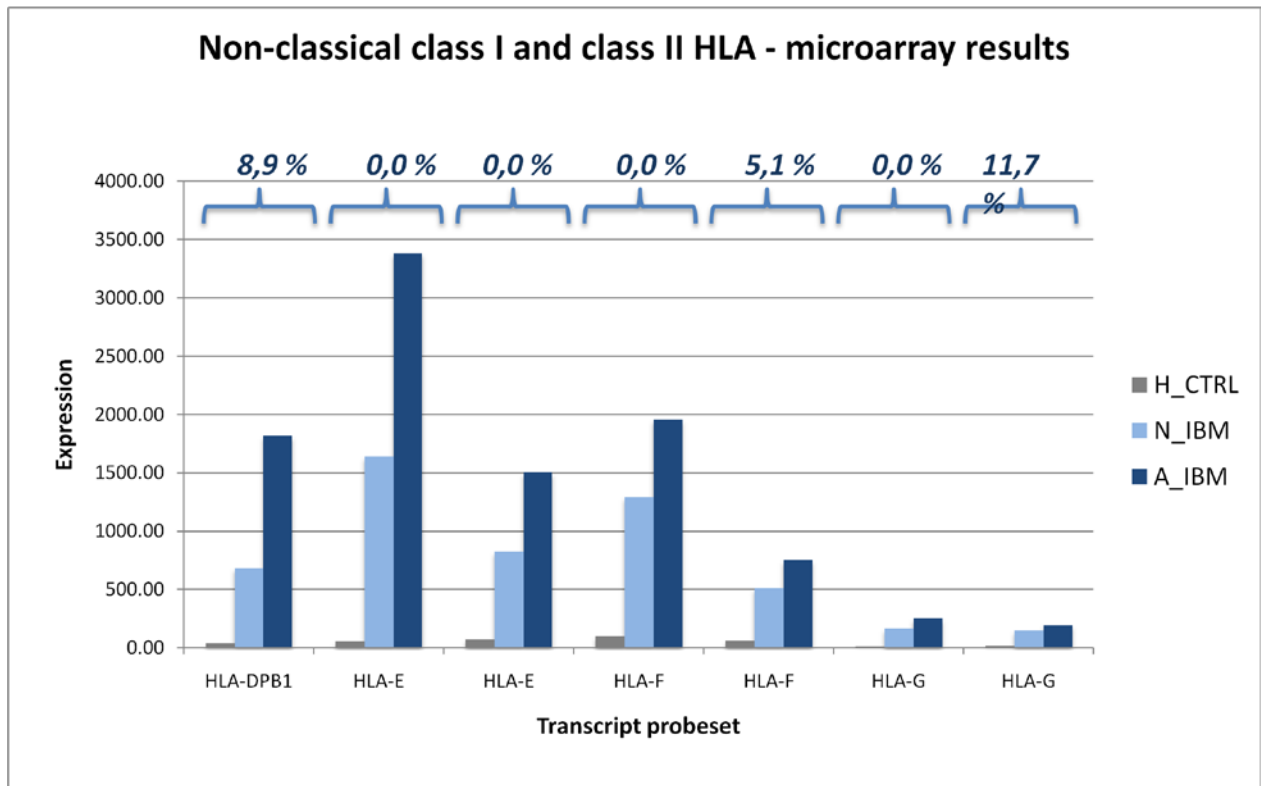


Figure 4.9: Microarray expression values of significantly regulated probesets – non-classical Class I HLA, and class II HLA transcripts. Presented here is same dataset as in Table 4.5. Expression values indicate a very strong expression of non-classical class I HLA in A_{IBM} myofibers, with a lower overexpression in N_{IBM}. The expression in H_{CTRL} myofibers is undetectable to very low. The q-values are all 20% or less (as indicated by the numbers above the brackets), indicating a high significance of the differential expression across all samples.

Two probesets of STAT1 were found to be differentially expressed with a q-value of 0%, thus being highly significant across all patients (**Figure 4.10**). STAT1 was strongly expressed in A_{IBM} and N_{IBM} and undetectable in H_{CTRL}. PSMB8, a major immunoproteasome component, was differentially regulated in A_{IBM} versus N_{IBM} (fold change = 2.86, **Figure 4.10**) with a q value of 0% as well.

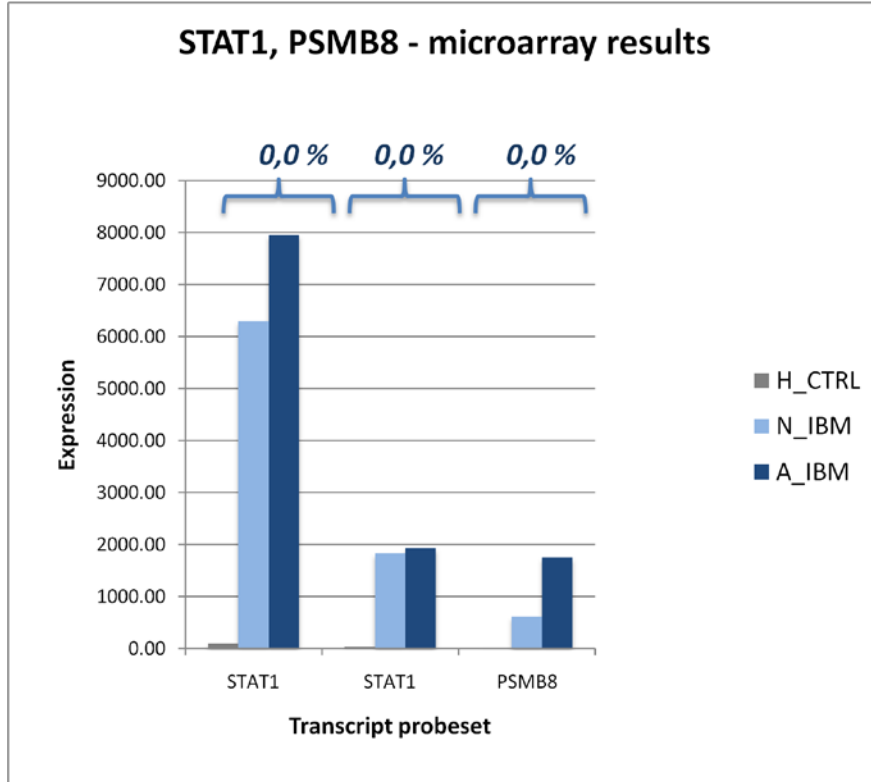


Figure 4.10: Microarray expression values of significantly regulated probesets – STAT1, and PSMB8 transcripts. Presented here is same dataset as in Table 4.5. Expression values indicate a very strong expression of STAT1 and PSMB8 in A_{IBM} myofibers, with a lower overexpression in N_{IBM}. The expression in H_{CTRL} myofibers is undetectable to very low. The respective q-values equal 0% (as indicated by the numbers above the brackets), indicating a very high significance of the differential expression across all samples.

Table 4.6 lists examples of transcripts relevant for inflammatory signaling and antigen presentation that were found to be upregulated in global microarrays from sIBM biopsies in previously published studies (Greenberg et al., 2002; Greenberg et al., 2005). The results presented in this work allow to attribute these regulation patterns to specific myofiber subsets. However, some of the transcripts had q-values > 20%, thus limiting the interpretation of these results.

Probeset ID	Gene Symbol	Results in this study (Fold increase)			Studies by other authors (Fold increase, IBM/ Healthy)
		A _{IBM} / H _{CTRL}	A _{IBM} / N _{IBM}	N _{IBM} / H _{CTRL}	
208812_x_at	HLA-C	21.69	1.43	15.19	10 to 19 (1)
221875_x_at	HLA-F	19.33	1.52	12.76	10 to 19 (1)
209480_at	HLA-DQB1	5.13	5.62	0.91	30 to 39 (1)
201137_s_at	HLA-DPB1	49.02	2.66	18.46	10 to 19 (1)
208306_x_at	HLA-DRB1	7.42	2.00	3.71	10 to 19 (1)
200887_s_at	STAT1	83.92	1.26	66.35	10 to 19 (1)
209040_s_at	PSMB8	432.37	2.86	151.40	93 (2)

Table 4.6: Comparison of results from the microarray analysis presented here to previously published microarray studies in patients with sIBM. Shown here are some of the transcripts that were previously demonstrated to be strongly upregulated in muscle biopsies from patients with sIBM versus non-diseased controls (Greenberg et al., 2002; Greenberg et al., 2005). Class I HLA, Class II HLA, as well as STAT1 and PSMB8 have previously been demonstrated as strongly upregulated. However, in this dissertation, the high upregulation of these transcripts could specifically be attributed to myofibers.

4.4 Evaluation of transcripts involved in antigen presentation and IFN γ -induced signaling by means of TaqMan quantitative PCR

4.4.1 TaqMan quantitative PCR analysis confirms global HLA-I upregulation in sIBM myofibers

The microarray dataset was confirmed and expanded by quantitative PCR. Amplified RNA from laser-microdissected A_{IBM}, N_{IBM} and H_{CTRL} myofibers was analyzed using TaqMan quantitative PCR. Relative expression values were calculated for all TaqMan results using the $2^{-\Delta CT}$ method (Schmittgen and Livak, 2008; Livak and Schmittgen, 2001a). A detailed explanation of TaqMan quantitative PCR analysis using the $2^{-\Delta CT}$ method can be found in methods section 3.3.12.

All members of the HLA-I class family were found to be overexpressed in AIBM compared to HCTRL myofibers (Figure 4.11). These results correspond with the microarray data presented in section 4.3.2 and with previously published immunohistological studies, and support the overall validity of the experimental approach presented here. Moreover, HLA-I were also upregulated in NIBM myofibers, confirming the ubiquitous upregulation previously seen on the protein level by immunohistochemistry (Karpati et al., 1988).

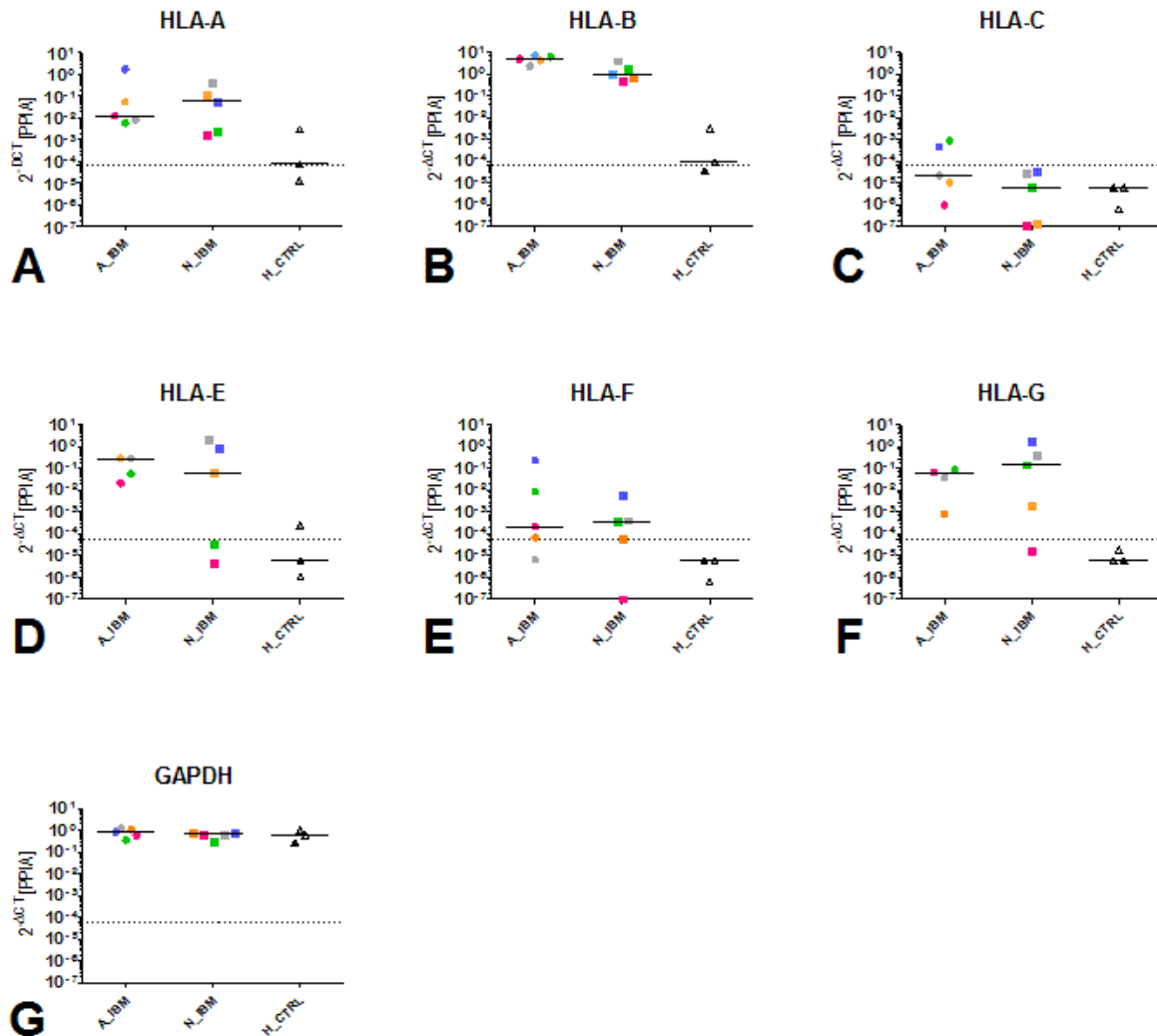


Figure 4.11: Comparison of transcript levels of Class I HLA and controls in attacked, non-attacked and healthy control myofibers using TaqMan Quantitative PCR (*legend continued on next page*).

Figure 4.11 (continued): Relative expression values were calculated using the $2^{-\Delta CT}$ method with PPIA (cyclophilin) as endogenous control. Each symbol represents the mean of triplicate experiments carried out on one sample. Five A_{IBM} samples (circles), five N_{IBM} samples (squares), and three H_{CTRL} samples (triangles) were included in the study. Colors correspond to individual patients (IBM-1, pink; IBM-2, green; IBM-3, grey; IBM-4, blue; IBM-5, yellow) and controls (C-1, white; C-2, grey; C-3, black) and medians are shown for each subset. The dashed line indicates the detection limit. **(A)** HLA-A, **(B)** HLA-B, **(C)** HLA-C, **(D)** HLA-E, **(E)** HLA-F, **(F)** HLA-G, **(G)** GAPDH. Data of HLA-E and -G from A_{IBM} of patient 4 were out of range (> 100) and are omitted here. HLA-A and HLA-B were strongly upregulated in both attacked and non-attacked sIBM myofibers. The non-classical HLA, namely HLA-E, HLA-F and HLA-G, displayed a pattern similar to that of HLA-A and HLA-B. GAPDH was used as an additional endogenous control. As expected, its expression pattern largely mirrors that of PPIA in that it is unchanged in all samples.

4.4.2 Differential regulation of IFN γ downstream effector transcripts

As described in section 4.3.2, a number of IFN- γ inducible molecules were found to be differentially upregulated in A_{IBM} versus N_{IBM} and H_{CTRL} myofibers. To determine the susceptibility of myofibers to IFN γ , the expression of both chains of the IFN γ receptor (IFNGR), as well as its major downstream mediator STAT1 was analyzed in A_{IBM} versus N_{IBM} and H_{CTRL} myofibers with TaqMan qPCR. Both IFNGR1 and IFNGR2 were upregulated in A_{IBM} . In N_{IBM} and H_{CTRL} myofibers, the expression of both IFNGR chains ranged below detection limit in the majority of cases (**Figure 4.12 A, B**). STAT1 was upregulated in A_{IBM} and below detection limit in N_{IBM} and in H_{CTRL} (**Figure 4.12 C**). Two other major downstream effector proteins of IFN γ , the immunoproteasome subunit PSMB8 (Kloetzel, 2001) and the Class II transactivator (CIITA) (van den Elsen et al., 2004) were upregulated in A_{IBM} compared to N_{IBM} and H_{CTRL} (**Figure 4.12 D, E**).

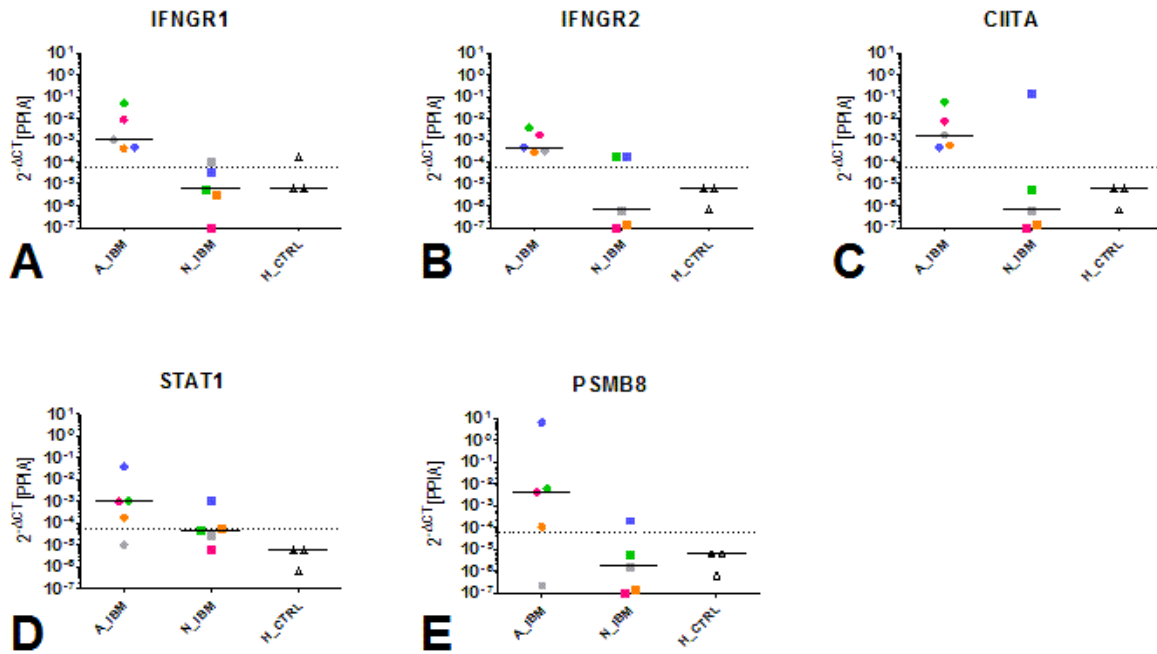


Figure 4.12: Comparison of transcript levels of IFNGR downstream signaling molecules and class II HLA in attacked, non-attacked and healthy control myofibers using TaqMan Quantitative PCR. Colors and symbols correspond to the legend explanation provided in **Figure 4.11**. Relative expression values were calculated as described. (A) IFNGR1, (B) IFNGR2, (C) STAT1, (D) PSMB8, (E) CIITA.

Next it was investigated whether upregulation of the IFN γ cascade leads to effective HLA-II induction in A_{IBM}. The expression of the respective α - and β -chains of HLA-DR, HLA-DP and HLA-DQ was analyzed. HLA-DRA and HLA-DRB were overexpressed in A_{IBM} in comparison to N_{IBM} and H_{CTRL} myofibers (**Figure 4.13 A, B**). The difference in overexpression between A_{IBM} and N_{IBM} was less striking in the case of HLA-DPA and HLA-DPB, however, there was the same tendency as in the DR transcripts (**Figure 4.13 C, D**). HLA-DQA and HLA-DQB showed a similar tendency, however with lower expression levels (**Figure 4.13 E, F**). Interestingly, in one of the patients (patient IBM-4) the levels of STAT1, PSMB8 and CIITA were significantly higher compared to the other patients, reflecting an inter-patient variability that is not surprising in a cohort of sIBM patients.

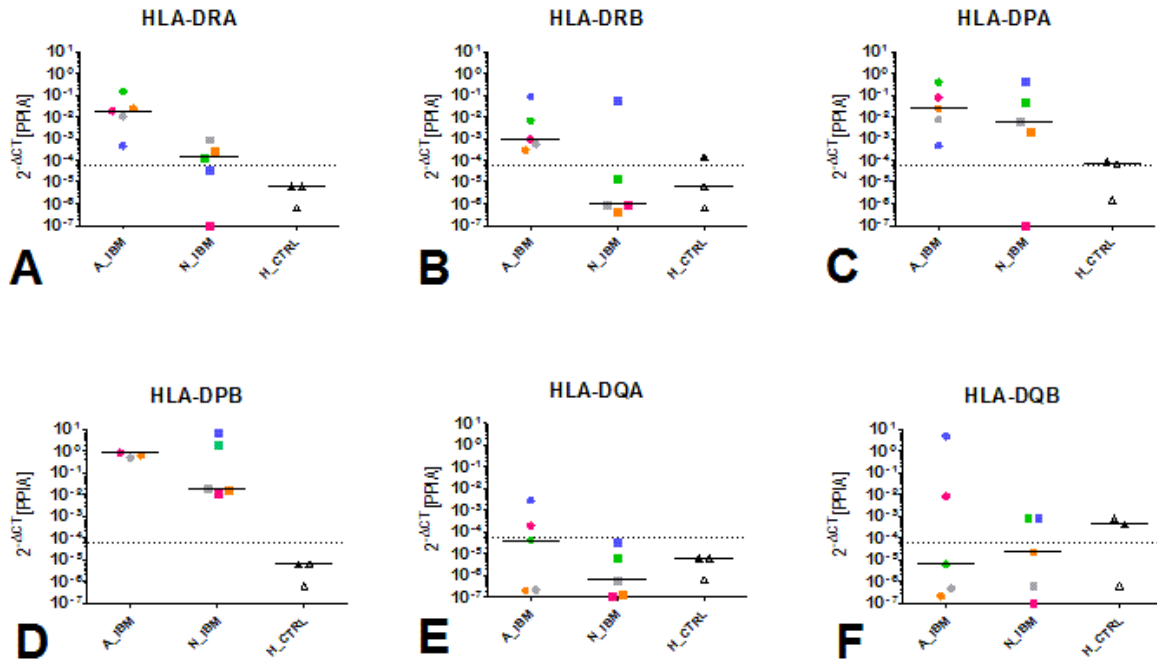


Figure 4.13: Comparison of transcript levels of class II HLA in attacked, non-attacked and healthy control myofibers using TaqMan Quantitative PCR. Colors and symbols correspond to the legend explanation provided in **Figure 4.11**. Relative expression values were calculated as described. (A) HLA-DRA, (B) HLA-DRB, (C) HLA-DPA, (D) HLA-DPB, (E) HLA-DQA, (F) HLA-DQB.

4.5 Confocal microscopy confirms differential IFNGR2 Expression in A₁IBM versus N₁IBM myofibers

Following binding of IFN γ , IFNGR1 is internalized in a complex with STAT1, while IFNGR2, also known as the inducible chain of the IFN γ receptor, remains on the cell membrane. To evaluate IFNGR2 protein expression, cryosections from sIBM patients and controls were double-stained for IFNGR2 and CD8. Immunofluorescence microscopy demonstrated that indeed, a IFNGR2 was expressed on a subset of myofibers of patients with sIBM (**Figure 4.14**).

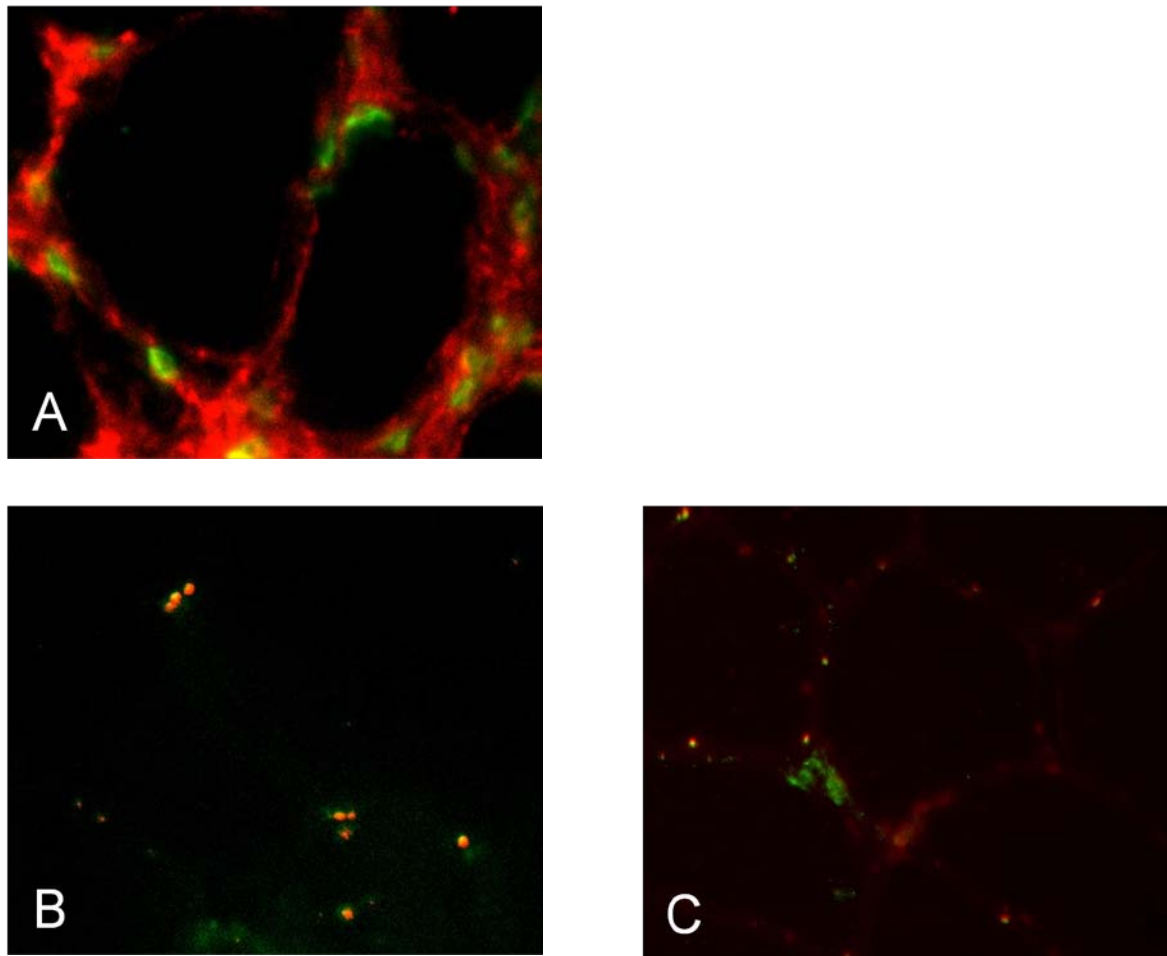


Figure 4.14: IFNGR2 expression in sIBM and healthy controls, visualized with immunofluorescence imaging. IFNGR2 (Alexa-594 in red) and CD8 (Alexa-488 in green) were stained as described in the methods section and visualized with immunofluorescence microscopy. A: A representative example from IBM patient IBM-5 is shown, demonstrating multiple CD8⁺ T cells (in yellow-green) attacking two myofibers, which appear positive for IFNGR2. The CD8⁺ T cells are positive for IFNGR2 as well. In addition to IFNGR2/ CD8 double staining of sIBM patients, technical control experiments were performed with rat Immunoglobulin G (rIgG) for anti-IFNGR2 antibody and mouse Immunoglobulin Isotype 1 (mIgG1) for anti-CD8 antibody) under identical experimental conditions (B). Biological control experiments were performed by staining muscle biopsy sections from healthy individuals in the same experiment (example from healthy control C-3, C).

As shown in **Figure 4.14 A**, myofiber membranes in sIBM were positive for IFNGR2, even though, importantly, not all myofibers expressed the same amount of IFNGR2 on their surface. However, since CD8⁺ T cells represent only a portion of the cells surrounding myofibers in

sIBM, and a number of the remaining, CD8-negative cells are likely to express IFNGR2 (e.g. macrophages), immunofluorescence microscopy made the differentiation between IFNGR-positive myofibers versus IFNGR2-positive/ CD8-negative cells surrounding the myofibers. The logical next step was therefore to examine IFNGR2 expression using confocal microscopy.

Figure 4.15 demonstrates examples of sIBM myofibers stained using the same protocol as in **Figure 4.14**, and imaged with confocal microscopy (as described in the methods, sections 3.3.5.3 and 3.3.6.2) using the highest resolution (63x objective). As shown in **Figure 4.15**, the IFNGR2 signal clearly localized to the myofiber membrane.

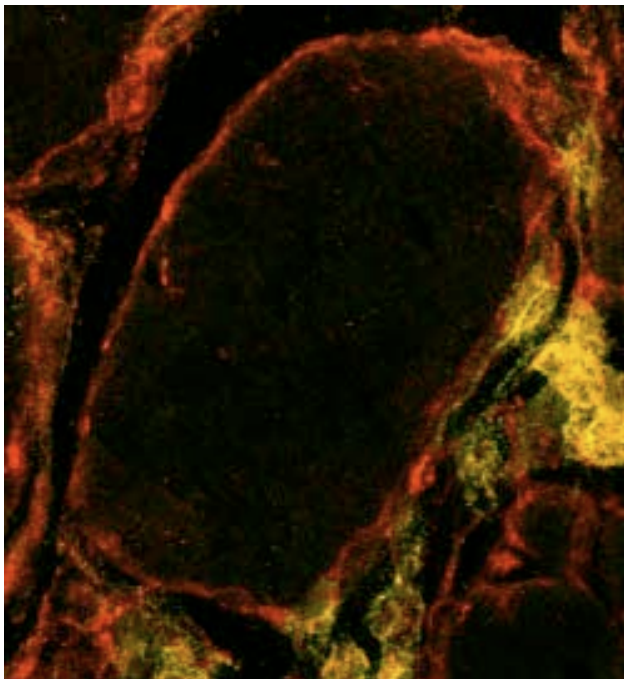


Fig. 4.15: IFNGR2 expression at the protein level in patients with sIBM. IFNGR2 (Alexa-594 in red) and CD8 (Alexa-488 in green) were stained as described in the methods section and visualized by confocal microscopy. Two CD8⁺ T cells are seen (double positive and thus visualized in yellow) in direct contact with the myofiber membrane. A number of additional CD8⁺ T cells appear in the perimysial space without establishing direct contact. The myofiber membrane is unequivocally positive for IFNGR2.

Negative control experiments were performed in the same experiment, examples shown in Figures 4.16 and 4.17.

IFNGR2 was not homogeneously distributed in sIBM biopsy samples. Some myofibers were positive for IFNGR2 along their entire surface, whereas others showed only partial, segmental membrane staining, and yet others were entirely negative. This heterogeneity of IFNGR2 surface staining was similar in all five sIBM patients included in the study (**Figure 4.16**, technical negative controls in **Figure 4.18**). By contrast, IFNGR2 was undetectable on myofibers from non-diseased controls (**Figure 4.17**).

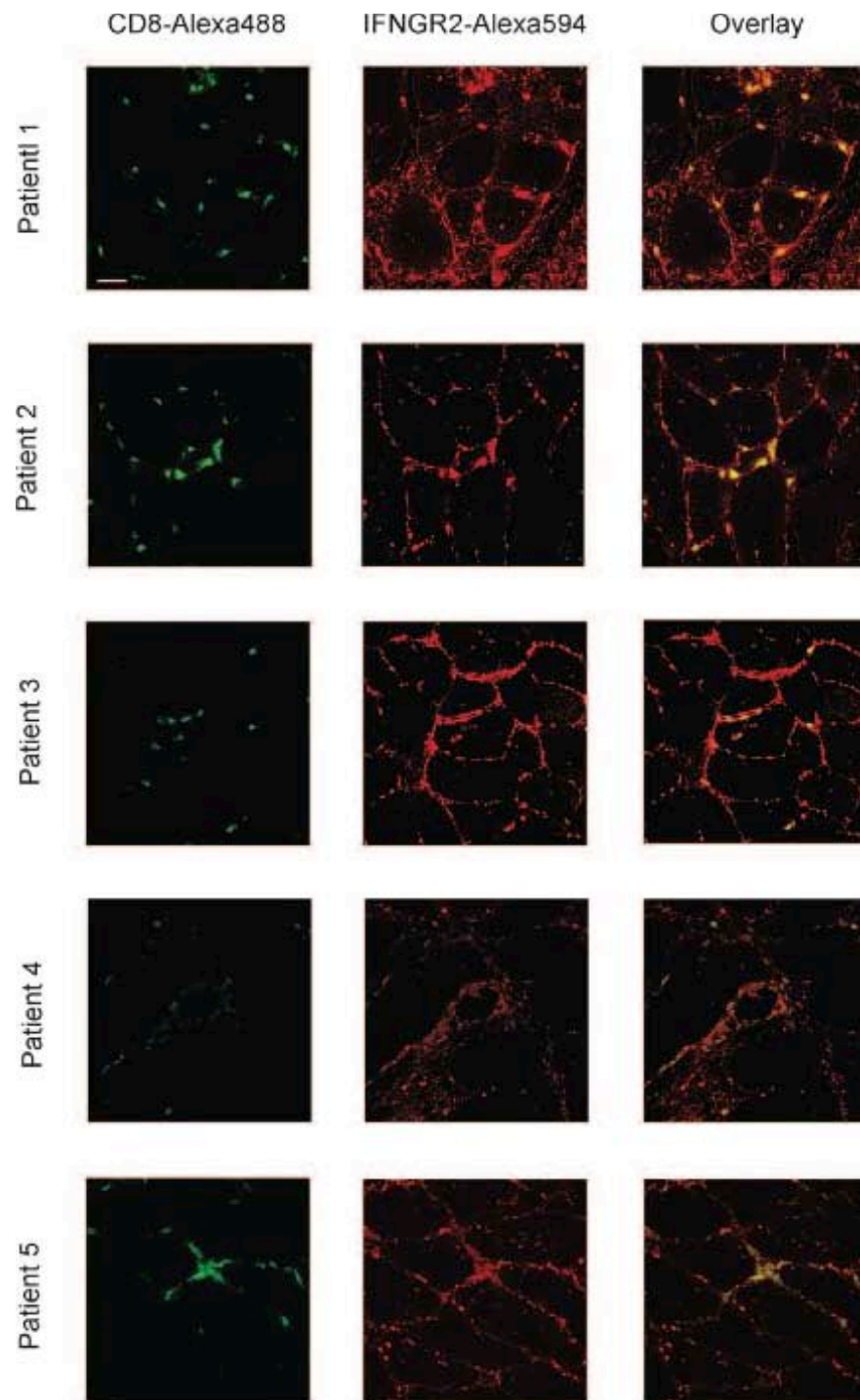


Fig. 4.16: IFNGR2 expression on the protein level in patients with sIBM. IFNGR2 (Alexa-594 in red) and CD8 (Alexa-488 in green) were stained as described in the methods section and visualized with confocal microscopy. Technical control experiments were performed with rIgG for anti-IFNGR2 antibody and mIgG1 for anti-CD8 antibody in the same experiment. Images are organized from left to right as follows: green channel (CD8), red channel (IFNGR2), overlay.

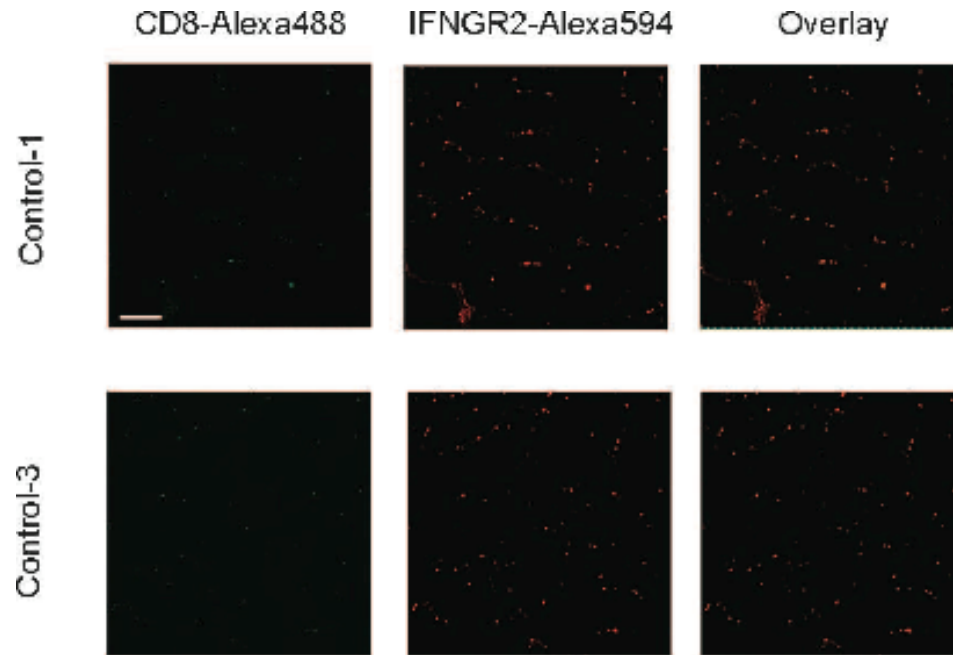


Fig. 4.17: Biological negative control experiments for the experiments described in Figure 4.10. IFNGR2 (Alexa-594 in red) and CD8 (Alexa-488 in green) were stained as described in the methods section and visualized with confocal microscopy. Biological control experiments were performed by staining muscle biopsy sections from healthy individuals under identical experimental conditions in parallel to the experiment described in Figure 4.11. Images are organized from left to right as follows: green channel (CD8), red channel (IFNGR2), overlay.

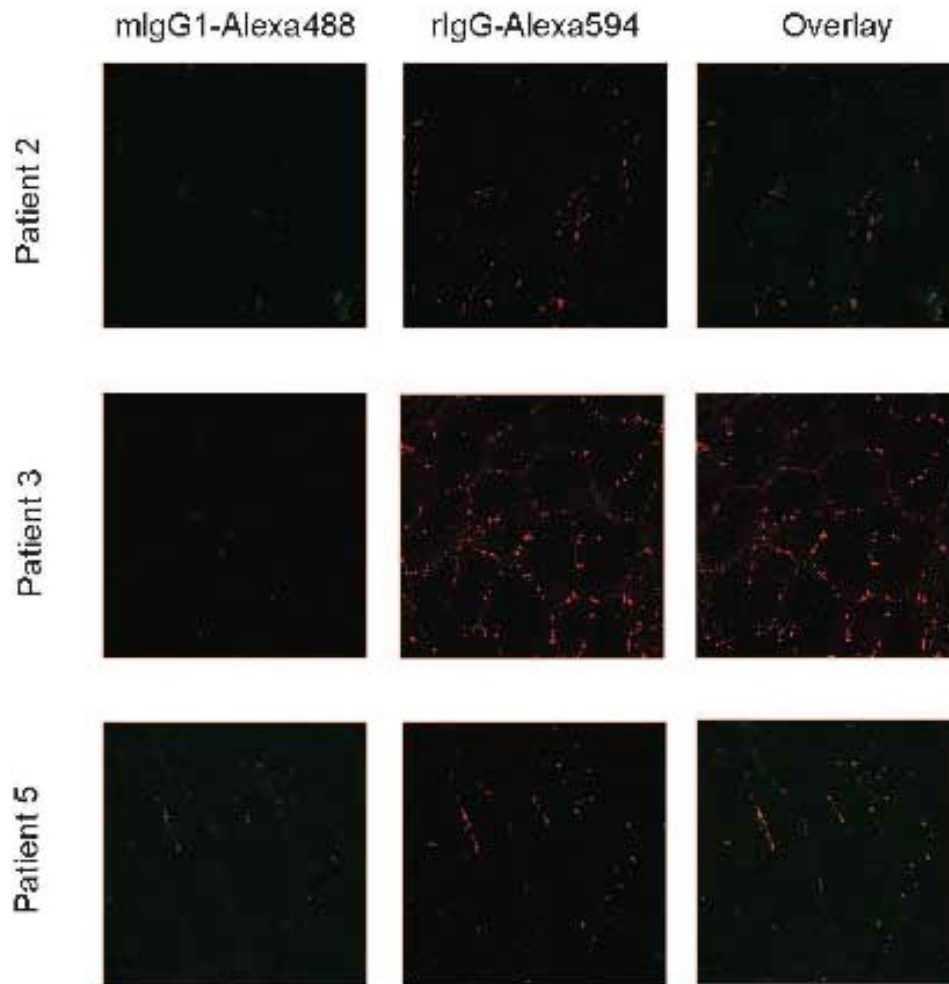


Fig. 4.18: Technical negative control experiments for the experiments described in Figure 4.10. rIgG (Alexa-594 in red) and mIgG1 (Alexa-488 in green) staining was performed as described in the methods section and visualized with confocal microscopy. Technical controls were performed by staining muscle biopsy sections from sIBM patients with rabbit Immunoglobulin G (rIgG) for anti-IFNGR2 antibody and mouse Immunoglobulin Isotype 1 (mIgG1) for anti-CD8 antibody under identical experimental conditions in parallel to the experiment described in Figure 4.11. Images are organized from left to right as follows: green channel (mIgG1), red channel (rIgG), overlay.

To investigate whether the degree of IFNGR2 expression might be related to the degree of inflammatory changes around individual myofibers, myofibers were classified into 4 groups based on IFNGR2 expression: group 1, > 80%; group 2, 50-80%; group 3, 20-50%, and group 4, < 20% surface staining (**Figure 4.19**).

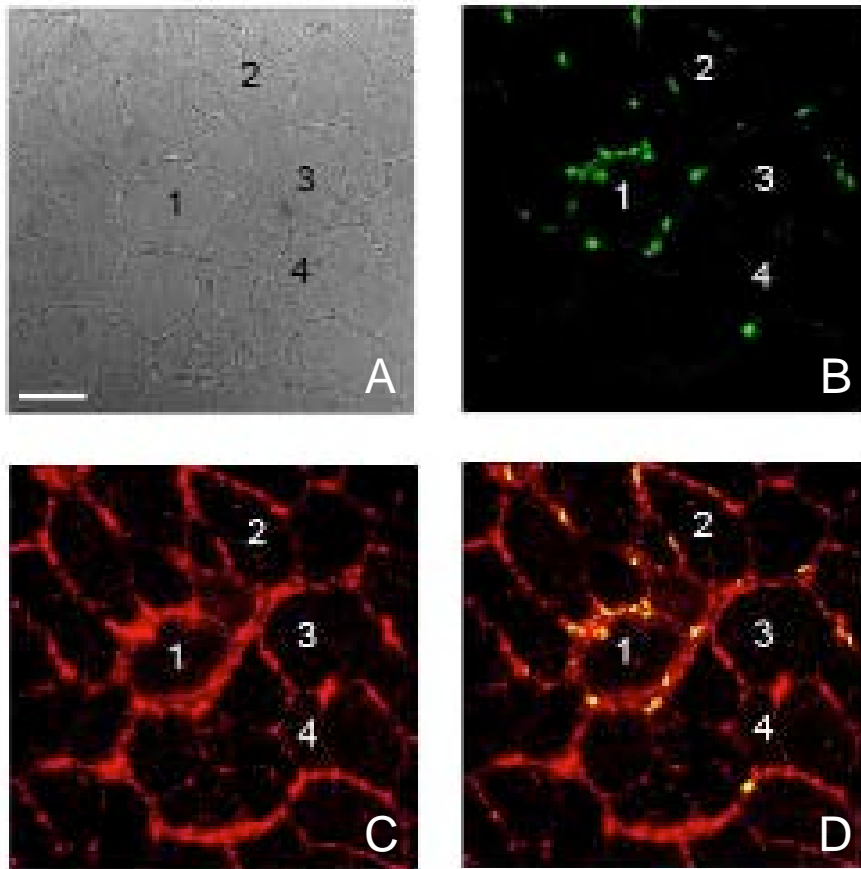


Figure 4.19: Immunohistochemistry demonstrates differential IFNGR2 expression in patients with sIBM. IFNGR2 (Alexa-594 in red, Figure C) and CD8 (Alexa-488 in green, Figure B) were stained as described in the methods section and visualized with confocal microscopy. While some myofibers were strongly positive for IFNGR2 along their entire surface, others were only segmentally positive, and yet others negative. The strongly positive myofibers were often heavily attacked by CD8⁺ T cells. Representative examples from one patient are shown. Four groups were defined according to IFNGR2 membrane positivity: Group 1 with >80% of the myofiber membrane positive for IFNGR2, Group 2 with 50-80%, Group 3 with 20-50%, and Group 4 with <20% of the myofiber membrane positive for IFNGR2. Transmission (A), green channel (CD8, B), red channel (IFNGR2, C), overlay. White scale bar, 50 μ m.

Cryosections from non-diseased control specimens stained in the same experiment were uniformly negative for IFNGR2 (as shown in **Figure 4.14 C**). For each myofiber classified as belonging to group 1 – group 4, the number of attacking CD8⁺ T cells was documented by two

independent investigators (the author (JI) and Mrs. Ingrid Eiglmeier (IE)) (**Figure 4.20**). Statistical analysis using the Mann-Whitney U-Test (methods section 3.3.14) was performed to determine whether the distributions of attacking CD8⁺ T cell numbers per myofiber in group 1 and group 4 differed significantly in all analyzed patients (as indicated by the asterisks in **Figure 4.20**). Median CD8⁺ T cell numbers in patient IBM-1 were 5 and 1 (observer IE, Mann-Whitney U = 9.5, p < 0.0001 (two-tailed)) and 6 and 1 (observer JI, Mann-Whitney U = 5.5, p < 0.0001 (two-tailed)). In patient IBM-2, median CD8⁺ T cell numbers were 4 and 0 (observer IE, Mann-Whitney U = 0, p < 0.0278 (two-tailed)) and 5 and 0.5 (observer JI, Mann-Whitney U = 0, p < 0.0223 (two-tailed)). In patient IBM-3, median CD8⁺ T cell numbers were 5 and 1 (observer IE, Mann-Whitney U = 3, p < 0.0072 (two-tailed)) and 5.5 and 1 (observer JI, Mann-Whitney U = 0.5, p < 0.0011 (two-tailed)). In patient IBM-5, median CD8⁺ T cell numbers were 6 and 0 (observer IE, Mann-Whitney U = 13, p < 0.0001 (two-tailed)) and 7 and 0 (observer JI, Mann-Whitney U = 10.5, p < 0.0001 (two-tailed)). The Mann-Whitney U-Test thus showed that the difference between group 1 and group 4 was statistically significant in all analyzed patients.

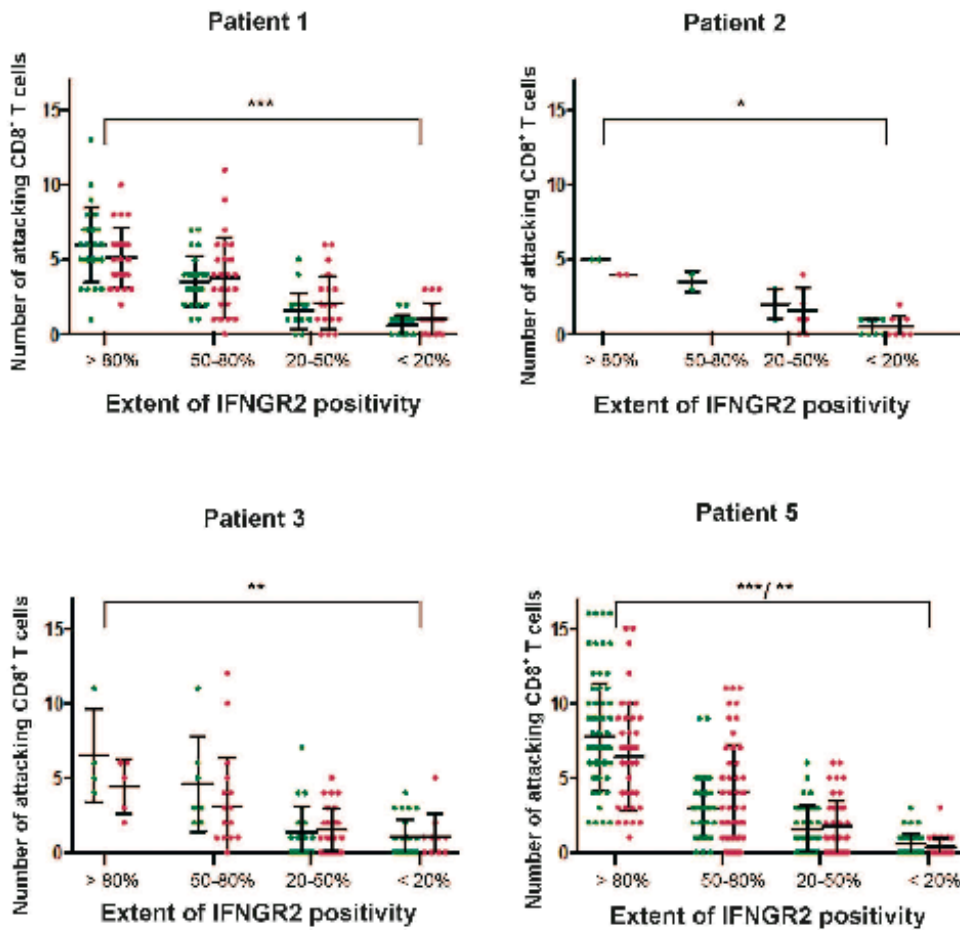


Figure 4.20: Relationship between extent of membrane positivity for IFNGR2 and number of adjacent CD8⁺ T cells. Each dot represents an individual myofiber. Each myofiber was assigned to a group according to the criteria discussed in the text and in Figure 4.19, and the number of adjacent CD8⁺ T cells was counted. In the graphs above, the number of adjacent CD8⁺ T cells was plotted against the respective group for each myofiber. Results from two independent observers (green and pink) are shown side by side. Mann-Whitney U tests were performed to determine statistical significance as illustrated by the asterisks (*** = $p < 0,0001$; ** = $p < 0,001$; * = $p < 0,01$). Patient IBM-4 was not included due to lack of material for a systematic analysis.

This analysis reveals a significant association between the density of the focal inflammatory infiltrate and the extent of IFNGR2 surface expression on a given myofiber, indicating that IFNGR2 is upregulated on myofibers by local mechanisms that can be attributed to the attacking CD8⁺ T cells (including T-cell-derived proinflammatory cytokines).

4.6 Upregulation of IFN γ - and TNF α - inducible chemokines

A number of TNF α -inducible genes were upregulated in A_{IBM} versus N_{IBM} and H_{CTRL}, albeit not reaching statistically significant q-values, The α chain of the TNF receptor, TNF-R1, showed an upregulation of 4.5-fold of A_{IBM} versus N_{IBM} as well as A_{IBM} versus H_{CTRL}, respectively. TNF α -induced protein 3 (TNFAIP3), a protein known to be dramatically induced by TNF α (Vereecke et al., 2009), showed a 2-fold upregulation of A_{IBM} versus N_{IBM} and 17-fold upregulation of A_{IBM} versus H_{CTRL}.

Since TNF α is known to induce CCL5 via STAT3 in vascular smooth muscle cells and many other non-lymphoid cell types (Kovacic et al., 2010), the transcriptional activity of the CCL5/STAT3 system was analyzed in laser microdissected myofiber subsets from patients with sIBM. Median values reflect a tendency for higher CCL5 and STAT3 expression in attacked myofibers compared to non-attacked myofibers and healthy controls (**Figure 4.21 A, B**), however, overall CCL5 and STAT3 expression was low, resulting in a considerable heterogeneity of CCL5 and STAT3 expression patterns across all patients and controls,

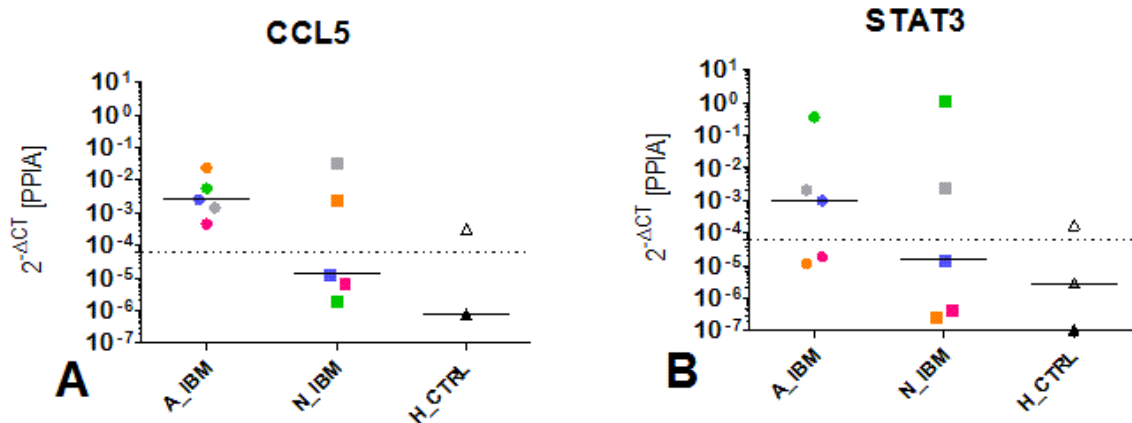


Figure 4.21: Comparison of transcript levels of CCL5 and STAT3 in attacked, non-attacked and healthy control myofibers using TaqMan Quantitative PCR. Colors and symbols correspond to the legend explanation provided in **Figure 4.11**. Relative expression values were calculated as described. While the expression levels were generally lower compared to the other transcripts, the same differential expression pattern could be observed, with attacked myofibers expressing higher levels of CCL5 and its transcription factor, STAT3, compared to non-attacked and healthy control myofibers.

Results

The microarray experiments (section 4.3.2) showed upregulation of IFN γ -inducible chemokines CXCL9 and CXCL10 in some of the samples, however, the q-values were rather high, indicating that the microarray data were not significant across all patients and controls (**Figure 4.22**)

Nevertheless, the regulation pattern indicated an upregulation of the two chemokines in A_{IBM} versus N_{IBM}.

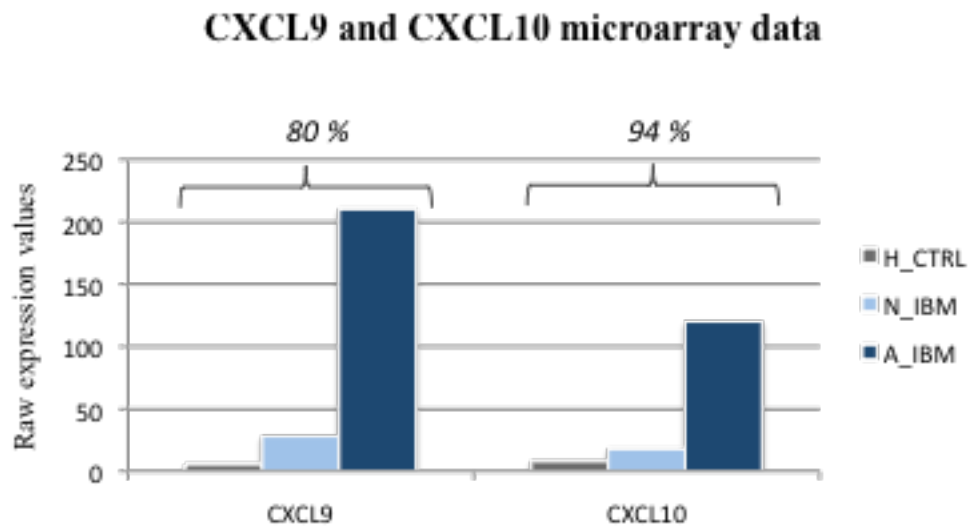


Figure 4.22: Microarray expression data of CXCL9 and CXCL10 in laser microdissected myofibers across all IBM patients and healthy controls. Raw expression values indicate a strong expression of both IFN γ -inducible chemokines in A_{IBM} myofibers only. The expression in N_{IBM} myofibers is borderline (expression values over 20 are considered present) and the chemokines are not detectable in H_{CTRL} myofibers. However, both transcripts are regulated with very high q-values of 80% and 94%, respectively (as indicated by the numbers above the brackets) and thus not significant across all samples.

TaqMan quantitative PCR was performed to investigate CXCL9 and CXCL10 mRNA expression in laser microdissected myofibers. However, in IBM patients 3 and 4 CXCL9 was not detectable by means of quantitative PCR. CXCL10 was not detectable in any of the IBM patient samples. **Figure 4.23** shows expression of CXCL9 in all IBM patients and healthy controls.

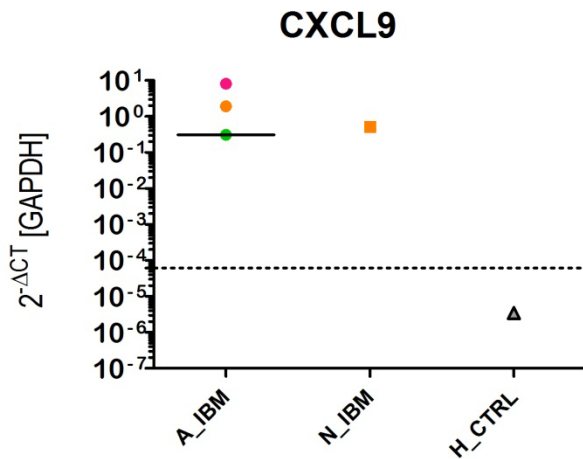


Figure 4.23: Comparison of transcript levels of CXCL9 in attacked, non-attacked and healthy control myofibers using TaqMan Quantitative PCR. Colors and symbols correspond to the legend explanation provided in Figure 4.8. Relative expression values were calculated as described. CXCL9 was only detectable in attacked myofibers from patients IBM-1, IBM-2 and IBM-5, as well as non-attacked myofibers from patient IBM-5. While not statistically significant, the data are in agreement with the differential expression pattern observed for other IFN γ -induced transcripts.

The expression of CXCL9 was further investigated on the protein level. The main difficulty when staining for chemokines is that these molecules are small and non-membrane-bound. They are therefore soluble and easily lost during a staining procedure that contains multiple washing steps. Several strategies were tested to improve chemokine staining results. The strategy that proved to be the most successful was to employ a protocol that includes steaming the cryosections in citrate buffer (methods section 3.3.5.6), a technique normally employed for the staining of paraffin-embedded tissue sections (Bradl M and Lassmann H, personal communication).

Results

The staining results definitely improved using the steaming protocol, however there was still a considerable variability between outcomes of identically performed experiments, leading to insufficient reproducibility (**Figure 4.24**).

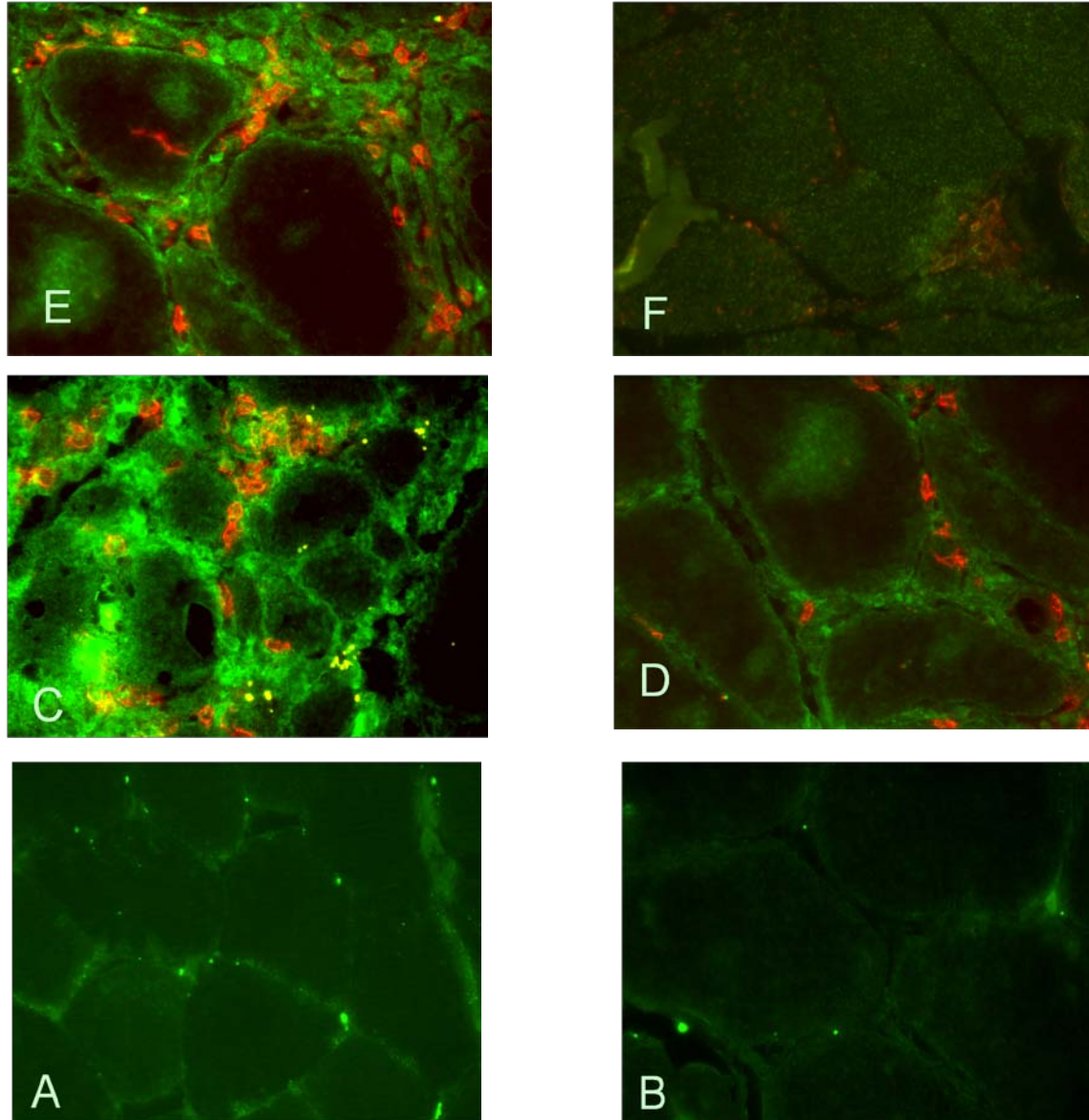


Figure 4.24 CXCL9 and CD8 double immunofluorescence staining in IBM patients. Figures C-E show examples of CXCL9-CD8 double immunofluorescence staining in IBM patient “IBM-1”; Figure F shows an example of the same staining in IBM patient “IBM-3”. These results were not reproducible in the other patients. Biological control experiments (healthy muscle stained with anti-CXCL9 antibody, as shown in Fig. A) and technical control experiments (IBM muscle treated with purified mouse IgG instead of the primary antibody, as shown in Fig. B) were performed.

CXCL9 and CXCL10 are both inducible by IFN γ , and bind to the same receptor, CXCR3 (Raju et al., 2003). It was hence interesting to investigate the expression of CXCR3 in sIBM to determine whether CXCR3 would colocalize with CD8. Double immunofluorescence staining for CXCR3 and CD8 was performed (**Figure 4.25**).

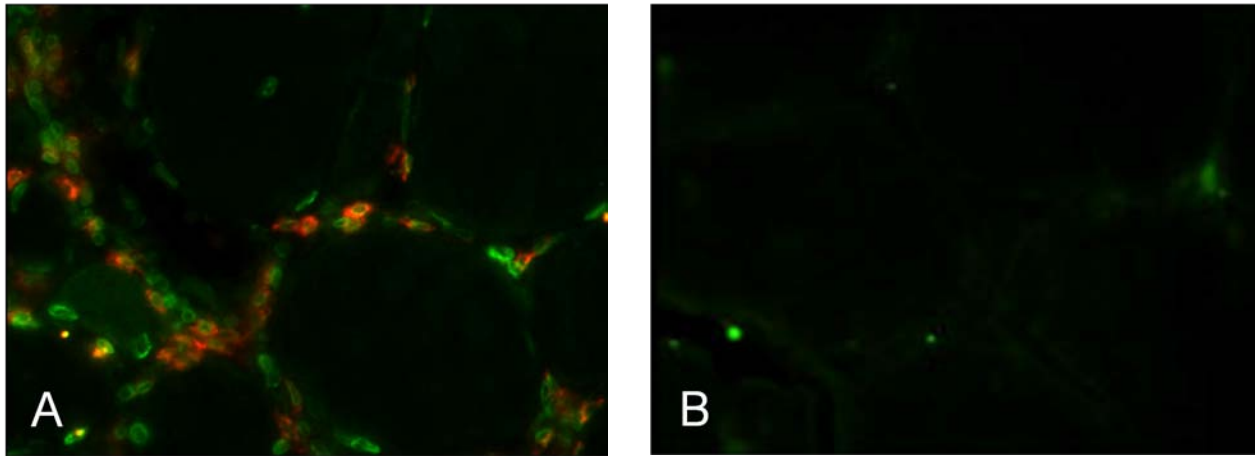


Figure 4.25: CXCR3 expression in sIBM lesions. Immunofluorescent staining was performed in sIBM patient 19116 (IBM-1) to colocalize CXCR3 (antibody labeled with Alexa-488, in green) and CD8 (antibody labeled with Cy-3, in red) (Figure A). Myofibers are seen surrounded by autoaggressive CD8⁺ T cells, as previously discussed. As expected, myofibers do not express CXCR3. The CD8⁺ T cells appear to be positive for CXCR3, underlining the importance of the chemoattractive properties of IFN γ -inducible CXCL9 and CXCL10. However, numerous cells are seen that are not CD8⁺, however do carry CXCR3 on their surface. Figure B shows a negative control experiment performed with Alexa-488-labeled mIgG2a on the same IBM patient.

4.7 Upregulation of class II HLA on the protein level

Immunofluorescent detection of HLA-II was attempted on the protein level. To detect HLA-II on the protein level, an antibody was used which recognizes HLA-DR, -DP, and DQ.

As illustrated in **Figure 4.26**, myofibers that were attacked by CD8⁺ T cells were strongly immunoreactive for HLA-II. This confirms the Taqman qPCR results (**Figure 4.13**) which demonstrated overexpression of HLA-DR, -DP and -DQ in attacked myofibers.

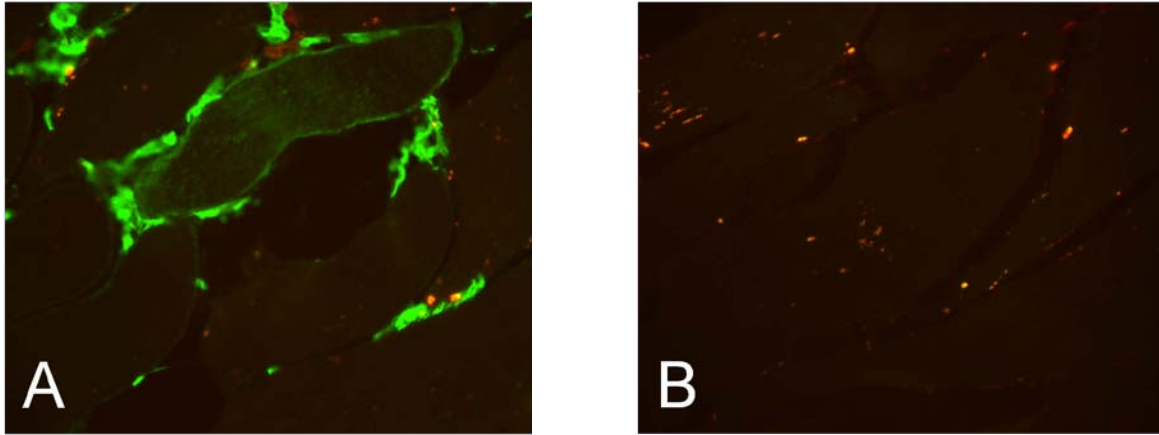


Figure 4.26: Colocalization of HLA-II (HLA-DR/-DP/-DQ) and CD8 in sIBM patient 2 (IBM-2). Figure A, myofibers attacked by CD8⁺ T cells (visualized with Cy3 in red) are strongly positive for HLA-II (visualized in green). In addition, there are numerous HLA-II⁺, CD8⁻ cells surrounding the myofibers. Figure B shows a negative control experiment performed with Alexa-488-labeled mIgG2a on the same IBM patient.

4.8 Upregulation of CIITA on the protein level

The detection of CIITA using immunofluorescence staining posed a very challenging task because of the presumed intracellular and intranuclear location of CIITA. A new protocol was established to account for the necessity of intranuclear staining. Sections were subjected to permeabilization with Triton X before incubation with the antibody as described in methods section 3.3.5.4.

Given the intranuclear localization of CIITA, it was necessary to visualize myofiber nuclei. For that purpose, DAPI (4',6-diamidino-2-phenylindole) was added to the protocol. As illustrated in **Figure 4.27**, CIITA staining was detectable in myofiber nuclei, co-localizing with DAPI. There was also a heterogeneously distributed positive cytoplasmic CIITA signal. A systematic evaluation of CIITA protein expression was not performed due to the difficulty of CIITA trafficking between the myofiber cytoplasm and nuclei.

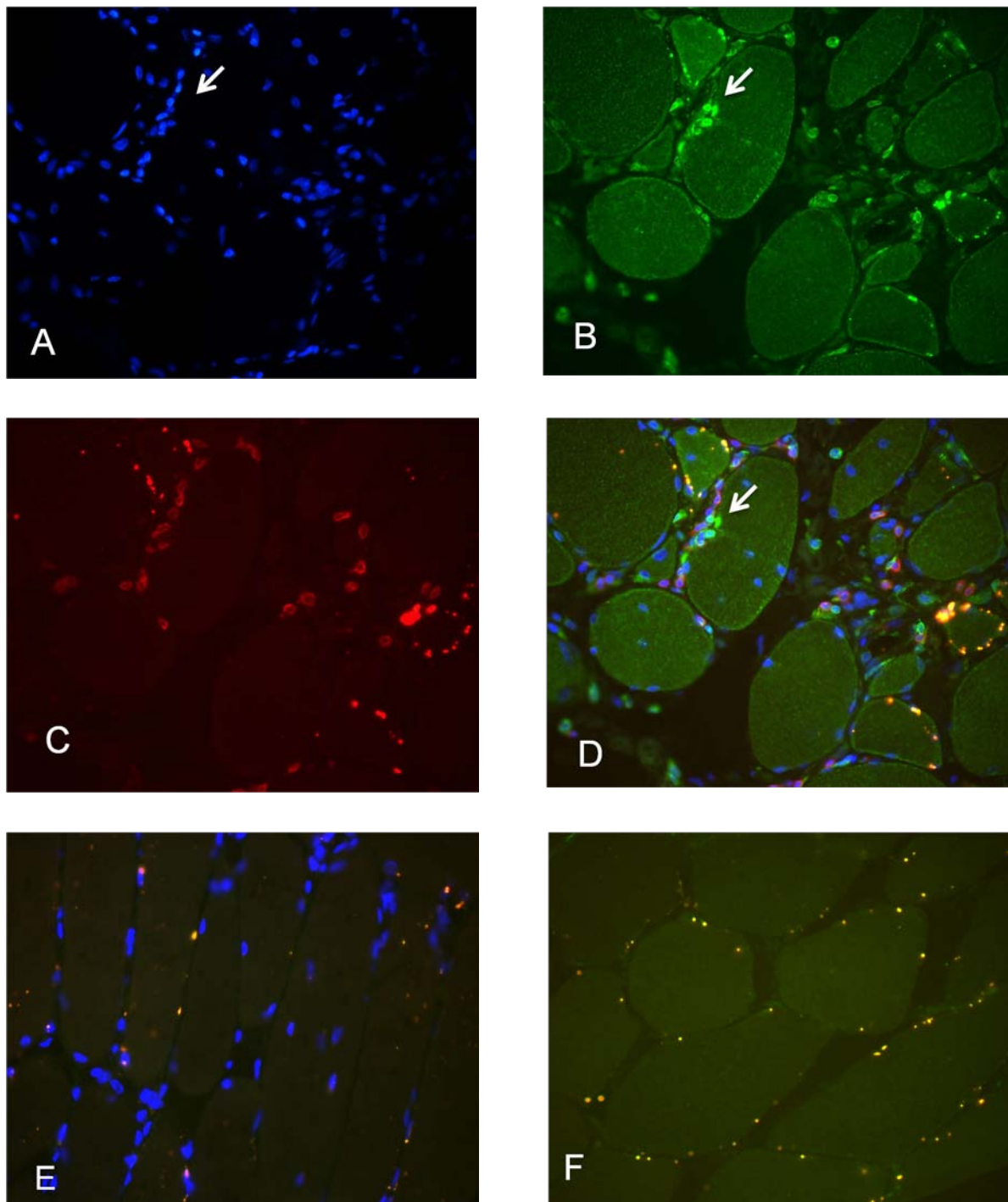


Figure 4.27: Colocalization of CIITA, CD8 and DAPI in sIBM patient 1 (IBM-1, Figure A-E) and healthy control C-1 (Figure F). Triple immunostaining of IBM-1 for nuclei (visualized with DAPI in blue, A), CIITA (visualized with Alexa488 in green, B) and CD8 (visualized with Cy3 in red, C). Overlay, D. Intranuclear staining could be used to detect individual myofibers with CIITA-positive nuclei (arrow) that were attacked by CD8⁺ T cells. E shows a technical control experiment (staining with isotype control antibodies of IBM-1). F, biological control experiment (C-1 double-immunostained for CD8 and CIITA in a parallel experiment).

4.9 RER1 – a novel candidate biomarker in sIBM and other amyloid-associated diseases

4.9.1 Microarray results indicate highly significant regulation of RER1 across all samples

The microarray analysis performed on laser microdissected A_{IBM}, N_{IBM} and H_{CTRL} myofibers was not hypothesis-driven. Rather, a global gene expression analysis comprising over 50,000 transcript probesets was carried out. The main focus of the research discussed in section 4.2 was centered on the regulation of proteins involved in the inflammatory response, in particular in antigen processing and presentation. After completion of this project, the microarray data were re-evaluated for other genes that were highly regulated across all patients and controls (i.e. such transcripts that had a low q-value of less than 20%). As illustrated in **Table 4.5**, a particularly striking example turned out to be the transcript RER1 (Retention in endoplasmic reticulum 1 (*S. cerevisiae*)) (**Figure 4.28**). While RER1 expression was remarkably high in all three healthy control samples, RER1 was downregulated below detection limits in all five patients with sIBM. As indicated by the strikingly low q-value of 0% (section 3.3.11), this result was mirrored in all five sIBM patients and all three healthy controls analyzed. This prompted a detailed investigation of RER1 expression in sIBM as well as other inflammatory and degenerative myopathies on the mRNA and the protein level.

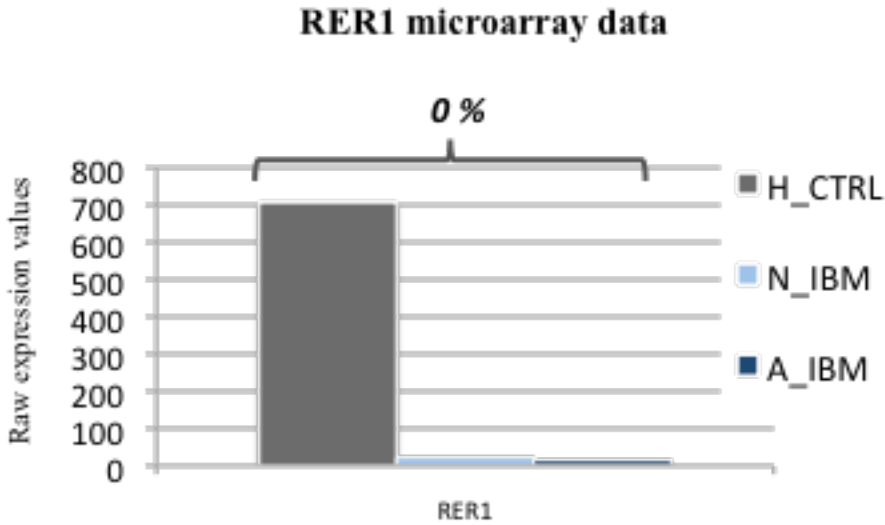


Figure 4.28: Raw microarray expression values of RER1 in laser microdissected myofibers across all IBM patients and healthy controls. Presented here is same dataset as in **Table 4.4**. Expression values indicate a very strong expression of RER1 in H_{CTRL} myofibers only. The transcript is undetectable in both A_{IBM} and N_{IBM} myofibers (expression values over 20 are considered present). The q-value is strikingly low with 0% (as indicated by the number above the bracket), rendering this result highly significant across all samples.

RER1 is the ubiquitously expressed human homolog of the *Saccharomyces cerevisiae* gene called “Retention in endoplasmic reticulum 1” and plays a role in the assembly of γ -Secretase, the key enzyme responsible for the biosynthesis of β -amyloid (Kaether et al., 2007). The highly significant downregulation of RER1 in IBM seen in laser microdissected myofibers initiated further investigation of RER1 mRNA and protein levels in sIBM and other myopathic disorders. Given the unique features of sIBM as being not only an inflammatory, but also a degenerative disease with β -amyloid deposition within myofibers, and given the potential role of RER1 in β -amyloid biosynthesis, the expression of RER1 was further analyzed. As discussed in section 5.2.2, RER1 downregulation might be an early, sensitive marker for sIBM diagnosis, as well as in differentiating “pure PM” versus “PM/ sIBM” versus “pure sIBM” (Chahin and Engel, 2008). This is particularly important given that PM may not be a standalone entity, but rather an early form of sIBM (van der Meulen et al., 2003; Amato et al., 1996; van der Meulen et al., 1998; Chahin and Engel, 2008) (section 1.3, section 5.2.2).

Given the physiological ubiquitous expression of RER1 (Yanai et al., 2005) a downregulation specific to myofibers most likely would be expected to manifest itself in an altered immunofluorescence staining pattern. Thus, staining was established for RER1 on muscle tissue cryosections; in addition to a TaqMan quantitative PCR protocol.

The evaluation of RER1 expression was approached in a clinically oriented manner, including normal and diseased controls. Eight healthy individuals, six patients diagnosed with PM, three patients diagnosed with “PM/sIBM”, nine patients diagnosed with sIBM, three patients diagnosed with DM, two patients diagnosed with MFM, and two patients diagnosed with DMD were included in the study (details are provided in **Table 3.2**, section 3.1).

4.9.2 RER1 protein expression patterns in inflammatory and degenerative myopathies compared with non-diseased controls

To detect RER1 protein expression in muscle biopsy cryosections, a staining protocol optimized for the available antibody (polyclonal rabbit-anti-human RER1, Sigma) was established as described in the methods section (**Table 3.8**, section 3.3.5.8).

Once the protocol was established, and a number of diseased and non-diseased samples were examined, a RER1 expression scoring system was developed differentiating three principal RER1 staining patterns (**Figure 4.29**): 1.) a pattern where most myofibers were strongly positive for RER1 (**Figure 4.29 A**); 2.) an intermediate pattern (**Figure 4.29 B**); and 3.) a pattern where most myofibers were negative for RER1 (**Figure 4.29 C**).

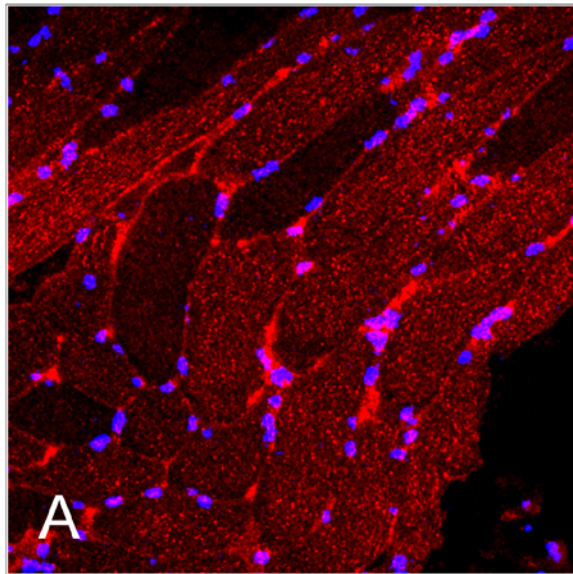
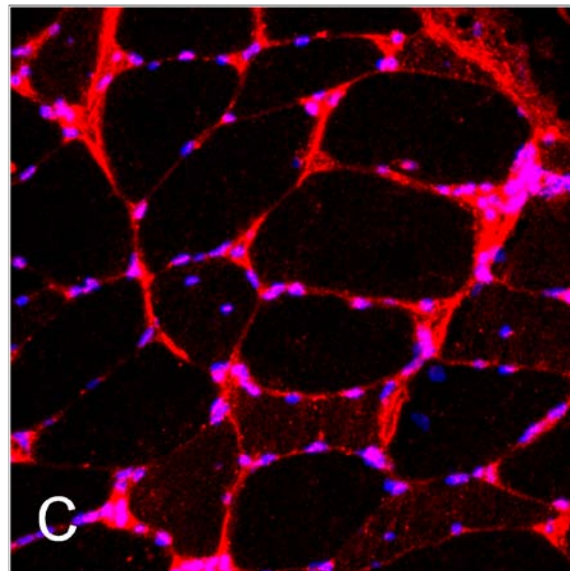
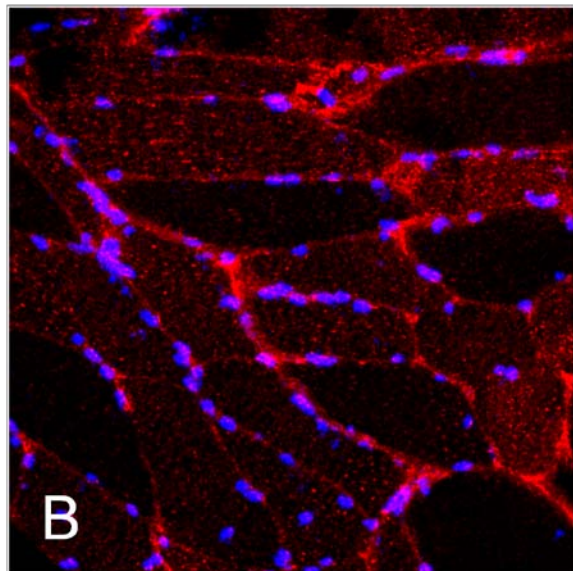


Figure 4.29: Establishment of a scoring system for RER1 expression according to RER1 staining patterns of axially cut myofibers. RER1 was visualized using a rabbit-anti-human RER1 unlabeled primary antibody and a goat-anti-rabbit secondary antibody labeled with Alexa-594 (red). Nuclear staining is visualized in blue using DAPI. Three principal RER1 staining patterns could be defined. 1.) a pattern where most myofibers were strongly positive for RER1 (A); 2.) an intermediate pattern (B); and 3.) a pattern where most myofibers were negative for RER1 (C).



After developing the scoring system outlined in **Figure 4.29**, six colleagues at the Department of Neuroimmunology of the Max Planck Institute of Neurobiology who were not involved in this project were presented with a total of 34 cases comprising sIBM, PM, PM/IBM, DM, Duchenne's muscular dystrophy (DMD), and normal controls (details are provided in **Table 3.2**, section 3.1), and asked to score all cases presented to them in a blinded fashion, i.e. the scorers did not know what disease entities they were evaluating. (examples shown in **Figures 4.30 to**

4.32) The scoring results were then evaluated for coherence and statistical significance, i.e. how well the score could discriminate between different disease entities.

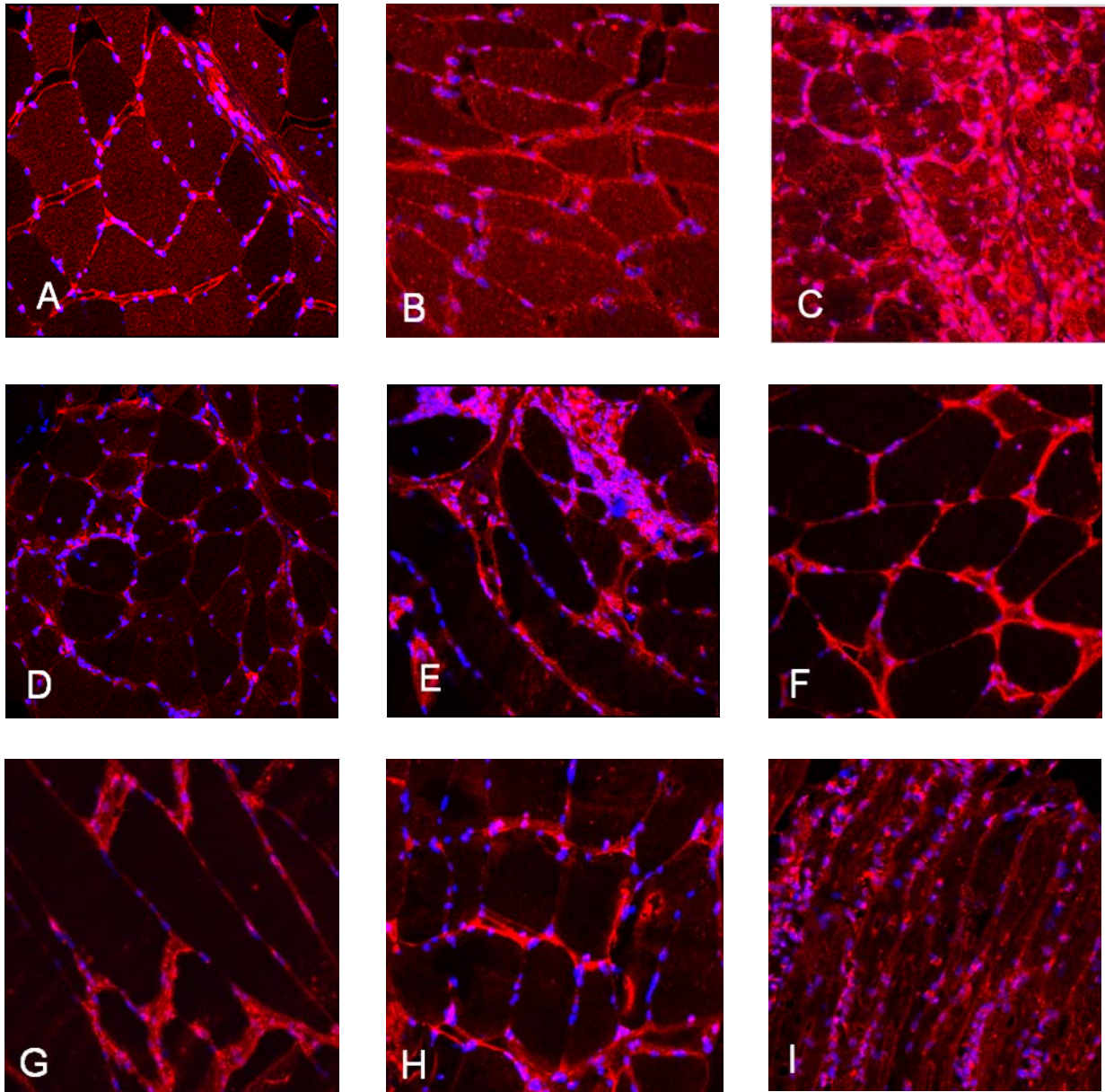


Figure 4.30: RER1 staining patterns in healthy and diseased muscle (part I). Muscle biopsy cryosections were stained for RER1 as described in the methods section. Nuclei were visualized with DAPI. Shown here are examples from non-diseased controls (A: 19400; B: 20350), patients with DM (C: 20589), patients with IBM (D: 27453; E: 18592), a patient with PM/IBM (F: 17336), patients with MFM (G: 22874; H: 23687); and a patient with DMD (I: 22208)

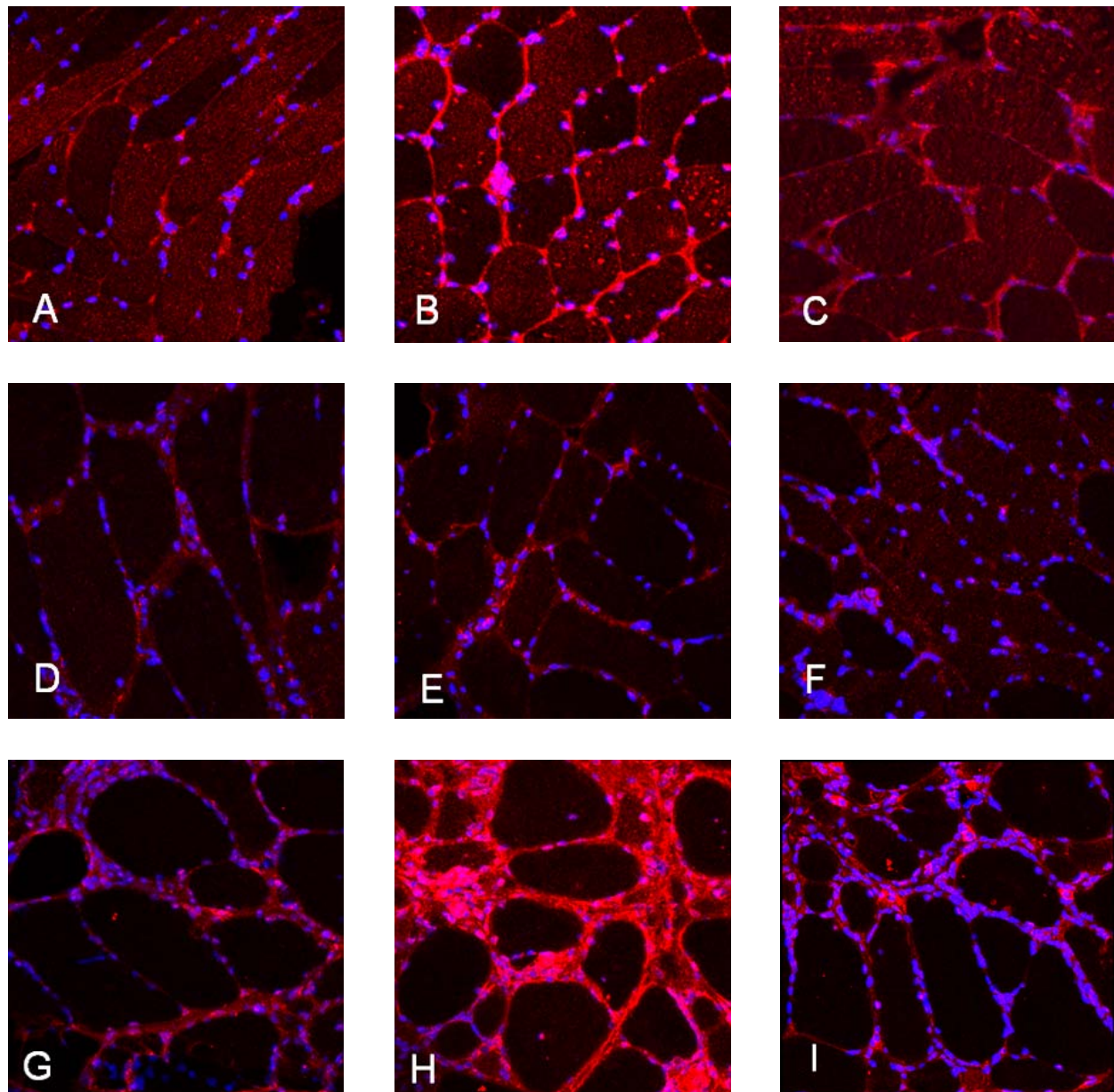


Figure 4.31: RER1 staining patterns in healthy and diseased muscle (part II). Muscle biopsy cryosections were stained for RER1 as described in the methods section. Nuclei were visualized with DAPI. Shown here are examples from non-diseased controls (A: 20387; B: 20239, C: 20059), patients with PM (D: 15701, E: 17936, F: 16288), and patients with IBM (G: 27464; H: 19116; I: 27525).

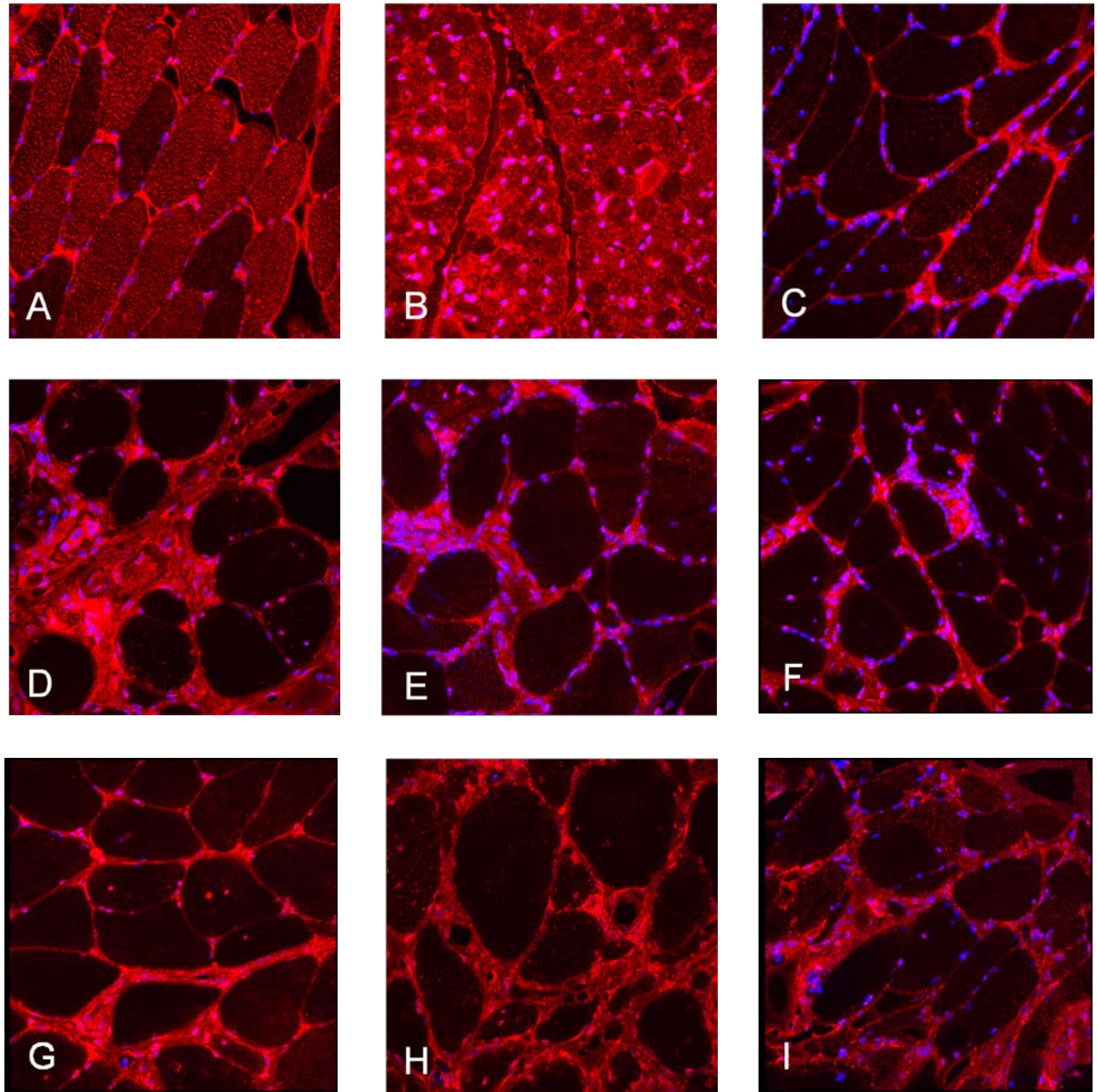


Figure 4.32: RER1 staining patterns in healthy and diseased muscle (part III). Muscle biopsy cryosections were stained for RER1 as described in the methods section. Nuclei were visualized with DAPI. Shown here are examples from a non-diseased control (A: 10804), a patient with DM (B: 27416), patients with PM (C: 16093; D: 15876; E: 18495), patients with PM/ IBM (F: 18747; G: 16646), and patients with IBM (H: 15551; I: 19142).

As shown in **Figure 4.33**, the coherence across the six scorers was very high, with very low standard error of the mean (SEM) values in each disease group. The mean score for both healthy controls and DM was 1 according to the system presented in **Figure 4.29**. The mean score for DMD was 1.5. The mean score for PM was 2.5. The mean score for “PM/IBM” was 3, and the mean score for IBM was 2.7.

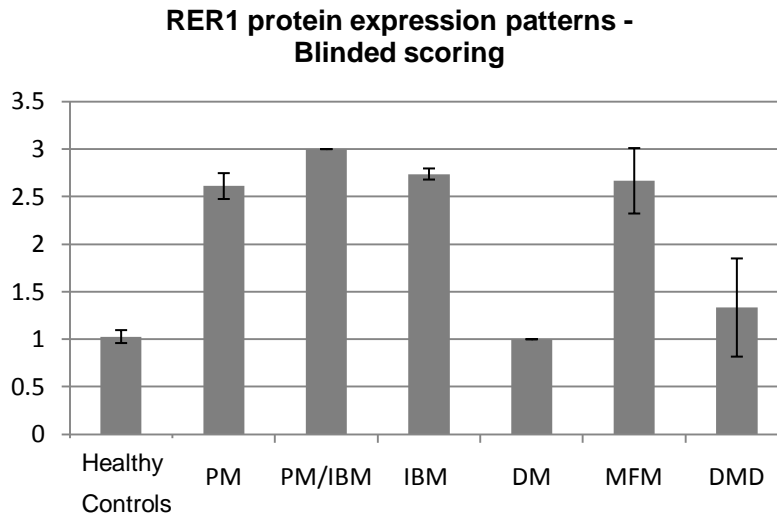


Figure 4.33: Blinded scoring results for RER1 staining patterns of 34 patients. Six researchers not involved in this project were presented with the scoring system outlined in Figure 4.29, based on which a muscle cross-section RER1 staining was to be rated with a score of 1 if most of the myofibers seen were RER1-positive, a score of 3 if most of the myofibers seen were RER1-negative, and a score of 2 in intermediate cases. The score for each evaluated disease group is shown on the y-axis, whereas the x-axis delineates the disease groups as described in the text.

Thus, healthy control myofibers and DM myofibers showed equally high RER1 expression. On the other hand, PM myofibers did not significantly differ from PM/IBM and IBM samples, in all cases the RER1 expression was very low to undetectable. This was also true for MFM. In DMD, the variability was the highest, due to the typical morphology of DMD myofibers, where it can be difficult to distinguish myofiber borders.

4.9.3 Analysis of RER1 mRNA expression in inflammatory and degenerative muscle diseases compared to non-diseased controls

Total RNA was isolated from each biopsy sample as described in the methods section 3.3.8.1. cDNA synthesis was performed following the protocol described in the methods section 3.3.12. TaqMan quantitative PCR was performed as described in methods section 3.3.13. As shown in **Figure 4.34**, median expression levels were highest in healthy controls and DM, and lowest in PM/IBM, IBM and MFM. In PM, there was a very strong heterogeneity in RER1 expression, resulting in a median expression level in the same range as control and DM samples. This however, mainly stemmed from two patient samples which yielded expression values considerably higher than all other samples (two outliers seen in **Figure 4.34**). Had the two outliers not been included in the analysis, the PM group would have yielded a much lower median RER1 expression ranging only slightly above the expression of RER1 in the PM/IBM, IBM, and MFM groups.

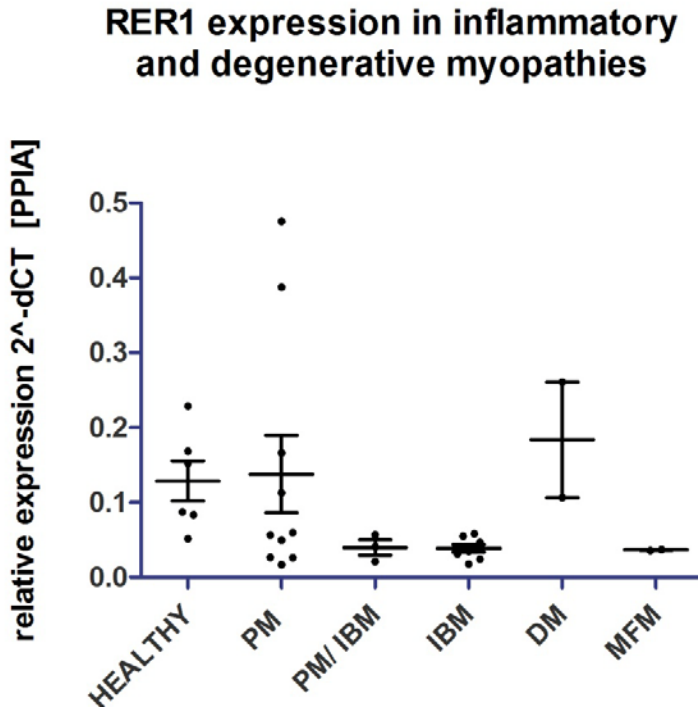


Figure 4.34: RER1 mRNA expression levels in all patients and controls. Relative expression values were calculated using the $2^{-\Delta CT}$ method with PPIA (cyclophilin) as endogenous control. Each circle represents the mean of triplicate experiments carried out on one individual. Medians are shown for each disease group. In accordance with the protein expression results, the control group and the DM group demonstrated high RER1 expression, while RER1 expression was low in PM/IBM, IBM and MFM. In PM, two outliers with high RER1 expression resulted in a median similar to the controls and DM. If these two patients were omitted, a much lower median would have resulted.

4.9.4 RER1 mRNA expression in laser microdissected myofibers versus muscle biopsy samples from patients with sIBM

In any given muscle biopsy, a high number of cells other than myofibers is present (fibrocytes, vascular endothelial cells, peripheral nerve cells and Schwann cells, all types circulating blood cells). Since RER1 is ubiquitously expressed under physiological conditions, it was interesting to see whether the observed RER1 downregulation was specific to the myofibers in IBM lesions. For that purpose, expression of RER1 was compared in RNA from laser microdissected myofibers versus total biopsy material in four patients with sIBM (**Figure 4.35**).

Comparison of myofiber-specific versus biopsy-specific RER1 expression confirmed the striking RER1 downregulation previously observed in the microarray analysis (**Figure 4.28**). This data shows that the observed RER1 downregulation in IBM compared to non-diseased muscle (**Figure 4.34**) can largely be attributed to IBM myofibers.

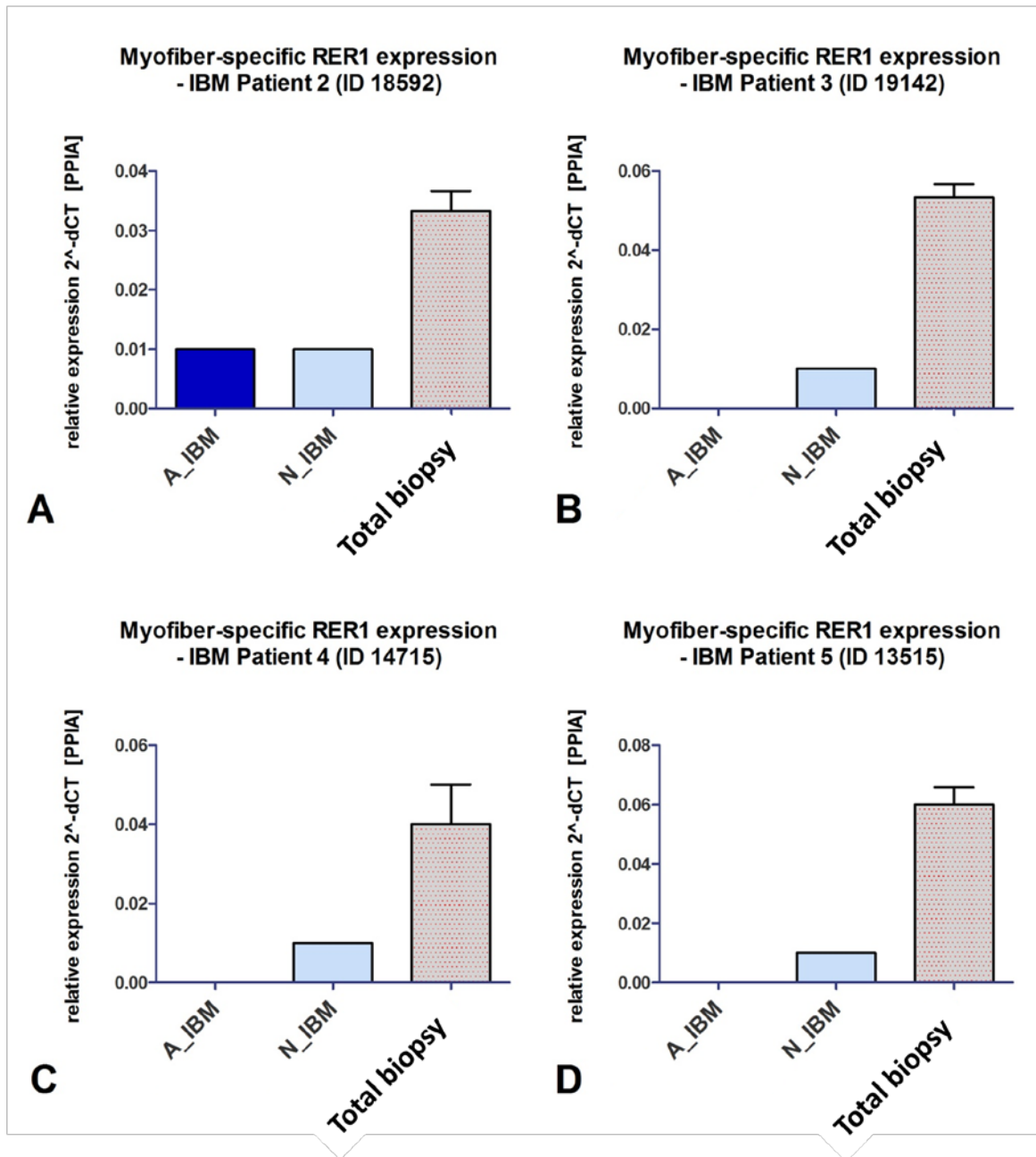


Figure 4.35 RER1 downregulation is myofiber-specific. RER1 expression was analysed with TaqMan qPCR in aRNA from laser microdissected myofibers of patients with IBM (section 4.3). Shown here is a comparison for myofiber-specific RER1 expression (A_IBM and N_IBM) versus RER1 expression in total biopsy material from the respective patient (A, IBM Patient 18592; B, IBM Patient 19142; C, IBM Patient 14715, D, IBM patient 13515). Each qPCR experiment was carried out in triplicate, measuring PPIA and RER1 expression in the same experiment. In all analysed cases, myofiber-specific relative RER1 expression was significantly lower than biopsy-specific RER1 expression.

4.9.5 Starvation of TE671 cells induces downregulation of RER1

RER1 was described very recently, hence its regulatory mechanisms at present are still unknown. Given the possible role of RER1 in the regulation of γ -secretase (Kaether et al., 2007), it was investigated whether mechanisms known to induce γ -secretase may have an impact on RER1 expression. Starvation is known to induce the amyloidogenic pathway via induction of γ -secretase in different cell types such as neurons and glia cells both *in vitro* and *in vivo* (Velliquette et al., 2005; Yu et al., 2005; LeBlanc et al., 1996). In addition, starvation of human vascular endothelial cells was shown to induce γ -secretase, specifically the PEN2 component, and thus upregulate A β 42 (Ma et al., 2010). Assuming that RER1 retains PEN2 in the ER (Kaether et al., 2007), and assuming that the expression of RER1 and PEN2 is reciprocally related, starvation should lead to a downregulation of RER1. Thus it was investigated whether starvation, a mechanism known to induce γ -secretase (Ma et al., 2010), would lead to a downregulation of RER1.

After multiple passages in RPMI-1640 (see methods section 3.3.15), human rhabdomyosarcoma TE671 cells were harvested untreated (time point 0) and after 3h and 24h in HBSS, respectively. RNA was isolated and TaqMan quantitative PCR was performed in triplicate experiments as described in section 4.4.3. **Figure 4.36** demonstrates that RER1 expression goes down three-fold after incubation in HBSS, significantly more than after incubation in RPMI.

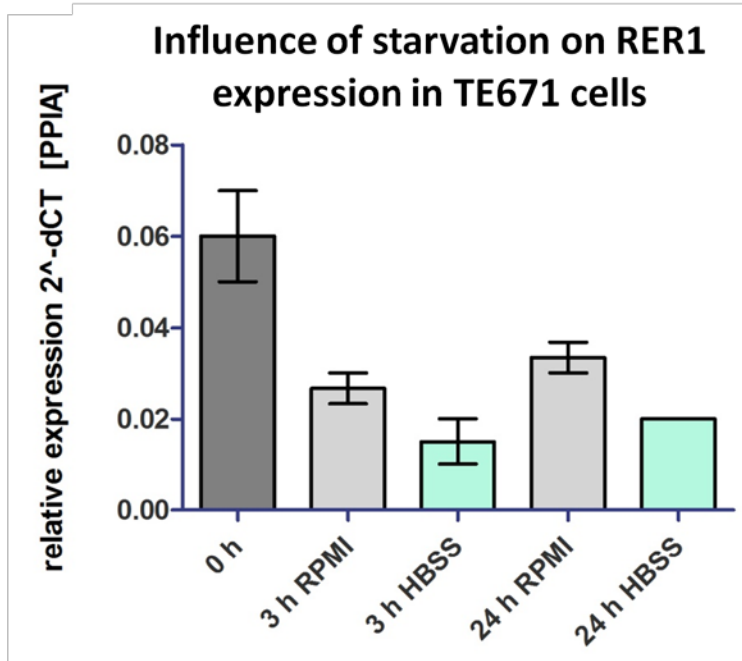


Figure 4.36: Influence of starvation of RER1 expression in human rhabdomyosarcoma TE671 cells.

TE671 cells were harvested fresh (time point 0), after 3h in RPMI and 24h in RPMI, respectively, as well as after 3h and 24h in HBSS, respectively. RNA was isolated and TaqMan quantitative PCR was performed in triplicate experiments as described in section 4.4.3. This experiment shows that RER1 expression is decreased after 3h of starvation, and remains low after 24h.

5. Discussion

sIBM is characterized by inflammatory infiltrates of CD8⁺ T cells focally surrounding and attacking non-necrotic myofibers (Arahata and Engel, 1984). The focal nature of the attacks implies that certain myofibers are heavily attacked, while other myofibers remain spared. The starting point for this dissertation was to individually sample and pool such attacked and non-attacked myofibers, respectively, as well as myofibers from control persons, and compare the transcriptomes of these three entities in a global, “bird’s view” approach with microarray technology. This required establishing a technique for the visualization of CD8⁺ T cells and HLA-ABC⁺ myofibers with minimum RNA degradation, as well as linear transcriptome amplification. The bird’s view approach revealed genes involved in antigen processing and presentation to be among the most significantly regulated transcripts. The expression of these genes was studied in detail on the mRNA and protein levels using quantitative PCR and immunohistochemistry. These data show that both classical and non-classical HLA-I are strongly upregulated in all myofibers in sIBM, while genes involved in IFN γ downstream signaling – first and foremost the IFN γ receptor – are specifically upregulated in attacked myofibers.

RER1, a transcript not previously associated with inflammatory myopathies, was found to be significantly regulated in the inflammatory myopathies. RER1 is a recently discovered chaperone involved in the assembly of γ -secretase subunits (ZZ Kaether C et al 2007). RER1 was significantly downregulated in attacked and non-attacked myofibers of sIBM patients, while being highly expressed in control persons. A transcriptional and protein expression study of 34 patients revealed that RER1 is downregulated in diseases where the amyloidogenic pathway plays an etiological role (sIBM, PM/sIBM, MFM), while being normal in purely inflammatory diseases such as DM, and that the downregulation of RER1 was specific to myofibers. An intriguing finding was that PM did not differ significantly from sIBM in terms of RER1 expression, supporting the hypothesis that PM may not even be a standalone condition (van der Meulen et al., 2003) and may in fact represent an early form of sIBM.

5.1 sIBM pathophysiology – inflammatory aspects

5.1.1 Ubiquitous upregulation of HLA-class I

In contrast to most other tissues, healthy muscle cells do not express HLA-I molecules. In the inflammatory myopathies, however, myofibers do strongly upregulate HLA-I (Emslie-Smith et al., 1989; Karpati et al., 1988; van der Pas et al., 2004). In sIBM, HLA-I expression is essentially ubiquitous on all myofibers (Dalakas, 2006a). The observed upregulation of HLA-I transcripts in both A_{IBM} and N_{IBM} is consistent with this well-established histological aspect. Both the “classical”, highly polymorphic HLA-I genes HLA-A, B and C, and the “nonclassical”, less polymorphic HLA-Ib genes HLA-E, F and G were overexpressed. This confirms and extends previous studies reporting that nonclassical HLA-G is upregulated on myofibers in inflammatory myopathies (Wiendl et al., 2000). Because upregulation of HLA-I on myofibers in sIBM appears to occur independently from the presence of local inflammatory cells (Dalakas, 2010b), and because it may occur in the absence of an $\text{IFN}\gamma$ signature (as shown by the results from N_{IBM}), it appears that HLA-I is upregulated by unknown triggers upstream of the $\text{IFN}\gamma$ -related changes. As indicated by the findings on overexpression of CCL5 and STAT3 (section 4.6), $\text{TNF}\alpha$, as well as other cytokines and chemokines, may potentiate the $\text{IFN}\gamma$ -induced signaling cascade in myofibers. These inflammatory processes may or may not be related to the degenerative changes in sIBM (Askanas and Engel, 2005; Askanas and Engel, 2008; Vatteemi et al., 2009).

Numerous viruses are known triggers for HLA-I upregulation across many different cell types. Hantaan virus specifically upregulates HLA-ABC in megakaryocytes (Lutteke et al., 2010), whereas Influenza A virus induces HLA-G in alveolar epithelial cells (LeBouder et al., 2009). The family of flaviviruses has even been shown to specifically induce HLA-I in human myoblasts (Bao et al., 1992). The flaviviruses are particularly intriguing in this context since flavivirus-induced HLA-ABC upregulation seems to occur independently from chemokines or cytokines, and thus to precede local inflammatory responses (Arnold et al., 2004). While no unequivocal link between viral infection and sIBM has been established, Dalakas and colleagues have repeatedly demonstrated an association between sIBM and HIV (Dalakas et al., 2007) as well as between sIBM and HTLV (Cupler et al., 1996), respectively. In a subset of HIV-infected

patients who developed sIBM, the focally attacking CD8⁺ T cells were HIV-specific, suggesting a cross-reaction with myofiber antigens (Dalakas et al., 2007).

Other causes for HLA-I upregulation include autoimmunity (Iwasa et al., 2010) and malignancy (Du and Wang, 2011). A factor uniting the very different etiologies behind HLA-I upregulation is the presence of cytokines and chemokines capable of inducing HLA-I (and HLA-II), namely TNF α and IFN γ .

At present, it remains uncertain what precise role the ubiquitous HLA-I overexpression plays in sIBM pathogenesis. In animal models, MHC-I overexpression coincided with inflammatory and degenerative myopathic changes, possibly related to an endoplasmic reticulum (ER) stress response (Nagaraju et al., 2000; Nagaraju et al., 2005; Li et al., 2009). Interestingly, HLA-I overload alone was sufficient for the development of myositis (Li et al., 2009). This finding supports the results presented here, namely that HLA-I upregulation on myofibers is the initial step of a cascade of pathophysiological events leading to the development of symptomatic disease. Since CD8⁺ T cells recognize HLA-I bound antigenic peptides, HLA-I expression is a definitive precondition for CD8⁺ T cell-mediated myofiber attack and injury. However, as demonstrated by the results presented in section 4.3, HLA-I is only a required but by no means sufficient precondition for a CD8⁺ T cell mediated attack, and HLA-I expression alone cannot explain the focal character of inflammatory infiltrates seen in sIBM.

5.1.2 Upregulation of IFN γ receptor in CD8⁺ T cell-attacked myofibers

The explorative microarray experiments (section 4.3) indicated overexpression of IFN γ -inducible transcripts in A_{IBM} versus N_{IBM}. The crucial upstream protein required for initiation of downstream IFN γ signaling is the IFN γ receptor (**Fig. 5.1, center**). The quantitative PCR results presented in section 4.4 suggest that the IFN γ receptor is only expressed by A_{IBM}, but not N_{IBM} or H_{CTRL} myofibers.

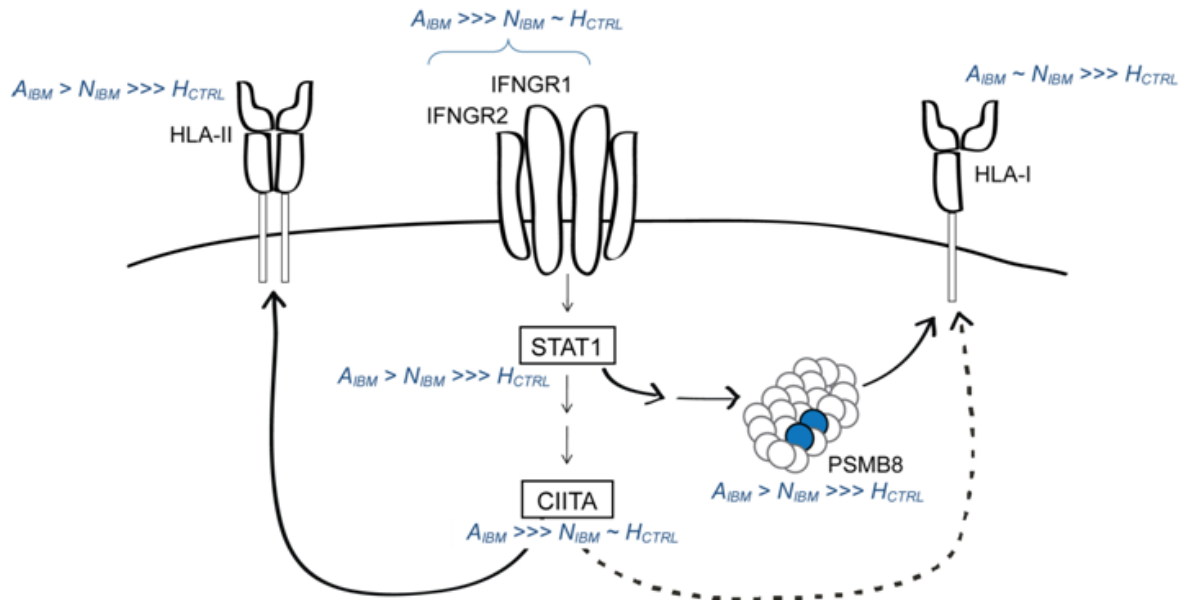


Figure 5.1: Changes in the molecular pattern of inflammatory signaling, antigen processing and presentation in attacked myofibers: scheme. HLA-I are upregulated in all IBM myofibers. IFN- γ induced CIITA results in a pronounced upregulation of HLA-II (continuous arrow) and a less pronounced upregulation of HLA-I (dotted arrow) (Gobin et al., 1997). However, the effect of CIITA cannot be held responsible for the initial, IFN- γ independent, probably ubiquitous HLA-I upregulation. Upregulation of IFN γ -pathway components IFNGR1 and IFNGR2 was shown in A_{IBM}, explaining the upregulation of IFN γ -inducible genes such as STAT1, CIITA, PSMB8 and HLA-II in A_{IBM}.

When IFN γ binds to its receptor, the complex of IFN γ , IFNGR1 and STAT1 translocates into the cell nucleus while IFNGR2 prevails on the cell membrane (Larkin, III et al., 2000; Ahmed and Johnson, 2006). Confocal microscopy revealed that IFNGR2 protein expression in sIBM muscle was heterogeneous and correlated with the presence of inflammatory cells. In order to quantify the relationship between inflammatory cells and segmental IFNGR2 expression, myofibers were assigned to one of four groups according to their extent of IFNGR2 surface staining and the number of attacking CD8⁺ T cells for each myofiber was documented, revealing a positive correlation between the extent of myofiber surface expression of IFNGR2 and the number of adjacent CD8⁺ T cells in all patients, and thereby confirming the quantitative PCR findings.

5.1.3 Upregulation of IFN γ -induced transcripts

The signal transducer and activator of transcription 1 (STAT1) is an important downstream component of the IFN γ signaling cascade. A role for STAT1 overexpression has previously been demonstrated for DM and PM (Illa et al., 1997). Quantitative PCR analysis revealed a differential expression of STAT1 in myofibers in sIBM, with overexpression of STAT1 in A_{IBM} versus N_{IBM} myofibers (**Figure 5.1**). This is in line with the observation that IFNGR2 is preferentially expressed in A_{IBM} myofibers.

A further IFN γ -inducible transcript found selectively overexpressed in A_{IBM} is the class II transactivator (CIITA). CIITA is the most pertinent transcription factor for the induction of HLA-II (Leibundgut-Landmann et al., 2004), however, CIITA can induce HLA-I to some extent as well (Gobin et al., 1998) (**Figure 5.1**). IFN γ is a strong regulator of CIITA and can upregulate CIITA in non-lymphoid cells (van den Elsen et al., 2004). The results of this dissertation show, for the first time, an overexpression of CIITA in CD8⁺ T cell-attacked myofibers of sIBM patients. Literature on the expression of HLA-II in sIBM myofibers is controversial. Global tissue profiling in inflammatory myopathies has shown increased amounts of HLA-DR, -DP, and -DQ in sIBM, however the cellular source remained unknown (Greenberg et al., 2002). Immunohistochemical studies addressing the expression of HLA-II on myofibers in inflammatory myopathies are few and far between. One study examined HLA-II expression in DM and PM, but not sIBM (Englund et al., 2001). In contrast to the results in sIBM presented in sections 4.4.2 and 4.7, the authors found HLA-DR expression to be independent of inflammatory infiltrates (Englund et al., 2001). The discrepancy might be related to differences between the different myopathies, since CD8⁺ T cells predominate in sIBM and CD4⁺ T cells predominate in DM, whereas PM is a heterogenous entity. Another possibility are technical reasons, e.g. different antibody reagents used for HLA-II staining. The pathogenic significance of IFN γ -induced HLA-class II upregulation is unknown, probably initiated by TNF α (Keller et al., 2010). Since the endomysial inflammatory infiltrates in sIBM predominantly consist of CD8⁺ T cells (Engel and Arahata, 1984), (auto-) antigen presentation to CD4⁺ T cells is unlikely.

The IFN γ -inducible catalytic proteasome subunit PSMB8 is another member of antigen-presentation and processing selectively upregulated in attacked myofibers. PSMB8 generates peptides which show an increased affinity for HLA-I (Kloetzel, 2001). Previous global microarray profiling studies in muscle biopsies from patients with inflammatory myopathies showed a strong overexpression of PSMB8 (Greenberg *et al.*, 2002; Greenberg *et al.*, 2005), without revealing the cellular source. The microarray and quantitative PCR data presented in sections 4.2 and 4.4.2 attribute upregulation of PSMB8 to A_{IBM} myofibers, pointing to an upregulated IFN γ signature in A_{IBM}.

Additional IFN γ -inducible transcripts are likely upregulated in A_{IBM}. Upregulation of the CCL5/STAT3 system was shown in A_{IBM} (section 4.6). CCL5 is known to attract activated T cells (Flier *et al.*, 2001; Kovacic *et al.*, 2010), and is synergistically upregulated by TNF α and IFN γ (Lee *et al.*, 2000; Hiroi and Ohmori, 2003). Thus the expression of CCL5 by myofibers would contribute to the local proinflammatory loop. A possible role for TNF α in inflammatory myopathies is supported by studies demonstrating that TNF α upregulated the TSP1/CD36/CD47 complex in cultured myoblasts (Salajegheh *et al.*, 2007). Synergistic effects between TNF α and IFN γ are thus likely to play a pathophysiological role in sIBM. Furthermore, previous studies in inflammatory myopathies have proposed that the myofibers themselves are capable of producing IFN γ -inducible, T-cell chemoattractant chemokines (Raju *et al.*, 2003; Tateyama *et al.*, 2009). In light of the capability of CXCL9 and CXCL10 to attract activated T cells this result might provide an explanation for why certain myofibers are attacked while others are spared. Clearly, the role of chemokines needs to be further explored in future studies.

The IFN γ -inducible chemokines CXCL9 or MIG (monokine induced by interferon gamma) and CXCL10 or IP-10 (IFN γ -inducible protein 10), as well as their common receptor CXCR3 have previously been shown to be strongly expressed on the myofibers, and CXCL9 and CXCL10 were also demonstrated to be expressed on a subset of autoinvasive CD8⁺ cells (Raju *et al.*, 2003). Moreover, both chemokines were shown to be produced by myotubes upon IFN γ stimulation. Thus, they can facilitate the recruitment of activated T cells to the muscle and perpetuate the self-sustaining nature of endomysial inflammation commonly seen in sIBM. This result expands upon previously published immunohistochemical studies (Raju *et al.*, 2003) and indicates that myofibers are indeed capable of producing chemokines upon IFN γ stimulation

and indicates, for the first time, an upregulation of IFN γ -inducible chemokines in individual myofiber cells on the mRNA level.

Technical challenges did not make it possible to demonstrate CXCL9 expression in all analyzed patients with sIBM. However, the CXCL9 expression data shows what seems to be a tendency towards overexpression of CXCL9 in A_{IBM} versus N_{IBM} and H_{CTRL}, however, these data did not reach statistical significance on the mRNA or protein level.

5.1.4 Comparison with other microarray studies in human inflammatory myopathies and animal models

Previous microarray studies in inflammatory and degenerative myopathies were carried out on biopsy tissue, thus not distinguishing between myofiber-derived transcripts versus transcripts overexpressed by leukocytes present in the biopsy (Greenberg *et al.*, 2002, 2005). Given the ability of myofibers to produce certain chemokines and other inflammatory proteins under specific circumstances (Hohlfeld *et al.*, 1993; Raju *et al.*, 2003; Tateyama *et al.*, 2009), it is all the more important to determine the source of transcripts upregulated in inflammatory myopathies. In the results presented here, for the first time, microarray analysis was performed on individually laser microdissected myofibers rather than total biopsy material, thus enabling to attribute some of the previously discovered gene expression alterations to myofibers rather than other cell types present in a muscle biopsy. Moreover, these results led to the discovery of a significant downregulation of RER1, a gene not previously intertwined with sIBM pathophysiology.

Global microarray studies previously reported by other authors have demonstrated a strong overexpression of HLA-I, HLA-II, PSMB8, a number of interferon-induced genes, and certain cytokines such as CCL5 and MIG (CXCL9) in sIBM. By comparison, the data presented here allow, for the first time, an attribution of expression pattern alterations to particular myofiber subsets. Myofiber-specific HLA-I upregulation was demonstrated in all myofibers in sIBM, whereas IFN γ -inducible transcripts, as well as transcripts required for IFN γ signaling, were found to be upregulated in A_{IBM} versus N_{IBM} and H_{CTRL}. On the other hand, immunoglobulins were absent in the myofiber-specific microarray studies, attributing the previously described

immunoglobulin overexpression to infiltrating B-cells (Greenberg et al., 2005; Bradshaw et al., 2007).

As discussed in section 5.1.1, overexpression of MHC-I alone was sufficient to create myositis-like symptoms and histopathological signs in a mouse model, including inflammatory infiltrates (Li et al., 2009). Microarray results presented by the same authors showed an upregulation of transcripts involved in ER and Golgi trafficking, which further supports the hypothesis that increased ER stress plays an important pathophysiological role in the development of inflammatory myopathies.

5.1.5 Inflammatory aspects of sIBM - conclusions and model

In conclusion, the results in sections 4.1 – 4.8 show that the receptor for IFN γ , as well as members of the downstream IFN γ signaling cascade, are selectively upregulated in attacked sIBM myofibers (**Figure 5.1**). This fact leads to a very basic question: which is the initial event in sIBM pathophysiology, a) focal inflammation, or b) focal upregulation of antigen presentation and processing pathways in the attacked myofiber? The results of sections 4.1 – 4.8 give rise to a hypothetical scenario that may help explain the focality of CD8⁺ T cell attack. As an initial step, the expression of HLA-I is induced ubiquitously across all myofibers by unknown proximal triggers (viruses, other infectious agents, cross-presentation, or other mechanisms).

Subsequently, a roaming CD8⁺ T cell by chance establishes contact with a myofiber, recognizing a HLA-I-associated antigen on a myofiber membrane. Antigen recognition and activation results in the secretion of proinflammatory cytokines and chemokines by the T cell, which in turn attracts and activates macrophages and other inflammatory cells. The inflammatory-cell-derived cytokines and chemokines upregulate IFN γ receptor expression on the attacked and possibly on adjacent myofibers. This in turn increases the susceptibility of the myofibers to IFN γ -mediated stimulation. IFN γ -mediated signaling results in a cascade of secondary changes in the attacked fibers, increasing their susceptibility to further inflammatory attack. In this way, an initial antigen recognition event by a CD8⁺ T cell on an HLA-I positive myofiber is amplified, leading to strong focal inflammatory changes and resulting in attack of the same myofiber by additional CD8⁺ T cells.

5.2 sIBM pathophysiology – degenerative aspects

5.2.1 Role of the amyloidogenic pathway in sIBM

As discussed in previous sections, there is a very strong concept that inflammatory and degenerative changes in sIBM are mutually related (Karpati and O'Ferrall, 2009; Schmidt et al., 2008). Consistent with this concept, the microarrays of laser microdissected myofibers (section 4.3.2) demonstrated APP and other degenerative markers such as embryonic myosin variants to be upregulated with reasonable q-values between 20% and 40 %.

Important degenerative aspects of sIBM are the accumulation of proteins in sIBM myofibers that are also found in Alzheimer's disease (AD) -affected brain tissue. This includes paired helical filaments of phosphorylated tau, Amyloid- β -precursor protein (β -APP), β - and γ -secretase, and the end product of the amyloidogenic pathway, oligomers of aggregated, congophilic Amyloid- β -42 (A β -42) (Askanas and Engel, 2008; Askanas et al., 2009; Vattemi et al., 2009). A β -42 could not be detected in polymyositis or undiseased muscle biopsy samples, whereas increased A β -42 were found in sIBM muscle biopsies, and immunohistochemically localized within sIBM myofibers (Nogalska et al., 2010). The link to the inflammatory pathways in sIBM may be hidden in the fact that certain chemokines, in particular IL-1 β , can upregulate intracellular β -Amyloid expression in cultured muscle cells, and indeed IL-1 β colocalized with β -Amyloid oligomers in biopsies of sIBM patients (Schmidt et al., 2008). While the pathophysiological role of β -Amyloid deposits in sIBM is not defined, it clearly sets sIBM apart from other inflammatory myopathies, and understanding the early steps in amyloid biosynthesis may shed light on sIBM pathophysiology.

5.2.2 RER1 – a novel potential early regulator of amyloid biosynthesis

While the importance of the amyloidogenic pathway is commonly acknowledged, the regulation of amyloid biosynthesis in sIBM remains unexplained. Previous studies have demonstrated presenilin-1, an important γ -secretase subunit to be upregulated (Askanas and Engel, 1998). However, γ -secretase is a complex multimeric machinery containing additional subunits the

absence of which render it unable to produce β -amyloid (Aph, PEN2, and nicastrin) (Spasic and Annaert, 2008). Understanding the assembly process of these subunits is only in the beginnings, and will be important to understand pathophysiology and improve diagnosis and therapy of all diseases involving amyloid biosynthesis.

As shown in the unbiased, “bird’s view”, microarrays from laser microdissected myofibers (section 4.3.2), RER1 was very strongly downregulated in myofibers from patients with sIBM (q value of 0%). RER1 is the ubiquitously expressed human homolog of the *Saccharomyces cerevisiae* gene called “Retention in endoplasmic reticulum 1” and plays a role in the assembly of γ -Secretase, the key enzyme responsible for the biosynthesis of β -amyloid (Kaether et al., 2007). The highly significant downregulation of RER1 in IBM seen in laser microdissected myofibers initiated further investigation of RER1 mRNA and protein levels in sIBM and other myopathic disorders.

Congophilic deposits currently are the major histological differentiation between sIBM and PM (Dalakas, 2010b). However, intracellular amyloid deposits have to accumulate for an extended time period before congophilic deposits can be detected. Given the potential role of RER1 in β -amyloid biosynthesis, RER1 downregulation might be an early, sensitive marker for sIBM diagnosis. This is particularly important in the context of determining “pure PM” versus “PM/sIBM” versus “pure sIBM” (Chahin and Engel, 2008) (section 1.3). As discussed in section 1.3, the original Bohan and Peter criteria (Bohan and Peter, 1975a; Bohan and Peter, 1975b), employ solely skin changes to distinguish PM from DM, and sIBM is not clearly defined. Many large-scale studies applying the Bohan and Peter criteria concluded that PM was the most common inflammatory myopathy (Hill et al., 2001; Love et al., 1991; Joffe et al., 1993). However, recent studies pointed out that PM indeed is the least common of the inflammatory myopathies, and that a large number of patients initially diagnosed with PM need to be re-diagnosed with sIBM at a later stage, based on resistance to treatment and histological findings (van der Meulen et al., 2003; Chahin and Engel, 2008).

It is well established that progressive deposition of β -amyloid, derived from β -amyloid precursor protein (APP), plays a major role in AD pathophysiology (Selkoe, 1989; Sisodia and Price, 1995). One of the major enzymes responsible for the production of β -Amyloid is γ -Secretase (Wolfe and Guenette, 2007). γ -Secretase represents a complex machinery consisting of four

subunits that have to be assembled within the endoplasmic reticulum (ER) and the cytoplasm before γ -Secretase can successfully cleave its substrates (Spasic and Annaert, 2008). AD research in the recent years has focused on the regulation and assembly of γ -Secretase, given its potential applicability as a drug target in future AD therapies (Woo et al., 2011).

5.2.3 Myofiber-specific RER1 downregulation demonstrated in laser microdissected sIBM myofibers

Comparison of myofiber-specific versus biopsy-specific RER1 expression confirmed the striking RER1 downregulation previously observed in the microarray analysis. This data shows that the observed RER1 downregulation in IBM compared to non-diseased muscle can largely be attributed to IBM myofibers. These results are in line with the initial hypothesis that RER1 downregulation is a prerequisite for the induction of β -amyloid biosynthesis, since cells other than myofibers contained in an IBM muscle biopsy, such as lymphocytes and fibroblasts, would not be expected to produce β -amyloid. This result would not have been possible without the laser microdissection approach.

5.2.4 RER1 mRNA and protein downregulation in sIBM versus other inflammatory and degenerative myopathies

Of all inflammatory myopathies, sIBM is the only entity where amyloid deposits can be found within myofibers. Despite sharing the monoclonally expanded CD8⁺ T cell infiltrates focally attacking myofibers with PM, sIBM does not respond to immunomodulatory treatment. The highly significant downregulation of RER1 mRNA seen in the microarray data (section 4.9.1) prompted the investigation of RER1 expression on the protein and the mRNA level in sIBM patients versus non-diseased controls, other inflammatory myopathies (PM/IBM, PM, DM), other degenerative myopathies involving amyloid deposition (MFM) and disease controls (DMD) (34 patients total, **Table 3.2**).

A scoring system was established based on RER1 protein expression in muscle biopsy cross-sections as detected using confocal imaging (**Figure 4.28**): high RER1 expression in myofibers (score of 1), intermediate RER1 expression in myofibers (score of 2), and low RER1 expression in myofibers (score of 3). Scoring of the 34 patient samples was performed by six colleagues not otherwise involved in the project. Indeed, the “purely inflammatory” disease DM and the control samples did show high RER1 expression, whereas sIBM patients demonstrated very low to no RER1 expression. The inflammatory infiltrates seen in sIBM served as an internal positive control, being strongly RER1-positive. Interestingly, PM/IBM, as well as PM, did show a RER1 downregulation close to that of the sIBM group. In light of the ongoing discussion on whether PM is an entity of its own (van der Meulen et al., 2003), these data are very interesting, and point in the direction of PM possibly being an early form of sIBM, where RER1 is already going down, while β -amyloid deposits have not yet accumulated to an extent detectable by Congo-red staining. Supporting the theory of RER1 downregulation corresponding with β -amyloid upregulation, RER1 was found to be downregulated in MFM. In DMD, the variability was the highest, due to the typical morphology of DMD myofibers, where it can be difficult to distinguish myofiber borders.

The protein expression data were correlated with TaqMan quantitative PCR data on the same 34 patient samples. Median expression levels were highest in healthy controls and DM, and lowest in PM/IBM, IBM and MFM (**Figure 4.34**). In PM, there was a very strong heterogeneity in RER1 expression, resulting in a median expression level in the same range as control and DM samples. This however, mainly stemmed from two patient samples which yielded expression values considerably higher than all other samples (two outliers seen in **Figure 4.34**). Had the two outliers not been included in the analysis, the PM group would have yielded a much lower median RER1 expression ranging only slightly above the expression of RER1 in the PM/IBM, IBM, and MFM groups. This further supports the notion derived from the protein expression data, namely that PM behaves similarly to IBM with regard to RER1 expression. The PM/IBM group, which behaved exactly like sIBM on both the protein and the mRNA level. The results presented here question the demarcation of PM as an entity of its own.

5.2.5 RER1 expression may predict the disease course in a patient with myositis

A particularly intriguing finding was that RER1 was downregulated to a large extent in some of the PM patient samples, raising the question whether PM might in fact be an early form of sIBM, where amyloid deposits are not yet detectable by Congo-red staining, however the amyloidogenic pathway has already been initiated via loss of RER1. A particularly striking case, patient 16825, was originally diagnosed as “PM”. The imaging and quantitative PCR experiments presented in sections 4.9.2 and 4.9.3, however, demonstrated complete downregulation of RER1 on the protein and the mRNA level. The patient’s clinical chart data were requested from Dr. Andrew Engel at the Mayo Clinic in Rochester, MN, and an evaluation of the patient’s clinical course revealed that he had been resistant to all immunomodulatory treatment options, and had a slowly progressive disease course. Moreover, a re-biopsy five years later revealed congophilic deposits and led to the re-classification of this patient as “sIBM”. The biopsy used in this dissertation, however, was the initial biopsy, which had not (yet) shown congophilic deposits. Thus, RER1 downregulation may be an early marker of amyloid biosynthesis, not only in sIBM, but also in all other diseases involving the amyloidogenic pathway, the most prominent being Alzheimer’s disease. This promising pathway clearly has to be further investigated in future studies.

It was no less interesting that RER1 also was downregulated in myofibrillar myopathy (MFM). MFM feature β -amyloid deposits and bears intriguing similarities to sIBM in that immunoproteasome induction and HLA-I upregulation play a role in both entities (Ferrer et al., 2004). Future work will show whether these shared characteristics are secondary effects or whether they may have pathophysiological implications.

5.2.6 Possible regulatory mechanisms of RER1

The importance of the amyloid biosynthesis pathway to Alzheimer’s disease has resulted in a significant research effort directed at understanding its regulation. One of the mechanisms proposed for the induction of γ -secretase is starvation: as shown by Ma and colleagues, starvation of human vascular endothelial cells (HUVEC) resulted in upregulation of γ -secretase

subunits APH1 and PEN2 (Ma et al., 2010). Given the putative inverse correlation of PEN2 and RER1 expression (ZZ Kaether et al 2007), it was investigated here whether starvation of human rhabdomyosarcoma cells would result in a downregulation of RER1 (section 4.9.5). As shown in section 4.9.5, starvation did indeed result in RER1 downregulation, suggesting that the induction of γ -secretase upon starvation may be triggered through a loss of RER1 expression. Starvation is a common mechanism in myofibers, as was shown particularly for sIBM (Lunemann et al., 2007). The possible association between starvation and RER1 thus opens up interesting opportunities for future exploration.

5.2.7 RER1: Conclusions and possible clinical and pathophysiological implications

It was shown here that sIBM, but not healthy muscle and DM, are clearly associated with myofiber-specific downregulation of RER1 (sections 4.9.1 – 4.9.4). This data further supports the importance of the amyloidogenic pathway for sIBM pathophysiology (Askanas and Engel, 2008; Dalakas, 2008). Aside from the pathophysiological implications, it appears that RER1 downregulation occurs long before the emergence of congophilic deposits (section 5.2.5). RER1 thus may be a potential early biomarker in the detection of sIBM.

The validity of classifying PM as a standalone disease has long been debated (van der Meulen et al., 2003; Chahin and Engel, 2008). The data shown in sections 4.9.1 – 4.9.4 imply that RER1 downregulation occurs in PM as well. Given the absence of congophilic amyloid deposits in PM, the results presented here give rise to the question whether PM might be an early form of sIBM, in which γ -secretase upregulation has already begun, however amyloid deposits have not (yet) accumulated.

5.3 Inclusion body myositis – a paradigm for the interplay of immunological and degenerative disease mechanisms

sIBM is traditionally classified within the group of inflammatory myopathies, which also include PM and DM (Dalakas, 2004). However, sIBM has two major distinguishing traits compared to

the other inflammatory myopathies: the myofibers harbor amyloid deposits and other degenerative markers, and sIBM is not responsive to any immunomodulatory treatment.

sIBM shares a number of intriguing similarities with Alzheimer's disease (AD) (Askanas and Engel, 2006): in AD, a major pathophysiological role has been established for β -amyloid, the same peptide that accumulates in sIBM myofiber "inclusions" (Mikol and Engel, 2004). Much evidence has been collected for the presence of β -amyloid in sIBM myofibers. It remains unknown, however, what possible pathophysiological role these intra-myofiber β -amyloid accumulations might play. One interesting link between inflammation and degeneration is the evidence that IL1- β induced β -amyloid in skeletal muscle cells, and that IL1- β colocalized with β -amyloid in sIBM biopsy cryosections (Schmidt et al., 2008). Furthermore, heat shock proteins such as α -B-crystallin that are known to be upregulated in the setting of inflammation, were shown to be associated with APP and β -amyloid in sIBM (Muth et al., 2009). Conversely, β -amyloid accumulation increased α -B-crystallin overexpression in sIBM, implicating that the degenerative changes may indeed precede the inflammatory mechanisms (Wojcik et al., 2006).

The regulation of RER1 expression remains still unknown. Two hypothetical scenarios are possible: on the one hand, inflammatory changes may trigger RER1 downregulation that in turn results in chronic accumulation of β -amyloid deposits. On the other hand, if the degenerative changes are what initially triggers sIBM, RER1 downregulation and subsequent β -amyloid accumulation may result in the production of chemokines and cytokines which in turn may attract inflammatory cells. The first scenario seems more likely in light of the results from RER1 expression in PM, a disease where inflammatory changes resemble sIBM, but no β -amyloid deposits are found. RER1 may thus be an important early switch in the initiation of amyloid biosynthesis, giving rise to potential early diagnosis of amyloidogenic disorders such as sIBM and Alzheimer's disease, as well as possible treatment options.

6. Summary

Sporadic inclusion body myositis (sIBM) is an enigmatic disease resistant to immunomodulatory treatment and featuring autoimmune and degenerative aspects: clonally expanded CD8⁺ T cells focally infiltrate uniformly HLA-I⁺ myofibers that harbor β -amyloid deposits. In a non-hypothesis-driven approach, CD8⁺ T cell-attacked and non-attacked myofibers were compared on the transcriptional level. To this end, cytosol of such attacked and non-attacked myofibers was isolated independently using laser microdissection. For comparison, healthy tissue was investigated. After linear transcriptome amplification, a transcriptome analysis was performed using microarray hybridization and quantitative PCR. RNA expression analysis was verified on the protein level by immunohistochemistry.

The most prominently regulated molecular patterns were those of antigen processing and presentation. HLA-I upregulation was observed on both attacked and non-attacked myofibers, while myofibers from healthy controls did not express HLA-I. HLA-II were overexpressed in attacked myofibers compared to non-attacked myofibers and healthy controls. A number of transcripts inducible by IFN γ , as well as the IFN γ receptor, were specifically induced in attacked myofibers. IFN γ receptor protein expression on myofiber membranes was demonstrated using confocal microscopy. It was shown that IFN γ receptor protein expression on myofiber membranes correlated with the extent of inflammatory CD8⁺ T cell infiltrates surrounding the myofibers. The differential upregulation of IFN- γ signaling is thus likely related to local inflammation, whereas the ubiquitous HLA-I upregulation is triggered further upstream by as-yet-unknown mechanisms.

In the unbiased global transcriptome analysis, RER1, a chaperone recently discovered to play a role in the assembly of γ -secretase, was statistically highly significantly downregulated in myofibers from patients with sIBM compared to control myofibers. This result prompted a case-control study of 36 patients on the transcriptional and the protein level, comparing RER1 expression levels in different inflammatory and degenerative myopathies. RER1 was found to be strongly downregulated in patients with sIBM, while being strongly expressed in healthy muscle and in DM, confirming the microarray results. Moreover, RER1 was downregulated in MFM, a degenerative myopathy featuring amyloid deposits, and, strikingly, PM, a disease which, while resembling sIBM, so far has been considered a standalone entity and a purely inflammatory condition. RER1 downregulation might be an early, sensitive molecular marker in diseases where amyloid biosynthesis plays a role, such as sIBM, and possibly PM, as well as neurodegenerative diseases such as Alzheimer's disease.

7. References

Ahmed,C.M. and Johnson,H.M. (2006). IFN-gamma and its receptor subunit IFNGR1 are recruited to the IFN-gamma-activated sequence element at the promoter site of IFN-gamma-activated genes: evidence of transactivational activity in IFNGR1. *J. Immunol.* *177*, 315-321.

Alzheimer's Association. 2010 Alzheimer's disease facts and figures. *Alzheimer's and Dementia* *6*, 158-194. 2010.

Ref Type: Generic

Amato,A.A., Gronseth,G.S., Jackson,C.E., Wolfe,G.I., Katz,J.S., Bryan,W.W., and Barohn,R.J. (1996). Inclusion body myositis: clinical and pathological boundaries. *Ann. Neurol.* *40*, 581-586.

Amemiya,K., Granger,R.P., and Dalakas,M.C. (2000). Clonal restriction of T-cell receptor expression by infiltrating lymphocytes in inclusion body myositis persists over time. *Studies in repeated muscle biopsies. Brain* *123 (Pt 10)*, 2030-2039.

Applied Biosystems. Application note: Real-Time PCR. 1-6. 2011.

Ref Type: Generic

Arahata,K. and Engel,A.G. (1984). Monoclonal antibody analysis of mononuclear cells in myopathies. I: Quantitation of subsets according to diagnosis and sites of accumulation and demonstration and counts of muscle fibers invaded by T cells. *Ann. Neurol.* *16*, 193-208.

Argov,Z. and Yarom,R. (1984). "Rimmed vacuole myopathy" sparing the quadriceps. A unique disorder in Iranian Jews. *J. Neurol. Sci.* *64*, 33-43.

Arnold,S.J., Osvath,S.R., Hall,R.A., King,N.J., and Sedger,L.M. (2004). Regulation of antigen processing and presentation molecules in West Nile virus-infected human skin fibroblasts. *Virology* *324*, 286-296.

Askanas,V. and Engel,W.K. (1998). Does overexpression of betaAPP in aging muscle have a pathogenic role and a relevance to Alzheimer's disease? Clues from inclusion body myositis, cultured human muscle, and transgenic mice. *Am. J. Pathol.* *153*, 1673-1677.

Askanas,V. and Engel,W.K. (2005). Sporadic inclusion-body myositis: a proposed key pathogenetic role of the abnormalities of the ubiquitin-proteasome system, and protein misfolding and aggregation. *Acta Myol.* *24*, 17-24.

Askanas,V. and Engel,W.K. (2006). Inclusion-body myositis: a myodegenerative conformational disorder associated with A β , protein misfolding, and proteasome inhibition. *Neurology* *66*, S39-S48.

References

- Askanas,V. and Engel,W.K. (2007). Inclusion-body myositis, a multifactorial muscle disease associated with aging: current concepts of pathogenesis. *Curr. Opin. Rheumatol.* *19*, 550-559.
- Askanas,V. and Engel,W.K. (2008). Inclusion-body myositis: muscle-fiber molecular pathology and possible pathogenic significance of its similarity to Alzheimer's and Parkinson's disease brains. *Acta Neuropathol.* *116*, 583-595.
- Askanas,V., Engel,W.K., and Nogalska,A. (2009). Inclusion body myositis: a degenerative muscle disease associated with intra-muscle fiber multi-protein aggregates, proteasome inhibition, endoplasmic reticulum stress and decreased lysosomal degradation. *Brain Pathol.* *19*, 493-506.
- Badrising,U.A., Schreuder,G.M., Giphart,M.J., Geleijns,K., Verschuuren,J.J., Wintzen,A.R., Maat-Schieman,M.L., van,D.P., van Engelen,B.G., Faber,C.G., Hoogendijk,J.E., de Jager,A.E., Koehler,P.J., de,V.M., and van Duinen,S.G. (2004). Associations with autoimmune disorders and HLA class I and II antigens in inclusion body myositis. *Neurology* *63*, 2396-2398.
- Bao,S., King,N.J., and Dos Remedios,C.G. (1992). Flavivirus induces MHC antigen on human myoblasts: a model of autoimmune myositis? *Muscle Nerve* *15*, 1271-1277.
- Bartoccioni,E., Gallucci,S., Scuderi,F., Ricci,E., Servidei,S., Broccolini,A., and Tonali,P. (1994). MHC class I, MHC class II and intercellular adhesion molecule-1 (ICAM-1) expression in inflammatory myopathies. *Clin. Exp. Immunol.* *95*, 166-172.
- Baugh,L.R., Hill,A.A., Brown,E.L., and Hunter,C.P. (2001). Quantitative analysis of mRNA amplification by in vitro transcription. *Nucleic Acids Res.* *29*, E29.
- Bender,A., Behrens,L., Engel,A.G., and Hohlfeld,R. (1998). T-cell heterogeneity in muscle lesions of inclusion body myositis. *J. Neuroimmunol.* *84*, 86-91.
- Bennett,L., Palucka,A.K., Arce,E., Cantrell,V., Borvak,J., Banchereau,J., and Pascual,V. (2003). Interferon and granulopoiesis signatures in systemic lupus erythematosus blood. *J. Exp. Med.* *197*, 711-723.
- Bohan,A. and Peter,J.B. (1975a). Polymyositis and dermatomyositis (first of two parts). *N. Engl. J. Med.* *292*, 344-347.
- Bohan,A. and Peter,J.B. (1975b). Polymyositis and dermatomyositis (second of two parts). *N. Engl. J. Med.* *292*, 403-407.
- Braak,H., Del,T.K., Rub,U., de Vos,R.A., Jansen Steur,E.N., and Braak,E. (2003). Staging of brain pathology related to sporadic Parkinson's disease. *Neurobiol. Aging* *24*, 197-211.
- Bradshaw,E.M., Orihuela,A., McArde,S.L., Salajegheh,M., Amato,A.A., Hafler,D.A., Greenberg,S.A., and O'Connor,K.C. (2007). A local antigen-driven humoral response is present in the inflammatory myopathies. *J. Immunol.* *178*, 547-556.

Buttice,G., Miller,J., Wang,L., and Smith,B.D. (2006). Interferon-gamma induces major histocompatibility class II transactivator (CIITA), which mediates collagen repression and major histocompatibility class II activation by human aortic smooth muscle cells. *Circ. Res.* 98, 472-479.

Chahin,N. and Engel,A.G. (2008). Correlation of muscle biopsy, clinical course, and outcome in PM and sporadic IBM. *Neurology* 70, 418-424.

Coux,O., Tanaka,K., and Goldberg,A.L. (1996). Structure and functions of the 20S and 26S proteasomes. *Annu. Rev. Biochem.* 65, 801-847.

Cupler,E.J., Leon-Monzon,M., Miller,J., Semino-Mora,C., Anderson,T.L., and Dalakas,M.C. (1996). Inclusion body myositis in HIV-1 and HTLV-1 infected patients. *Brain* 119 (Pt 6), 1887-1893.

Dalakas,M.C. (1991). Polymyositis, dermatomyositis and inclusion-body myositis. *N. Engl. J. Med.* 325, 1487-1498.

Dalakas,M.C. (2004). Molecular pathogenesis of inflammatory myopathies and future therapeutic strategies. *Suppl Clin. Neurophysiol.* 57, 288-303.

Dalakas,M.C. (2005). Autoimmune muscular pathologies. *Neurol. Sci.* 26 *Suppl 1*, S7-S8.

Dalakas,M.C. (2006a). Inflammatory, immune, and viral aspects of inclusion-body myositis. *Neurology* 66, S33-S38.

Dalakas,M.C. (2006b). Sporadic inclusion body myositis--diagnosis, pathogenesis and therapeutic strategies. *Nat. Clin. Pract. Neurol.* 2, 437-447.

Dalakas,M.C. (2007). Autoimmune inflammatory myopathies. *Handb. Clin. Neurol.* 86, 273-301.

Dalakas,M.C. (2008). Interplay between inflammation and degeneration: using inclusion body myositis to study "neuroinflammation". *Ann. Neurol.* 64, 1-3.

Dalakas,M.C. (2010a). Immunotherapy of myositis: issues, concerns and future prospects. *Nat. Rev. Rheumatol.* 6, 129-137.

Dalakas,M.C. (2010b). Inflammatory muscle diseases: a critical review on pathogenesis and therapies. *Curr. Opin. Pharmacol.*

Dalakas,M.C. (2011). Immunotherapy of Inflammatory Myopathies: Practical Approach and Future Prospects. *Curr. Treat. Options. Neurol.*

Dalakas,M.C., Rakocevic,G., Shatunov,A., Goldfarb,L., Raju,R., and Salajegheh,M. (2007). Inclusion body myositis with human immunodeficiency virus infection: four cases with clonal expansion of viral-specific T cells. *Ann. Neurol.* 61, 466-475.

References

- Decker,T., Muller,M., and Stockinger,S. (2005). The yin and yang of type I interferon activity in bacterial infection. *Nat. Rev. Immunol.* 5, 675-687.
- Dimitri,D., Benveniste,O., Dubourg,O., Maisonobe,T., Eymard,B., Amoura,Z., Jean,L., Tiev,K., Piette,J.C., Klatzmann,D., Herson,S., and Boyer,O. (2006). Shared blood and muscle CD8+ T-cell expansions in inclusion body myositis. *Brain* 129, 986-995.
- Du,C. and Wang,Y. (2011). The immunoregulatory mechanisms of carcinoma for its survival and development. *J. Exp. Clin. Cancer Res.* 30, 12.
- Du,J. and Murphy,R.M. (2010). Characterization of the interaction of beta-amyloid with transthyretin monomers and tetramers. *Biochemistry* 49, 8276-8289.
- Dustin,M.L. and Long,E.O. (2010). Cytotoxic immunological synapses. *Immunol. Rev.* 235, 24-34.
- Emslie-Smith,A.M., Arahata,K., and Engel,A.G. (1989). Major histocompatibility complex class I antigen expression, immunolocalization of interferon subtypes, and T cell-mediated cytotoxicity in myopathies. *Hum. Pathol.* 20, 224-231.
- Engel,A.G. and Arahata,K. (1984). Monoclonal antibody analysis of mononuclear cells in myopathies. II: Phenotypes of autoinvasive cells in polymyositis and inclusion body myositis. *Ann. Neurol.* 16, 209-215.
- Englund,P., Lindroos,E., Nennesmo,I., Klareskog,L., and Lundberg,I.E. (2001). Skeletal muscle fibers express major histocompatibility complex class II antigens independently of inflammatory infiltrates in inflammatory myopathies. *Am. J. Pathol.* 159, 1263-1273.
- Ferrer,I., Carmona,M., Blanco,R., Moreno,D., Torrejon-Escribano,B., and Olive,M. (2005). Involvement of clusterin and the aggresome in abnormal protein deposits in myofibrillar myopathies and inclusion body myositis. *Brain Pathol.* 15, 101-108.
- Ferrer,I., Martin,B., Castano,J.G., Lucas,J.J., Moreno,D., and Olive,M. (2004). Proteasomal expression, induction of immunoproteasome subunits, and local MHC class I presentation in myofibrillar myopathy and inclusion body myositis. *J. Neuropathol. Exp. Neurol.* 63, 484-498.
- Ferrer,I. and Olive,M. (2008). Molecular pathology of myofibrillar myopathies. *Expert. Rev. Mol. Med.* 10, e25.
- Fidzianska,A., Rowinska-Marcinska,K., and Hausmanowa-Petrusewicz,I. (2004). Coexistence of X-linked recessive Emery-Dreifuss muscular dystrophy with inclusion body myositis-like morphology. *Acta Neuropathol.* 107, 197-203.
- Figarella-Branger,D., Civatte,M., Bartoli,C., and Pellissier,J.F. (2003). Cytokines, chemokines, and cell adhesion molecules in inflammatory myopathies. *Muscle Nerve* 28, 659-682.

- Flier, J., Boorsma, D.M., van Beek, P.J., Nieboer, C., Stoof, T.J., Willemze, R., and Tensen, C.P. (2001). Differential expression of CXCR3 targeting chemokines CXCL10, CXCL9, and CXCL11 in different types of skin inflammation. *J. Pathol.* *194*, 398-405.
- Fornai, F., Lenzi, P., Gesi, M., Ferrucci, M., Lazzeri, G., Natale, G., Ruggieri, S., and Paparelli, A. (2003). Recent knowledge on molecular components of Lewy bodies discloses future therapeutic strategies in Parkinson's disease. *Curr. Drug Targets. CNS. Neurol. Disord.* *2*, 149-152.
- Gobin, S.J., Peijnenburg, A., van, E.M., van, Z.M., Van den Berg, R., and van den elsen, P.J. (1998). The RFX complex is crucial for the constitutive and CIITA-mediated transactivation of MHC class I and beta2-microglobulin genes. *Immunity.* *9*, 531-541.
- Goebels, N., Michaelis, D., Engelhardt, M., Huber, S., Bender, A., Pongratz, D., Johnson, M.A., Wekerle, H., Tschopp, J., Jenne, D., and Hohlfeld, R. (1996). Differential expression of perforin in muscle-infiltrating T cells in polymyositis and dermatomyositis. *J. Clin. Invest* *97*, 2905-2910.
- Gough, D.J., Levy, D.E., Johnstone, R.W., and Clarke, C.J. (2008). IFN γ signaling-does it mean JAK-STAT? *Cytokine Growth Factor Rev.* *19*, 383-394.
- Gouras, G.K., Almeida, C.G., and Takahashi, R.H. (2005). Intraneuronal A β accumulation and origin of plaques in Alzheimer's disease. *Neurobiol. Aging* *26*, 1235-1244.
- Greenberg, S.A. (2010). Dermatomyositis and type 1 interferons. *Curr. Rheumatol. Rep.* *12*, 198-203.
- Greenberg, S.A., Bradshaw, E.M., Pinkus, J.L., Pinkus, G.S., Burleson, T., Due, B., Bregoli, L., O'Connor, K.C., and Amato, A.A. (2005). Plasma cells in muscle in inclusion body myositis and polymyositis. *Neurology* *65*, 1782-1787.
- Greenberg, S.A., Sanoudou, D., Haslett, J.N., Kohane, I.S., Kunkel, L.M., Beggs, A.H., and Amato, A.A. (2002). Molecular profiles of inflammatory myopathies. *Neurology* *59*, 1170-1182.
- Griggs, R.C. (2006). The current status of treatment for inclusion-body myositis. *Neurology* *66*, S30-S32.
- Hill, C.L., Zhang, Y., Sigurgeirsson, B., Pukkala, E., Mellemkjaer, L., Airio, A., Evans, S.R., and Felson, D.T. (2001). Frequency of specific cancer types in dermatomyositis and polymyositis: a population-based study. *Lancet* *357*, 96-100.
- Hilton-Jones, D., Miller, A., Parton, M., Holton, J., Sewry, C., and Hanna, M.G. (2010). Inclusion body myositis: MRC Centre for Neuromuscular Diseases, IBM workshop, London, 13 June 2008. *Neuromuscul. Disord.* *20*, 142-147.
- Hiroi, M. and Ohmori, Y. (2003). The transcriptional coactivator CREB-binding protein cooperates with STAT1 and NF-kappa B for synergistic transcriptional activation of the CXC ligand 9/monokine induced by interferon-gamma gene. *J. Biol. Chem.* *278*, 651-660.

References

- Hofbauer,M., Wiesener,S., Babbe,H., Roers,A., Wekerle,H., Dornmair,K., Hohlfeld,R., and Goebels,N. (2003). Clonal tracking of autoaggressive T cells in polymyositis by combining laser microdissection, single-cell PCR, and CDR3-spectratype analysis. *Proc. Natl. Acad. Sci. U. S. A* *100*, 4090-4095.
- Hohlfeld,R., Goebels,N., and Engel,A.G. (1993). Cellular mechanisms in inflammatory myopathies. *Baillieres Clin. Neurol.* *2*, 617-635.
- Hu,X. and Ivashkiv,L.B. (2009). Cross-regulation of signaling pathways by interferon-gamma: implications for immune responses and autoimmune diseases. *Immunity.* *31*, 539-550.
- Huizing,M. and Krasnewich,D.M. (2009). Hereditary inclusion body myopathy: a decade of progress. *Biochim. Biophys. Acta* *1792*, 881-887.
- Illa,I., Gallardo,E., Gimeno,R., Serrano,C., Ferrer,I., and Juarez,C. (1997). Signal transducer and activator of transcription 1 in human muscle: implications in inflammatory myopathies. *Am. J. Pathol.* *151*, 81-88.
- Irizarry,R.A., Bolstad,B.M., Collin,F., Cope,L.M., Hobbs,B., and Speed,T.P. (2003). Summaries of Affymetrix GeneChip probe level data. *Nucleic Acids Res.* *31*, e15.
- ISAACS,A. and LINDENMANN,J. (1957). Virus interference. I. The interferon. *Proc. R. Soc. Lond B Biol. Sci.* *147*, 258-267.
- Iwasa,K., Kato-Motozaki,Y., Furukawa,Y., Maruta,T., Ishida,C., Yoshikawa,H., and Yamada,M. (2010). Up-regulation of MHC class I and class II in the skeletal muscles of myasthenia gravis. *J. Neuroimmunol.* *225*, 171-174.
- Jain,A., Sharma,M.C., Sarkar,C., Bhatia,R., Singh,S., and Handa,R. (2007). Major histocompatibility complex class I and II detection as a diagnostic tool in idiopathic inflammatory myopathies. *Arch. Pathol. Lab Med.* *131*, 1070-1076.
- Jego,G., Palucka,A.K., Blanck,J.P., Chalouni,C., Pascual,V., and Banchereau,J. (2003). Plasmacytoid dendritic cells induce plasma cell differentiation through type I interferon and interleukin 6. *Immunity.* *19*, 225-234.
- Joffe,M.M., Love,L.A., Leff,R.L., Fraser,D.D., Targoff,I.N., Hicks,J.E., Plotz,P.H., and Miller,F.W. (1993). Drug therapy of the idiopathic inflammatory myopathies: predictors of response to prednisone, azathioprine, and methotrexate and a comparison of their efficacy. *Am. J. Med.* *94*, 379-387.
- Junker,A., Ivanidze,J., Malotka,J., Eiglmeier,I., Lassmann,H., Wekerle,H., Meinl,E., Hohlfeld,R., and Dornmair,K. (2007). Multiple sclerosis: T-cell receptor expression in distinct brain regions. *Brain* *130*, 2789-2799.
- Kaether,C., Scheuermann,J., Fassler,M., Zilow,S., Shirotani,K., Valkova,C., Novak,B., Kacmar,S., Steiner,H., and Haass,C. (2007). Endoplasmic reticulum retention of the gamma-secretase complex component Pen2 by Rer1. *EMBO Rep.* *8*, 743-748.

- Karpati,G. and O'Ferrall,E.K. (2009). Sporadic inclusion body myositis: pathogenic considerations. *Ann. Neurol.* *65*, 7-11.
- Karpati,G., Pouliot,Y., and Carpenter,S. (1988). Expression of immunoreactive major histocompatibility complex products in human skeletal muscles. *Ann. Neurol.* *23*, 64-72.
- Keller,C.W., Fokken,C., Turville,S.G., Lunemann,A., Schmidt,J., Munz,C., and Lunemann,J.D. (2010). TNF-alpha induces macroautophagy and regulates MHC class II expression in human skeletal muscle cells. *J. Biol. Chem.*
- Kloetzel,P.M. (2001). Antigen processing by the proteasome. *Nat. Rev. Mol. Cell Biol.* *2*, 179-187.
- Koffman,B.M., Rugiero,M., and Dalakas,M.C. (1998). Immune-mediated conditions and antibodies associated with sporadic inclusion body myositis. *Muscle Nerve* *21*, 115-117.
- Kovacic,J.C., Gupta,R., Lee,A.C., Ma,M., Fang,F., Tolbert,C.N., Walts,A.D., Beltran,L.E., San,H., Chen,G., St,H.C., and Boehm,M. (2010). Stat3-dependent acute Rantes production in vascular smooth muscle cells modulates inflammation following arterial injury in mice. *J. Clin. Invest* *120*, 303-314.
- LaFerla,F.M. and Oddo,S. (2005). Alzheimer's disease: Abeta, tau and synaptic dysfunction. *Trends Mol. Med.* *11*, 170-176.
- Larkin,J., III, Johnson,H.M., and Subramaniam,P.S. (2000). Differential nuclear localization of the IFNGR-1 and IFNGR-2 subunits of the IFN-gamma receptor complex following activation by IFN-gamma. *J. Interferon Cytokine Res.* *20*, 565-576.
- LeBlanc,A.C., Xue,R., and Gambetti,P. (1996). Amyloid precursor protein metabolism in primary cell cultures of neurons, astrocytes, and microglia. *J. Neurochem.* *66*, 2300-2310.
- LeBouder,F., Khoufache,K., Menier,C., Mandouri,Y., Keffous,M., Lejal,N., Krawice-Radanne,I., Carosella,E.D., Rouas-Freiss,N., and Riteau,B. (2009). Immunosuppressive HLA-G molecule is upregulated in alveolar epithelial cells after influenza A virus infection. *Hum. Immunol.* *70*, 1016-1019.
- Lee,A.H., Hong,J.H., and Seo,Y.S. (2000). Tumour necrosis factor-alpha and interferon-gamma synergistically activate the RANTES promoter through nuclear factor kappaB and interferon regulatory factor 1 (IRF-1) transcription factors. *Biochem. J.* *350 Pt 1*, 131-138.
- Leibundgut-Landmann,S., Waldburger,J.M., Krawczyk,M., Otten,L.A., Suter,T., Fontana,A., Acha-Orbea,H., and Reith,W. (2004). Mini-review: Specificity and expression of CIITA, the master regulator of MHC class II genes. *Eur. J. Immunol.* *34*, 1513-1525.
- Li,C.K., Knopp,P., Moncrieffe,H., Singh,B., Shah,S., Nagaraju,K., Varsani,H., Gao,B., and Wedderburn,L.R. (2009). Overexpression of MHC class I heavy chain protein in young skeletal

References

muscle leads to severe myositis: implications for juvenile myositis. *Am. J. Pathol.* 175, 1030-1040.

Lindberg,C., Oldfors,A., and Tarkowski,A. (1994). Restricted use of T cell receptor V genes in endomysial infiltrates of patients with inflammatory myopathies. *Eur. J. Immunol.* 24, 2659-2663.

Livak,K.J. and Schmittgen,T.D. (2001a). Analysis of relative gene expression data using real-time quantitative PCR and the $2^{-(\Delta\Delta C(T))}$ Method. *Methods* 25, 402-408.

Livak,K.J. and Schmittgen,T.D. (2001b). Analysis of relative gene expression data using real-time quantitative PCR and the $2^{-(\Delta\Delta C(T))}$ Method. *Methods* 25, 402-408.

Love,L.A., Leff,R.L., Fraser,D.D., Targoff,I.N., Dalakas,M., Plotz,P.H., and Miller,F.W. (1991). A new approach to the classification of idiopathic inflammatory myopathy: myositis-specific autoantibodies define useful homogeneous patient groups. *Medicine (Baltimore)* 70, 360-374.

Lunemann,J.D., Schmidt,J., Dalakas,M.C., and Munz,C. (2007). Macroautophagy as a pathomechanism in sporadic inclusion body myositis. *Autophagy.* 3, 384-386.

Lutteke,N., Raftery,M.J., Lalwani,P., Lee,M.H., Giese,T., Voigt,S., Bannert,N., Schulze,H., Kruger,D.H., and Schonrich,G. (2010). Switch to high-level virus replication and HLA class I upregulation in differentiating megakaryocytic cells after infection with pathogenic hantavirus. *Virology* 405, 70-80.

Ma,J.F., Wang,H.M., Li,Q.Y., Zhang,Y., Pan,J., Qiang,Q., Xin,X.Y., Tang,H.D., Ding,J.Q., and Chen,S.D. (2010). Starvation triggers Abeta42 generation from human umbilical vascular endothelial cells. *FEBS Lett.* 584, 3101-3106.

Mastaglia,F.L. (2009). Sporadic inclusion body myositis: variability in prevalence and phenotype and influence of the MHC. *Acta Myol.* 28, 66-71.

Mastaglia,F.L., Needham,M., Scott,A., James,I., Zilko,P., Day,T., Kiers,L., Corbett,A., Witt,C.S., Allcock,R., Laing,N., Garlepp,M., and Christiansen,F.T. (2009). Sporadic inclusion body myositis: HLA-DRB1 allele interactions influence disease risk and clinical phenotype. *Neuromuscul. Disord.* 19, 763-765.

Mattson,M.P. (2004). Pathways towards and away from Alzheimer's disease. *Nature* 430, 631-639.

McDouall,R.M., Dunn,M.J., and Dubowitz,V. (1989). Expression of class I and class II MHC antigens in neuromuscular diseases. *J. Neurol. Sci.* 89, 213-226.

Mikol,J. and Engel,A.G. (2004). Inclusion Body Myositis. In *Myology.*, A.G.Engel and C.Franzini-Armstrong, eds. (New York: McGraw-Hill), pp. 1367-1388.

- Miller, F.W. (2005). Inflammatory myopathies: polymyositis, dermatomyositis, and related conditions. In *Arthritis and Allied Conditions: A Textbook of Rheumatology*, W.Koopman and L.Moreland, eds. (Philadelphia, PA: Lippincott Williams & Wilkins), pp. 1593-1620.
- Munz, C., Lunemann, J.D., Getts, M.T., and Miller, S.D. (2009). Antiviral immune responses: triggers of or triggered by autoimmunity? *Nat. Rev. Immunol.* 9, 246-258.
- Murphy, K.M., Travers, P., and Walport, M. (2008a). Antigen Presentation to T Lymphocytes. In *Immunobiology*, K.M.Murphy, P.Travers, and M.Walport, eds. (London, UK: Taylor & Francis), pp. 183-218.
- Murphy, K.M., Travers, P., and Walport, M. (2008b). Autoimmunity and Transplantation. In *Immunobiology*, K.M.Murphy, P.Travers, and M.Walport, eds. (London: Taylor & Francis), pp. 599-654.
- Murphy, K.M., Travers, P., and Walport, M. (2008c). Basic Concepts in Immunology. In *Immunobiology*, K.M.Murphy, P.Travers, and M.Walport, eds. (London, UK: Taylor & Francis), pp. 1-27.
- Muth, I.E., Barthel, K., Bahr, M., Dalakas, M.C., and Schmidt, J. (2009). Proinflammatory cell stress in sporadic inclusion body myositis muscle: overexpression of alphaB-crystallin is associated with amyloid precursor protein and accumulation of beta-amyloid. *J. Neurol. Neurosurg. Psychiatry* 80, 1344-1349.
- Nagaraju, K., Casciola-Rosen, L., Lundberg, I., Rawat, R., Cutting, S., Thapliyal, R., Chang, J., Dwivedi, S., Mitsak, M., Chen, Y.W., Plotz, P., Rosen, A., Hoffman, E., and Raben, N. (2005). Activation of the endoplasmic reticulum stress response in autoimmune myositis: potential role in muscle fiber damage and dysfunction. *Arthritis Rheum.* 52, 1824-1835.
- Nagaraju, K., Raben, N., Loeffler, L., Parker, T., Rochon, P.J., Lee, E., Danning, C., Wada, R., Thompson, C., Bahtiyar, G., Craft, J., Hooft Van, H.R., and Plotz, P. (2000). Conditional up-regulation of MHC class I in skeletal muscle leads to self-sustaining autoimmune myositis and myositis-specific autoantibodies. *Proc. Natl. Acad. Sci. U. S. A* 97, 9209-9214.
- Needham, M. and Mastaglia, F.L. (2007). Inclusion body myositis: current pathogenetic concepts and diagnostic and therapeutic approaches. *Lancet Neurol.* 6, 620-631.
- Nishino, I., Noguchi, S., Murayama, K., Driss, A., Sugie, K., Oya, Y., Nagata, T., Chida, K., Takahashi, T., Takusa, Y., Ohi, T., Nishimiya, J., Sunohara, N., Ciafaloni, E., Kawai, M., Aoki, M., and Nonaka, I. (2002). Distal myopathy with rimmed vacuoles is allelic to hereditary inclusion body myopathy. *Neurology* 59, 1689-1693.
- Nogalska, A., D'Agostino, C., Engel, W.K., Klein, W.L., and Askanas, V. (2010). Novel demonstration of amyloid-beta oligomers in sporadic inclusion-body myositis muscle fibers. *Acta Neuropathol.* 120, 661-666.
- Pestka, S. (1997). The interferon receptors. *Semin. Oncol.* 24, S9.

References

- Powers,A.C. (2008). Diabetes Mellitus. In Harrison's Principles of Internal Medicine, A.S.Fauci, E.Braunwald, D.L.Kasper, S.L.Hauser, D.L.Longo, J.L.Jameson, and J.Loscalzo, eds. (NYC, NY: McGraw-Hill Companies).
- Prchal,M., Pilz,A., Simma,O., Lingnau,K., von,G.A., Strobl,B., Muller,M., and Decker,T. (2009). Type I interferons as mediators of immune adjuvants for T- and B cell-dependent acquired immunity. *Vaccine 27 Suppl 6*, G17-G20.
- Price,P., Witt,C., Allcock,R., Sayer,D., Garlepp,M., Kok,C.C., French,M., Mallal,S., and Christiansen,F. (1999). The genetic basis for the association of the 8.1 ancestral haplotype (A1, B8, DR3) with multiple immunopathological diseases. *Immunol. Rev. 167*, 257-274.
- Raju,R., Vasconcelos,O., Granger,R., and Dalakas,M.C. (2003). Expression of IFN-gamma-inducible chemokines in inclusion body myositis. *J. Neuroimmunol. 141*, 125-131.
- Rizza,P., Moretti,F., and Belardelli,F. (2010). Recent advances on the immunomodulatory effects of IFN-alpha: implications for cancer immunotherapy and autoimmunity. *Autoimmunity 43*, 204-209.
- Ronnlom,L. and Alm,G.V. (2003). Systemic lupus erythematosus and the type I interferon system. *Arthritis Res. Ther. 5*, 68-75.
- Sadeh,M., Gadoth,N., Hadar,H., and Ben-David,E. (1993). Vacuolar myopathy sparing the quadriceps. *Brain 116 (Pt 1)*, 217-232.
- Salajegheh,M., Raju,R., Schmidt,J., and Dalakas,M.C. (2007). Upregulation of thrombospondin-1(TSP-1) and its binding partners, CD36 and CD47, in sporadic inclusion body myositis. *J. Neuroimmunol. 187*, 166-174.
- Schmidt,J., Barthel,K., Wrede,A., Salajegheh,M., Bahr,M., and Dalakas,M.C. (2008). Interrelation of inflammation and APP in sIBM: IL-1 beta induces accumulation of beta-amyloid in skeletal muscle. *Brain 131*, 1228-1240.
- Schmittgen,T.D. and Livak,K.J. (2008). Analyzing real-time PCR data by the comparative C(T) method. *Nat. Protoc. 3*, 1101-1108.
- Schroder,K., Hertzog,P.J., Ravasi,T., and Hume,D.A. (2004). Interferon-gamma: an overview of signals, mechanisms and functions. *J. Leukoc. Biol. 75*, 163-189.
- Seitz,S., Schneider,C.K., Malotka,J., Nong,X., Engel,A.G., Wekerle,H., Hohlfeld,R., and Dornmair,K. (2006). Reconstitution of paired T cell receptor alpha- and beta-chains from microdissected single cells of human inflammatory tissues. *Proc. Natl. Acad. Sci. U. S. A 103*, 12057-12062.
- Sekul,E.A. and Dalakas,M.C. (1993). Inclusion body myositis: new concepts. *Semin. Neurol. 13*, 256-263.

Selcen,D., Ohno,K., and Engel,A.G. (2004). Myofibrillar myopathy: clinical, morphological and genetic studies in 63 patients. *Brain* *127*, 439-451.

Selkoe,D.J. (1989). Amyloid beta protein precursor and the pathogenesis of Alzheimer's disease. *Cell* *58*, 611-612.

Semino-Mora,C. and Dalakas,M.C. (1998). Rimmed vacuoles with beta-amyloid and ubiquitinated filamentous deposits in the muscles of patients with long-standing denervation (postpoliomyelitis muscular atrophy): similarities with inclusion body myositis. *Hum. Pathol.* *29*, 1128-1133.

Sisodia,S.S. and Price,D.L. (1995). Role of the beta-amyloid protein in Alzheimer's disease. *FASEB J.* *9*, 366-370.

Sivakumar,K., Semino-Mora,C., and Dalakas,M.C. (1997). An inflammatory, familial, inclusion body myositis with autoimmune features and a phenotype identical to sporadic inclusion body myositis. Studies in three families. *Brain* *120* (Pt 4), 653-661.

Spasic,D. and Annaert,W. (2008). Building gamma-secretase: the bits and pieces. *J. Cell Sci.* *121*, 413-420.

Stark,G.R. (2007). How cells respond to interferons revisited: from early history to current complexity. *Cytokine Growth Factor Rev.* *18*, 419-423.

Stark,G.R., Kerr,I.M., Williams,B.R., Silverman,R.H., and Schreiber,R.D. (1998). How cells respond to interferons. *Annu. Rev. Biochem.* *67*, 227-264.

Storey,J.D. and Tibshirani,R. (2003). Statistical methods for identifying differentially expressed genes in DNA microarrays. *Methods Mol. Biol.* *224*, 149-157.

Tateyama,M., Fujihara,K., Misu,T., and Itoyama,Y. (2009). CCR7+ myeloid dendritic cells together with CCR7+ T cells and CCR7+ macrophages invade CCL19+ nonnecrotic muscle fibers in inclusion body myositis. *J. Neurol. Sci.* *279*, 47-52.

van den Elsen,P.J., Holling,T.M., Kuipers,H.F., and Van der Stoep,N. (2004). Transcriptional regulation of antigen presentation. *Curr. Opin. Immunol.* *16*, 67-75.

van der Meulen,M.F., Bronner,I.M., Hoogendijk,J.E., Burger,H., van Venrooij,W.J., Voskuyl,A.E., Dinant,H.J., Linssen,W.H., Wokke,J.H., and de,V.M. (2003). Polymyositis: an overdiagnosed entity. *Neurology* *61*, 316-321.

van der Meulen,M.F., Hoogendijk,J.E., Jansen,G.H., Veldman,H., and Wokke,J.H. (1998). Absence of characteristic features in two patients with inclusion body myositis. *J. Neurol. Neurosurg. Psychiatry* *64*, 396-398.

References

- van der Pas,J., Hengstman,G.J., ter Laak,H.J., Borm,G.F., and van Engelen,B.G. (2004). Diagnostic value of MHC class I staining in idiopathic inflammatory myopathies. *J. Neurol. Neurosurg. Psychiatry* 75, 136-139.
- Van Gelder,R.N., von Zastrow,M.E., Yool,A., Dement,W.C., Barchas,J.D., and Eberwine,J.H. (1990). Amplified RNA synthesized from limited quantities of heterogeneous cDNA. *Proc. Natl. Acad. Sci. U. S. A* 87, 1663-1667.
- Vattemi,G., Nogalska,A., King,E.W., D'Agostino,C., Checler,F., and Askanas,V. (2009). Amyloid-beta42 is preferentially accumulated in muscle fibers of patients with sporadic inclusion-body myositis. *Acta Neuropathol.* 117, 569-574.
- Velliquette,R.A., O'Connor,T., and Vassar,R. (2005). Energy inhibition elevates beta-secretase levels and activity and is potentially amyloidogenic in APP transgenic mice: possible early events in Alzheimer's disease pathogenesis. *J. Neurosci.* 25, 10874-10883.
- Vereecke,L., Beyaert,R., and van,L.G. (2009). The ubiquitin-editing enzyme A20 (TNFAIP3) is a central regulator of immunopathology. *Trends Immunol.* 30, 383-391.
- Wang,Y., Liu,D., Chen,P., Koeffler,H.P., Tong,X., and Xie,D. (2008). Negative feedback regulation of IFN-gamma pathway by IFN regulatory factor 2 in esophageal cancers. *Cancer Res.* 68, 1136-1143.
- Wiendl,H., Behrens,L., Maier,S., Johnson,M.A., Weiss,E.H., and Hohlfeld,R. (2000). Muscle fibers in inflammatory myopathies and cultured myoblasts express the nonclassical major histocompatibility antigen HLA-G. *Ann. Neurol.* 48, 679-684.
- Wojcik,S., Engel,W.K., McFerrin,J., Paciello,O., and Askanas,V. (2006). AbetaPP-overexpression and proteasome inhibition increase alphaB-crystallin in cultured human muscle: relevance to inclusion-body myositis. *Neuromuscul. Disord.* 16, 839-844.
- Wolfe,M.S. and Guenette,S.Y. (2007). APP at a glance. *J. Cell Sci.* 120, 3157-3161.
- Woo,H.N., Baik,S.H., Park,J.S., Gwon,A.R., Yang,S., Yun,Y.K., and Jo,D.G. (2011). Secretases as therapeutic targets for Alzheimer's disease. *Biochem. Biophys. Res. Commun.* 404, 10-15.
- Wu,Z. and Irizarry,R.A. (2004). Preprocessing of oligonucleotide array data. *Nat. Biotechnol.* 22, 656-658.
- Yanai,I., Benjamin,H., Shmoish,M., Chalifa-Caspi,V., Shklar,M., Ophir,R., Bar-Even,A., Horn-Saban,S., Safran,M., Domany,E., Lancet,D., and Shmueli,O. (2005). Genome-wide midrange transcription profiles reveal expression level relationships in human tissue specification. *Bioinformatics.* 21, 650-659.
- Young,H.A. and Bream,J.H. (2007). IFN-gamma: recent advances in understanding regulation of expression, biological functions, and clinical applications. *Curr. Top. Microbiol. Immunol.* 316, 97-117.

Yu, W.H., Cuervo, A.M., Kumar, A., Peterhoff, C.M., Schmidt, S.D., Lee, J.H., Mohan, P.S., Mercken, M., Farmery, M.R., Tjernberg, L.O., Jiang, Y., Duff, K., Uchiyama, Y., Naslund, J., Mathews, P.M., Cataldo, A.M., and Nixon, R.A. (2005). Macroautophagy--a novel Beta-amyloid peptide-generating pathway activated in Alzheimer's disease. *J. Cell Biol.* *171*, 87-98.

8. Curriculum vitae

Name	Jana Ivanidze
Date of Birth	April 26, 1984
Place of Birth	Kiev, Ukraine
Nationality	German
Family status	Single

Work experience

Since January 2011 Radiology resident, Institute of Clinical Radiology, LMU, Munich

Training

Since April 2007 PhD Student, Max Planck Institute of Neurobiology, Department of Neuroimmunology, Martinsried/
Institute of Clinical Neuroimmunology, LMU, Munich
PhD Program: Medical Life Sciences and Technology, TUM, Munich.

Medical Education

October 2003 – November 2009 Medical Studies, LMU, Munich
Degree: State Examination, grade “A” (1.83)

Internship (practical training): Internal Medicine, Departments of Cardiology and Hematology/ Oncology, LMU, Munich
Surgery, Departments of Neurosurgery and Vascular Surgery, LMU, Munich
Radiology, Institute for Clinical Radiology, LMU, Munich

High School Education

St. Anna-Gymnasium (grammar school), Munich.
Degree: Baccalaureate (Abitur), grade “A” (1.3)

9. Published data from the manuscript

Jana Ivanidze, Reinhard Hoffmann, Hanns Lochmüller, Andrew G. Engel, Reinhard Hohlfeld*, and Klaus Dornmair*. Inclusion Body Myositis: Laser microdissection reveals differential upregulation of IFN gamma signaling cascade in attacked versus non-attacked myofibers. *American Journal of Pathology (manuscript accepted on May 31st, 2011).*

Jana Ivanidze, Reinhard Hoffmann, Hanns Lochmüller, Andrew G. Engel, Reinhard Hohlfeld, and Klaus Dornmair. Loss of Retention in endoplasmic reticulum 1 (RER1) expression in Sporadic inclusion body myositis: a novel marker for β -amyloid biosynthesis? *Neurology. (manuscript submission in preparation).*

Jana Ivanidze, Andrew G. Engel, Reinhard Hohlfeld, and Klaus Dornmair. Inclusion Body Myositis: Interferon Gamma Signaling in HLA-I⁺ Myofibers attacked by CD8⁺ T-Cells. Abstract and oral presentation at the 10th International Congress of Neuroimmunology, Barcelona, Spain.